

ANALYSIS ON DEVELOPMENT OF INCREMENTAL RING ROLLING
PROCESS

A THESIS SUBMITTED TO
THE GRADUATE SCHOOL OF NATURAL AND APPLIED SCIENCES
OF
MIDDLE EAST TECHNICAL UNIVERSITY

BY

MUİN SÜLEYMAN ÖZTOP

IN PARTIAL FULFILLMENT OF THE REQUIREMENTS
FOR
THE DEGREE OF MASTER OF SCIENCE
IN
MECHANICAL ENGINEERING

DECEMBER 2006

Approval of the Graduate School of Natural and Applied Sciences

Prof. Dr. Canan ÖZGEN
Director

I certify that this thesis satisfies all the requirements as a thesis for the degree of Master of Science.

Prof. Dr. S. Kemal İDER
Head of Department

This is to certify that we have read this thesis and that in our opinion it is fully adequate, in scope and quality, as a thesis for the degree of Master of Science.

Prof. Dr.-Ing. A. Erman TEKKAYA
Co-Supervisor

Prof. Dr. Zafer DURSUNKAYA
Supervisor

Examining Committee Members

Assoc. Dr. Suat KADIOGLU (METU, ME) _____

Prof. Dr. Zafer DURSUNKAYA (METU, ME) _____

Prof. Dr. A. Erman TEKKAYA (ATILIM UNIV.) _____

Asst. Prof. Dr. Merve ERDAL (METU, ME) _____

Assoc. Prof. Dr. Uğurhan AKYÜZ (METU, CE) _____

I hereby declare that all information in this document has been obtained and presented in accordance with academic rules and ethical conduct. I also declare that, as required by these rules and conduct, I have fully cited and referenced all material and results that are not original to this work.

Name, Last Name: MUİN SÜLEYMAN, ÖZTOP

Signature :

ABSTRACT

ANALYSIS ON DEVELOPMENT OF INCREMENTAL RING ROLLING PROCESS

Öztop, Muin Süleyman

M.Sc., Department of Mechanical Engineering

Supervisor : Prof. Dr. Zafer Dursunkaya

Co-Supervisor: Prof. Dr.-Ing. A. Erman Tekkaya

December 2006, 192 pages

In this study, a novel incremental ring rolling process used in production of rings with various cross sections is examined. A basic type of this process is investigated numerically, using commercial finite element programs; MSC Superform, MSC Marc. The user defined subroutines are also utilized for flexibility in modeling. The aim of modeling is to determine the material flow for geometrical analysis, strain/stress distribution for tool force analysis and residual stresses, in a cost effective way. The process has instabilities and requires large number of incremental stages to complete a full finite element simulation. The full models are reliable but costly hence the numerical studies are focused on reliable simplified models with lower computation time. Different approaches are developed: three-dimensional segment model, improved segment model, velocity coupling model. The results of these models are compared with experimentally verified full models. Numerical parameters such as mesh type, step size, convergence ratio are examined. After verification of the model different applications to of the process is developed and physical parameters affecting the process are discussed; such as the tool path .

Keywords: Incremental Ring Rolling , Flexible Ring Rolling Analysis, Finite Element Method,

ÖZ

KADEMELİ YÜZÜK OVALAMA İŞLEMİNİN GELİŞTİRİLMESİNİN ANALİZİ

Öztop, Muin Süleyman

Yüksek Lisans, Makina Mühendisliği Bölümü

Tez Danışmanı: Prof. Dr. Zafer Dursunkaya

Yardımcı Danışman: Prof. Dr.-Ing. A. Erman Tekkaya

Aralık 2006, 192 sayfa

Bu çalışmada, çeşitli bilezik kesitlerinin üretiminde kullanılabilen yeni kademeli bilezik ovalama işlemi incelenmiştir. Bu işlemin, temel bir basamağının sayısal modellemelerinde ve analizlerinde, MSC Superform, MSC Marc gibi ticari yazılımlar kullanılmıştır. Ayrıca, kullanıcı tabanlı alt programlarla modellemede esneklik sağlanmıştır. Bu analizlerin amacı, geometri analizi için malzeme akışını belirleme, ve işlem sonrası kalıcı gerilme ve gerinimlerin dağılımlarını maliyeti azaltarak saptamaktır. İşlem sırasında bir çok dengesizlik görülmektedir ve işlemin üç boyutlu tam modelleri fazla sayıda kademeli olarak çözüldüklerinde düzgün sonuç vermektedir. Tam modeller güvenilir ancak çözüm zamanı göz önüne alındığında maliyetlidir. Bu nedenle bu çalışmada, basitleştirilmiş, daha kısa süreli çözümlene zamanı gerektiren ve güvenilir olan modeller üzerine odaklanılmıştır. Üç boyutlu kısmi model, geliştirilmiş kısmi model ve hız eşleştirmeli model gibi değişik yaklaşımlar geliştirilmiştir. Modellerin sonuçları, deneysel olarak doğrulamaları yapılmış tam modellerle karşılaştırılmıştır. Modellemede en iyi sayısal parametreleri belirleme çalışmaları incelenmiştir. Ayrıca prosesi etkileyen fiziksel parametreler de, takım yolu gibi, ele alınmıştır.

Keywords: Esnek Yüzük Ovalama İşlemi , Sonlu Elemanlar Methodu,

To Memory of My Father

ACKNOWLEDGMENTS

The author wishes to express his deepest gratitude to his supervisors; Prof. Dr.-Ing. A. Erman Tekkaya and Prof. Dr. Zafer Dursunkaya, for their guidance, advice, criticism, encouragements and insight throughout the research.

The author also would like to express his appreciation to Omer Music for his guidance, unlimited help during the research and also for his incredible friendship.

The author would like to thank to managers in ORS Bearing Company; Dr. Feridun Özhan and Turan Savaş for their great support and generosity in opening their facilities for experiments.

The author would also like to express his gratefulness to Dr. Julian Allwood, for his valuable comments and advices throughout the meetings.

The author would also like to express his gratefulness to his friends Özer, Mithat Barış, Bülent, Ceyhun, Oya, Evin, Asli, Murat and Tuğçe for envying his life and for their supports. The author would like to thank to his ex-colleagues in TUBITAK-SAGE, especially to Mahmut Beşir for his consideration and support.

Finally the author would like to thank his mother Selma Öztop, his aunt Sema Çetinel, his sister Şeyma and his brother Mecit for their support and patience throughout the research.

The travel expenditures for academic activities throughout this research are funded by TUBITAK-BAYG and British Council.

The author is grateful to TUBITAK-BAYG for supporting him with the National Master of Science Scholarship during twelve months of research.

TABLE OF CONTENTS

ABSTRACT	iv
ÖZ	v
ACKNOWLEDGMENTS	vii
TABLE OF CONTENTS	viii
LIST OF TABLES	xii
LIST OF FIGURES	xiv
CHAPTERS	
1.INTRODUCTION	1
1.1 Incremental Forming Processes	1
1.1.1 Roll Forging	5
1.1.2 Roll Forming	6
1.1.3 Cross-Wedge Rolling	7
1.1.4 Spinning.....	8
1.1.5 Roll Bending	10
1.1.6 Radial Forging	12
1.1.7 Rotary Forging/Orbital Forging	13
1.1.8 Rotary Swaging.....	15
1.1.9 Flat/Profile Rolling.....	17
1.1.10 Ring Rolling.....	18
2.LITERATURE SURVEY	26
2.1 General Characteristics of Incremental Forming Process for Numerical Modelling	27
2.2 Numerical Modelling of Incremental Forming Processes (IFP)	30
2.2.1 Roll Forging	30
2.2.2 Roll Forming (RF)	31
2.2.3 Cross-Wedge Rolling (CWR).....	32
2.2.4 Spinning.....	34
2.2.5 Roll Bending	36

2.2.6	<i>Radial Forging</i>	37
2.2.7	<i>Rotary Forging/Orbital Forging</i>	39
2.2.8	<i>Rotary Swaging</i>	40
3.2.9	<i>Flat/Profile Rolling</i>	41
2.2.10	Ring Rolling	42
2.2.11	<i>Discussion</i>	59
2.3	Theory of X-Ray Diffractometer Residual Stress Measurement.....	61
2.3.1	Equations for X-Ray Strain Calculations	62
2.3.2	Equations for X-Ray Stress Calculations	64
2.3.3	Layer Removal by Electro Polishing and Correction of Layers.....	67
3	PROBLEM DEFINITION.....	69
3.1	Definition of the process	69
3.2	Need for Analysis	73
3.3	Aim and Scope of the Study.....	75
4	EXPERIMENTAL STUDIES	76
4.1	Plan of the Experiments	77
4.2	Machine and tooling	77
4.3	Measurement Equipments and Methodology.....	79
4.4	Series of Experiments	83
4.4.1	<i>First Series of Experiments</i>	83
4.4.2	<i>Second Series of Experiments</i>	85
4.4.3	<i>Third Series of Experiments</i>	90
4.4.4	<i>The Experiment conducted for numerical modeling</i>	97
5	NUMERICAL MODELS.....	101
5.1	Numerical Models for Conventional Ring Rolling	103
5.1.1	<i>Two-Dimensional (2D) Full Models</i>	104
5.1.2	<i>Two-Dimensional (2D) Segment Model</i>	111
5.1.3	<i>3D Full Model</i>	112
5.1.4	<i>3D Segment Model</i>	115
5.2	Numerical Models for Incremental Ring Rolling.....	118

5.2.1	3D Full Models	119
5.2.2	3D Segment Model	123
5.2.3	3D Segment Model with Soft Elastic Region	124
5.2.4	3D Velocity Coupling Model	127
6.	APPLICATION OF NUMERICAL MODELS	137
6.1	3D Segment Model for Conventional Ring Rolling	139
6.1.1	<i>Geometrical Comparison</i>	139
6.1.2	Total Equivalent Strain Analysis	140
6.1.3	<i>Residual Stress Analysis</i>	141
6.1.4	<i>Accuracy and Computation Time</i>	143
6.2	3D Full Model for Incremental Ring Rolling	144
6.2.1	<i>Geometrical Comparison</i>	145
6.2.2	Total Equivalent Strain Comparison	146
6.2.3	<i>Residual Stress Comparison</i>	148
6.2.4	<i>Accuracy and Computation Time</i>	151
6.2.5	<i>Material Flow Characterization</i>	152
6.3	3D Segment Modeling for Incremental Ring Rolling	153
6.3.1	<i>Geometrical Comparison</i>	153
6.3.2	<i>Total Equivalent Strain Comparison</i>	154
6.3.3	<i>Residual Stress Comparison</i>	155
6.3.4	<i>Accuracy and Computation Time</i>	157
6.4	3D Segment Model with Soft Elastic Region	158
6.4.1	<i>Geometrical Comparison</i>	158
6.4.2	<i>Total Equivalent Strain Comparison</i>	159
6.4.3	<i>Residual Stress Comparison</i>	160
6.4.4	<i>Accuracy and Computation Time</i>	161
6.5	3D Velocity Coupling Model	162
6.5.1	<i>Geometrical Comparison</i>	163
6.5.2	<i>Total Equivalent Strain Comparison</i>	164
6.5.3	<i>Residual Stress Comparison</i>	166

6.5.4	<i>Accuracy and Computation Time</i>	171
6.6	Comparisons of all models.....	171
6.6.1	<i>Geometrical Comparison</i>	171
6.6.2	<i>Total Equivalent Strain Comparison</i>	172
6.6.3	<i>Residual Stress Comparison</i>	174
6.6.4	<i>Accuracy and Computation Time</i>	177
7.	DISCUSSION AND CONCLUSION.....	179
8.	RECOMMENDATIONS AND FURTHER STUDIES.....	182
	REFERENCES	184

LIST OF TABLES

<i>Table 1.1 Schematic representation of incremental deformation process with rotational motion (Standring 2006)</i>	3
<i>Table 2.1 Summary of X-ray stress determination equations</i>	66
<i>Table 3.1 Mechanical and metallurgical properties of bearing steel (Music 2005)</i>	71
<i>Table 4.1 Ring rolling machine specification</i>	79
<i>Table 4.2 Axis movements with hardware limitations</i>	80
<i>Table 4.3 Dimensions of deformed ring.....</i>	87
<i>Table 4.4 The final profiles of the rings.....</i>	91
<i>Table 4.5 Variation in residual stresses for different configurations.....</i>	96
<i>Table 5.1 Summary of presented models</i>	102
<i>Table 5.2 Comparison of variations in stress for different relative force tolerances</i>	108
<i>Table 5.3 Mesh topologies used in model.....</i>	121
<i>Table 5.4 Error in total equivalent strain for different modulus of elasticity values.</i>	126
<i>Table 5.5 Error in total equivalent strain for different thickness of elastic region</i>	126
<i>Table 6.1 Summary of analyzed models.....</i>	138
<i>Table 6.2 Geometrical comparison of 3D segment model for conventional ring rolling.....</i>	139

Table 6.3 Geometrical comparison of 3D Full Model for different meshes ...	145
Table 6.4 Accuracy and computation time of the 3D Full Models.....	151
Table 6.5 Geometrical comparison of 3D Segment Model	154
Table 6.6 Geometrical comparison of 3D Segment Model with Soft Elastic Region	159
Table 6.7 Geometrical comparison of velocity coupling method at low deformation.....	163
Table 6.8 Geometrical comparison of velocity coupling method at high deformation.....	164
Table 6.9 Accuracy and computation time of the velocity coupling models.	171
Table 6.10 Geometrical comparison of all models.....	172
Table 6.11 Accuracy and computation time comparison of all models.....	177

LIST OF FIGURES

Figure 1.1 Sample produced with a) simple upsetting b) orbital forming....	2
Figure 1.2 Flat strip of cold metal passes through several stages of bending (Lindgren 2005)	5
Figure 1.3 Cross wedge rolling with two wedge shaped tools mounted on rollers (Piedrahita 2005).	8
Figure 1.4 Setup of spinning process (Sebastiani 2006)	9
Figure 1.5 a) Three-roll bending process (Hu 2001) b)Operational sequence of four-roll thin plate bending (Lin 2000)	11
Figure 1.6 A schematic diagram showing the arrangement of the forging dies in the radial forging machine (Ghaei 2005)	13
Figure 1.7 Types of rotary forging process (Standring 2006)	14
Figure 1.8 A simple representation of components in a conventional rotary swaging (Rathmann 2004).....	16
Figure 1.9 Kinematical classification of rolling process, applicable to both hollow and solid workpieces (Lange 1985)	17
Figure 1.10 Schematic representation of the main parts of the cold ring rolling machine at ORS (Music 2005)	19
Figure 1.11 Classification of bearing profiles.	22
Figure 1.12 Examples of difficult to produce sections in bearings.....	23
Figure 2.1 a) Non-uniform Mesh for symmetrical model b) deformation sequences for the process (Fang 2002)	34
Figure 2.2 Meshing strategies for spinning of a circular blank(Sebastiani, 2006).	39

Figure 2.3 Representation of a forged (a) and rolled (b) cross section from the same original dimensions and reduction (Wen 1998)	42
Figure 2.4 The coordinate system for the analysis and the geometrical configurations of rectangular plain ring rolling. (Tszeng and Altan 1991)..	44
Figure 2.5 Variation of mean axial spread $\Delta w/w_0$ with height reduction $\Delta H/H_0$ for plain ring rolling (Tszeng and Altan 1991).	45
Figure 2.6 Physical modelling of a ring rolling process (Joun 1998)	46
Figure 2.7 Comparison of simulation results for different forging factors.	47
Figure 2.8 Change in thickness reduction (Utsunomiya 2002).	49
Figure 2.9 Deformation model of ring rolling (Takizawa 2001)	50
Figure 2.10 Comparison of the partial model with the full model	51
Figure 2.11 Some of the results of ALE model of ring rolling (Davey2002) compared to results of Mamalis	52
Figure 2.12 Mesh systems defined in the model (Kim 1991)	54
Figure 2.13 Slide spread variation with reduction of height (Kim 1991)	54
Figure 2.14 The diameter increase with respect to the thickness reduction (Xie 2000)	55
Figure 2.15 Comparison of analysis results and actual rolled dimensions of CV joint cage (actual dimensions are in the parentheses) (Sawamiphakdi 2002)	57
Figure 2.16 Ring growth due to projection of nodal velocities in ring rolling (Montmitonnet 2006)	58
Figure 2.17 Ring growth elimination by cubic spline method (Montmitonnet 2006).	59
Figure 2.18 Definition of spatial and material coordinate systems (Noyan 1987).	62

Figure 2.19 $d_{\phi\psi}$ vs. $\sin^2 \psi$ behaviors a) Regular, $\varepsilon_{13} = \varepsilon_{23} = 0$; b) Regular, $\varepsilon_{13}, \varepsilon_{23} \neq 0$ c) Irregular, no condition	64
Figure 3.1 a) Representation of incremental ring rolling process (Allwood 2005) b) Cross-section view of part	70
Figure 3.2 Bearing steel flow curves from various sources (Music 2005)	72
Figure 4.1 Machine set-up for the experiment.....	80
Figure 4.2 Goniometer, TSA and X-Y Stage	81
Figure 4.2 The schematic representation of first series of experiments.....	83
Figure 4.2 Sketch of the ring shape at different stages of the experiment.....	84
Figure 4.5 Sketch of the ring shape at different stages of the experiment.....	85
Figure 4.6 Sketch of the ring shape at different stages of the experiment.....	86
Figure 4.7 a) The schematic view of the process	88
Figure 4.8 Axial residual stress distribution on outer face	89
Figure 4.9 Tangential residual stress distribution on outer face.....	89
Figure 4.10 Axial residual stress distribution on inner face	89
Figure 4.11 Tangential residual stress distribution on inner face.....	90
Figure 4.12 Tangential and axial residual stress distribution on a) inner face; b) outer face of the ring in edge aligned mandrel configuration.	93
Figure 4.13 Tangential and axial the residual stress distribution on a) inner face; b) outer face of the ring in center aligned mandrel	95
Figure 4.14 Axial residual stress distribution on outer face in the experiment for validation.	98
Figure 4.15 Tangential residual stress distribution on outer face in the experiment for validation.	99

Figure 4.16 Axial residual stress distribution on inner face in the experiment for validation.	99
Figure 4.17 Tangential residual stress distribution on inner face in the experiment for validation.	100
Figure 5.1 Plane strain model with load control option	104
Figure 5.2 Mesh topologies used in the analyses (Music 2005)	106
Figure 5.3 Circumferential stress distribution in radial direction for different mesh topologies and for $\xi=0.01$	107
Figure 5.4 The 2D segment model; a) initial b) final configuration.....	111
Figure 5.5 Residual Von Mises equivalent stress distribution for different mesh topologies (Music 2005)	114
Figure 5.6 The elements of 3D segment model.....	116
Figure 5.7 The residual stress distribution on a) outer surface b) inner surface of the rings for two different methods of cycle	117
Figure 5.8 Schematic representation of the model and the set of analysis	120
Figure 5.9 Equivalent residual stress distribution on the a) outer b) inner surface of the ring, for different mesh topologies.....	122
Figure 5.9 a) 3D Segment Model b) 3D Segment model with soft elastic region	125
Figure 5.10 The imaginary boundary planes, cut for velocity profile analysis.....	128
Figure 5.11 Normal velocities of the nodes on the mid of the planes are given	128
Figure 5.12. Simple tying constraint (MSC. MARC VOLUME A, 2005)	130
Figure 5.13 The relation of angular configurations of any retained and the tied node.	133
Figure 5.14 Representation of change in segment angle	135

Figure 6.1 Total equivalent strain comparison of 3D segment model for conventional ring rolling.....	140
Figure 6.2 Comparison of residual stress distribution in a) circumferential axial directions for different segment angles	143
Figure 6.3 Total equivalent strain distribution on a) outer b) inner rfaces of the ring	147
Figure 6.4 Residual stress distribution on the a) circumferential b) axial direction on the outer surface of the ring, for different mesh topologies	149
Figure 6.5 (Residual stress distribution on the a) circumferential b) axial direction)on the inner surface of the ring, for different mesh topologies	150
Figure 6.6 (Residual stress distribution on the a) circumferential b) axial direction)on the outer surface of the ring, for different mesh topologies	151
Figure 6.7 Material flow characterization with different sets of models	152
Figure 6.8 Total equivalent strain distributions for 3D Segment Model	155
Figure 6.9 Residual equivalent stress distribution on the a) outer b) inner surface of the ring, for different segment angles	156
Figure 6.11 Material flow on the boundary plane	157
Figure 6.12 Accuracy and computation time of the model.....	158
Figure 6.13 Total equivalent strain distributions comparison for 3D Segment Model with Soft Elastic Region.....	160
Figure 6.14 Accuracy of the model for different modulus of elasticity.	162
Figure 6.15 Total equivalent strain distributions comparison for velocity coupling model (1.1 mm of bite)	165
Figure 6.16 Total equivalent strain distributions comparison for velocity coupling model (2.2 mm of bite)	166
Figure 6.17 Circumferential deformation of the ring	167
Figure 6.18 Residual stress distribution in the a) circumferential b) axial direction, on the outer surface of the ring, for different mesh topologies	169

Figure 6.18 (continued) Residual stress distribution in the c) circumferential d) axial direction, on the inner surface of the ring, for different mesh topologies	170
Figure 6.19 Total equivalent strain comparison of all models on the a) outer b) inner surfaces	173
Figure 6.20 Residual stress distribution in the circumferential direction on the outer surface of the ring, for all models.....	175
Figure 6.21 Residual stress distribution in the axial direction on the outer surface of the ring, for all models.....	175
Figure 6.22 Residual stress distribution in the circumferential direction on the inner surface of the ring, for all models.....	176
Figure 6.23 Residual stress distribution in the axial direction on the inner surface of the ring, for all models.....	177

CHAPTER 1

INTRODUCTION

In this chapter, a brief introduction of incremental deformation processes with rotational motion is given; the applications, benefits and disadvantages of these processes are mentioned. Among these processes the conventional ring rolling is presented in detail. The products that ring rolling is utilized are classified. After product identification, the needs of improvements on the conventional ring rolling process are defined, and finally evolution of incremental ring rolling is explained. The expected benefits of this new process are stated and pitfalls are also examined. In the proceeding chapters experimental and numerical investigation on this process will be presented.

1.1 Incremental Forming Processes

The incremental forming processes are broad groups in manufacturing techniques. These processes can be defined as operations in which local forces are applied repeatedly upon workpiece by using simple tools. The number of working cycles on the workpiece may reach from several hundreds to thousands. The incremental forming processes are used for increasing flexibility with using simple kinematics and with reduction of the power needed. The formed part is expected to be near-net shape part. These result in reduction in investment costs and operating expenses by using simple machines to perform simple processes.

The incremental forming processes generally have superior formability characteristics compared to conventional forming processes. In addition to formability, many incrementally formed products exhibits better mechanical

characteristics as a result of favorable grain orientation. In *Figure 1.1*, there are two samples from same material formed with two different methods are shown. The first one is obtained with simple upsetting, and after a height reduction of 67%, the cracking at the edges starts. The identical sample is formed using orbital forging with a 2° degree tool angle and the cracking starts after a height reduction of 83 % (Pauskar 2006). In orbital forming lower deformation force is exerted on the workpiece.



Figure 1.1 Sample produced with a) simple upsetting b) orbital forming (Pauskar 2006)

In many incremental forming process the simplicity is concerned in terms of kinematics and tooling. There are many incremental processes that the kinematics is not complex and the tooling is simple and vice versa. However there are few of them in which both kinematics and the tooling are both complex. The simplicity of the kinematics can be defined as the easiness of the contact formation between workpiece and tool interface, flexibility in direction of motion of the tool during operation, and simple deformation characteristic that can be solved easily using analytical and numerical tools. The simplicity of the tooling is not only easiness in production of tools but also the flexibility of the tools. Multi-stage production is not desired in an incremental process. Single-stage production with a general purpose tool is expected. The tools are expected to be used in forming different type of products.

The evolution of the incremental processes is mainly based on the idea of near-net shape forming. Many conventional forming operations are succeeded by machining operations which cause loss in mechanical characteristics. The lower deformation forces, simplicity in the kinematics and the tooling are directly reflected to the investment cost and production cost of the operation. The construction of simple machine and using flexible tools decrease the depreciation. In addition, the lower amount of power for deformation decreases the production cost.

In many type of incremental processes, rotational motion exists. There are three features for the rotational motion: in the first one the workpiece rotates; in the second one, the tool rotates; and in the last one, both workpiece and the tools rotate. In addition to rotational motion the translational motion for the workpiece and the tools are also given separately or simultaneously. In *Table 1.1*, the type of the motions for workpiece and tools and the relationship between the motion direction of the workpiece and the tools are given. The table adopted from Standing's works (Standing 2006).

Table 1.1 Schematic representation of incremental deformation process with rotational motion (Standing 2006)

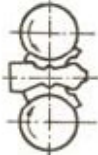
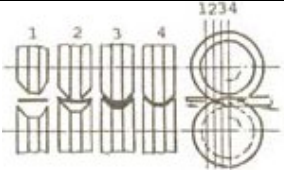
No	Name of Process	Schematic Diagram	Motion Types of Workpiece	Motion Types of Tools	Relation between motion direction of workpiece and tool
1	Roll Forging		—	○	⊥
2	Roll Forming		—	○	⊥

Table 1.1 (Continued) Schematic representation of incremental deformation process with rotational motion (Standing 2006)

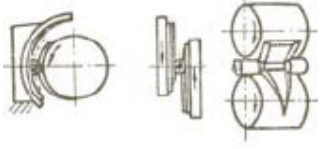
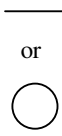
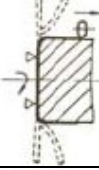
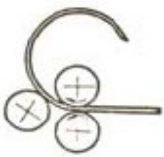
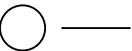
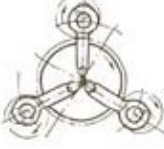
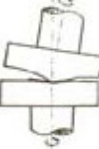
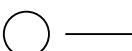
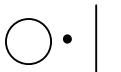
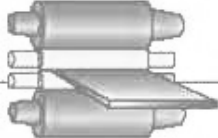
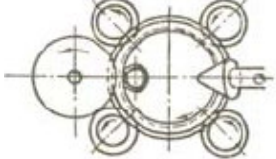
No	Name of Process	Schematic Diagram	Motion Types of Workpiece	Motion Types of Tools	Relation between motion direction of workpiece and tool
3	Cross Wedge Rolling				
4	Spinning				
5	Roll Bending				
6	Radial Forging				
7	Rotary Forging		stationary or 		
8	Rotary Swaging				

Table 1.1(Continued) Schematic representation of incremental deformation process with rotational motion (Standing 2006)

No	Name of Process	Schematic Diagram	Motion Types of Workpiece	Motion Types of Tools	Relation between motion direction of workpiece and tool
9	Flat /Profile Rolling		—	○	
10	Ring Rolling		○	○ •	

1.1.1 Roll Forging

In roll forging, a bar stock, round or flat is placed between die rollers which reduces the cross-section and increases the length to form parts such as axles, leaf springs etc. The rollers are rotated and workpiece has a translational motion perpendicular to rolling axis. Roll-forging can be used in both the pre-forming procedure and the finish forming procedure of forging process. It has remarkable advantages such as high productivity; high utilization rate of material, good labor condition, simple equipment structure, long life of the rolling dies and so on. In addition, due to the rational stream-line-distribution of metal fibers and uniformly distributed metallographic structure, roll-forging products exhibit better mechanical properties and reliability than those manufactured by die-forging or machining (Cai 2005). Roll forging techniques are utilized in production of many important parts such as front axles of automobiles, connecting rod of the diesel engine, taper leaf springs for vehicles, turbine blades, and ploughshares, etc. (Fu 2005, Cai 1994). The capacity of the equipment used in roll-forging is much

smaller than that is used in die-forging and because the roll-forming is a steady deformation process (Cai 1994), the high and big workshops and huge foundations are unnecessary, consequently, the investment in equipment and civil construction is saved significantly. The roll-forming technique makes it possible to manufacture large forging parts at lower-cost (Cai 2005).

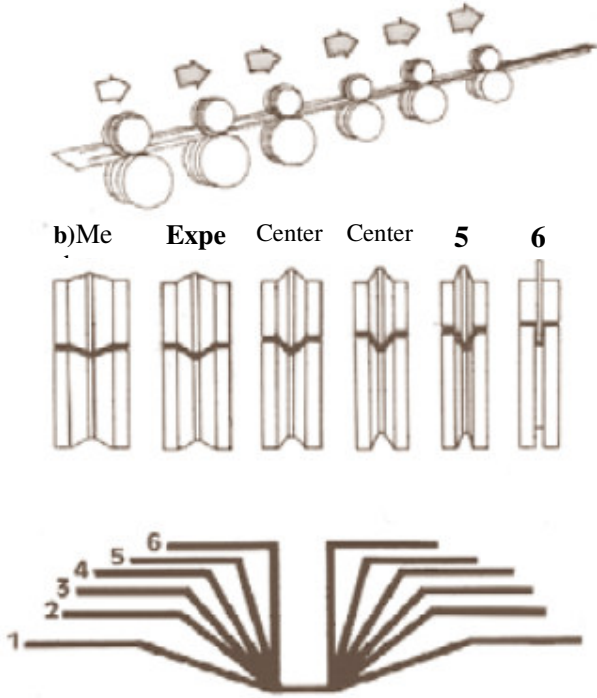


Figure 1.2 Flat strip of cold metal passes through several stages of bending (Lindgren 2005).

1.1.2 Roll Forming

In roll forming, a flat strip of sheet metal is incrementally formed through pairs of rolls without changing its thickness. The direction of motion of the strip is perpendicular to rotational axis. It is a progressive motion process of forming flat strip of cold metal through several stages of bending as shown in **Figure 1.2**. The metal strip is bent by passing through a series of rolls. The process adds both stiffness and strength to the roll formed material. The products of roll-forming

process are channels, gutters, siding, panels, frames, pipes and tubing, etc. The roll forming process is very robust; provide it is set up correctly. There are only small variations in the geometry of the produced profiles. The tolerances, spring-back, tearing and buckling of the strip are some of the critical parameters which have to be considered (Fu 1989). The benefit of the process in comparison to other metal forming processes is that auxiliary operations such as punch, welding, clenching etc. can be included and thus it is possible to produce profiles which are directly ready to use. The tools for a cold roll forming machines are expensive and therefore trial and errors when designing a machine are costly (Lindgren 2005).

1.1.3 Cross-Wedge Rolling

Cross-wedge rolling is a hot metal forming process in which a hot cylindrical billet is fed longitudinally through two identical wedge-shaped and counter-rotating rollers (*Figure 1.3*). The cross-wedge rolling is commonly performed with two flat tools or with wedge mounted rollers, but there is another method performed using three rollers on which wedges are mounted. There are two motion types for the billet; it rotates between the rollers or moves axially parallel to rolling axis. The billet is plastically deformed while rotating through the action of the dies (Piedrahita 2005). The final shape is obtained after one rotation of the rollers. Cross-wedge rolling processes are used mainly in the manufacturing of stepped shafts and axis. Automotive transmission shafts are generally produced with this method. It has many advantageous in terms of mechanical behavior of finished product and the precision obtained. However there are limited applications of the process in the industry. The main reason for this is related to the difficulties during design of tools. It is difficult to guarantee the stability of forming during process, the main process parameter concerning stability is the accuracy in the structural and geometrical design of the tools. The main type of defect occurs during the process is the internal cracks in the axial part of the workpiece. This defect is a result of the nature of the process. During the forming stage high stresses are induced and these stresses change in every quadrant of circle value and sign

appear. In other words these highly induced stresses are cyclic tensile (negative) and compressive (positive) stresses. The main risk result of this alternating stress is the occurrence of internal cracks in the workpiece due to low-cycle material fatigue. The application of hollowed charges in the place of full ones eliminates the risk of internal cracks, since the cracks are generally initiated in axial areas (Bartnicki 2005). The other types of defects are ovality or squeezing of workpiece between dies. The process parameters such as rotational speed, tooling geometry are vital in preventing this problem.

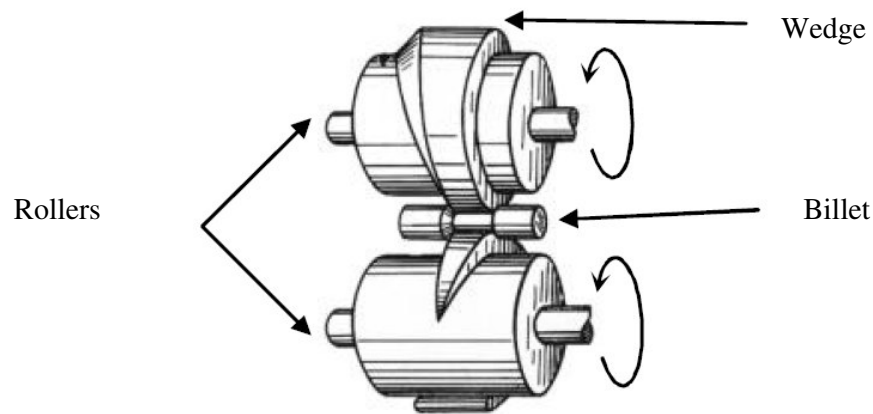


Figure 1.3 Cross wedge rolling with two wedge shaped tools mounted on rollers (Piedrahita 2005).

1.1.4 Spinning

Spinning is a process to form flat sheet metal blanks to hollow shapes by a simple tool called roller which exerts force incrementally to bend the flat metal onto a die or mandrel having the same surface geometry with the final product. The blanks are clamped rigidly against the mandrel by means of a tailstock and the shape of the mandrel bears the final profile of the desired product, **Figure 1.4** shows the schematic view of the process (Sebastiani 2006). During the process, both the

mandrel and blank are rotated while the spinning tool contacts the blank and progressively induces a change in its shape according to the profile of the mandrel. As the roller is applied locally on the workpiece, the total forming forces are reduced significantly compared to conventional press forming (Wong 2003). This does not only increase the possibilities in terms of large reductions and change in shape with less complex tooling, but also reduces the required load capacity and cost of the forming machine. All cold working metals can be spun; hot working is applied in exceptional cases. As it is for most cold metal forming processes, spun parts exhibit a fully worked, compacted grain structure as well as a characteristic surface finish. Moreover, high working rates induce a high level of cold work hardening, which leads to good fatigue strength and reduced notch sensitivity with the other mechanical properties mentioned above. The conventional spinning is carried out with only one spinning roller. In exceptional cases, however, this is not enough. When spinning heavy-gauge or high strength material it is better to use two rollers symmetrically positioned for better accuracy.

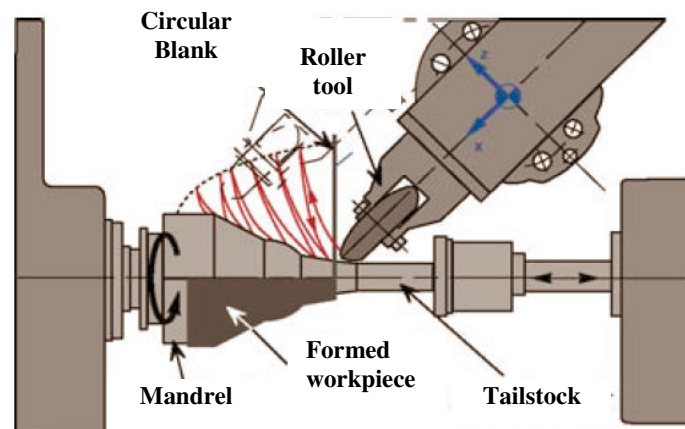


Figure 1.4 Setup of spinning process (Sebastiani 2006).

Spinning is a great means for manufacturing low cost rapid prototypes in metal, because it requires a minimum of time and money to produce parts. An average part can be spun in five to ten (5-10) minutes once one is familiar with the

process. Smooth parabolic curves (bell form) are ideal for spinning as the metal is comfortable deforming along a parabolic curve. The venturi form of velocity stacks for racing car carburetors are the common application of the spinning technology. There are several types of spinning; tube spinning and conical spinning etc. The tube spinning is an effective process for producing large thin-walled cylindrical workpieces and is used widely in industrial production. In tube spinning, where the tubular blank rotates with the mandrel whilst the roller undergoes axial feeding movement, the thickness reduces and the length increases. The roller touches the parts of the tubular blank, and plastic area is only in the region of the part around the contact zone, so that the deformation is restrained strongly by the surrounding metal. This method enhances the mechanical properties of the tubes, by providing fairly aligned grain-structure. Another type of spinning process is conical spinning. Conventional spinning is a convenient way to produce conical shapes from flat blank plates, however reducing thickness of a blank conical shape can also be employed. By this method, the mechanical properties of previously formed or machined conical shapes are enhanced and better accuracy in tolerances is obtained.

1.1.5 Roll Bending

Roll bending is a continuous form of three-point bending, where metal sheet can be bent to a desired curvature on forming rolls. Both tubes and cones can be produced by the machine. The conventional roll bending machines consist of three rollers of which rotational axis are parallel to direction of workpiece (***Figure 1.5a***), (Hu 2001). However, the process has a type employed with four-rollers. The four-roll plate bender consists of a pair of top and bottom rolls to pinch a bend plate (sequence 1, ***Figure 1.5b***), as well as a pair of left and right side rolls whose positions are suitably adjusted in a pre-set direction to achieve different finished curvature of bend plate (sequences 2 and 4, ***Figure 1.5b***)(Lin 2000). The continuous roll-bending process is executed by driving the top roll to convey the plate when either the left or right side roll is set to a required position. The most

important advantage of continuous four-roll plate bending process over the three roll ones is the flexibility of four-roll plate bending. This is a result of the main process parameter of, the roller leveling. By adding a new roller, the degree of leveling increases so the flexibility increases. In other words, operation modes of bending increases. The steady continuous roll-bending mode (sequences 4-6, **Figure. 1.5b**) is applied to achieve uniform circular configuration for the major portion of bend plate. The edge bending mode, which consists of two sub-modes: edge pre-bending mode (sequence 2, **Figure 1.5b**) and edge continuous roll-bending mode (sequence 3, Fig. 1.5b) has the function of reducing the length of non-circular edge zone as much as possible.

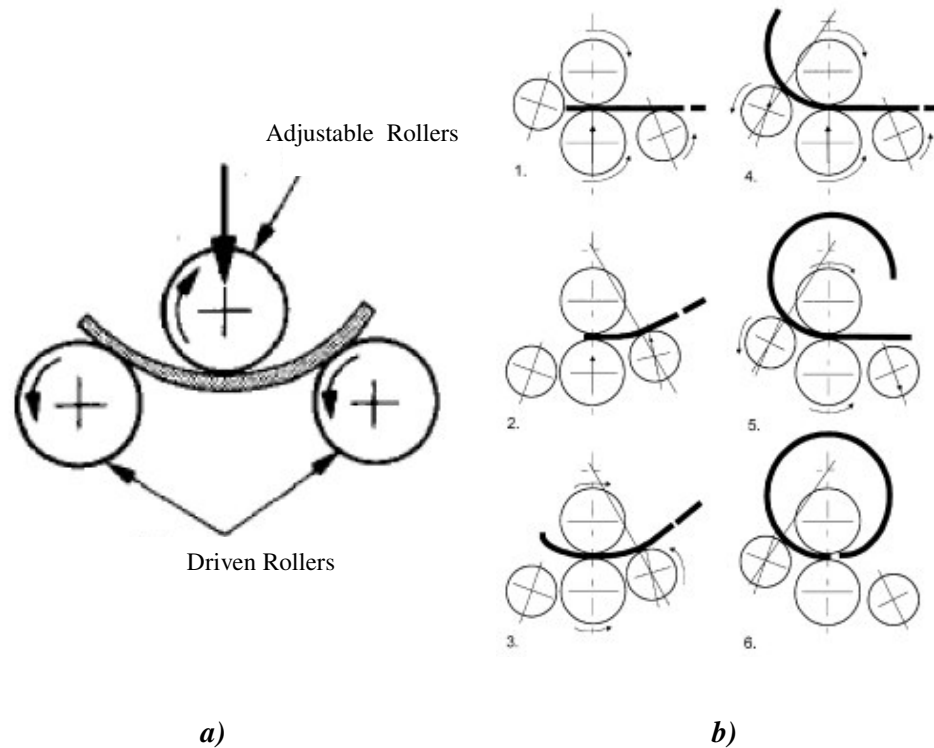


Figure 1.5 a) Three-roll bending process (Hu 2001) **b)**Operational sequence of four-roll thin plate bending (Lin 2000)

The main products of the roll bending processes are cylinders for pressure tanks; boilers; corrugated pipes; cones hoppers; regular and irregular shapes from structural sections for submarines, aircraft and nuclear reactors. The process can be performed using many materials such as carbon and alloy steels, aluminum alloys and titanium alloys (Hu 2001).

1.1.6 Radial Forging

Radial forging is a hot or cold forging process utilizing two or more radially moving anvils or dies, for producing solid or tubular components with or without profile. Radial forging is a cost-effective and material-saving forming process for reducing the cross-sections and creating internal profiles for tubes such as rifling of gun barrels. Usually a mandrel is used inside a tubular workpiece to create internal profile and/or size the internal diameter, but the process can also be performed without a mandrel when workpiece geometry does not allow utilizing it or the internal surface quality is not critical. Moreover, in stepped shafts and tubes, often there is a fillet connecting two different sections. If it is possible to produce that fillet during the forging process, the process could be more cost effective (Ghaei 2005). The advantages of radial forging are: smooth surface finish (by cold forging), considerable material or weight savings, preferred fiber structure, minimum notch effect, and increased material strength (Tszeng 1987).

Deformation in radial forging results from a large number of short stroke and high speed pressing operations by two or four hammer dies, while workpiece rotates and axially advances between the hammers after each blow. Dies are arranged radially around the workpiece, as shown in ***Figure 1.6*** (Ghaei 2005). Among parameters affecting the deformation pattern and quality of the forged product, the die shape is very important. Generally, the die shape is made of two sections, the inlet section, which forms a conical surface and the die land, which is cylindrical.

The forged components processed by radial forging will generally have higher residual stresses and undergo some deflections after forging due to the resultant high residual stresses, thus losing dimensional accuracy and having risk of fatigue.

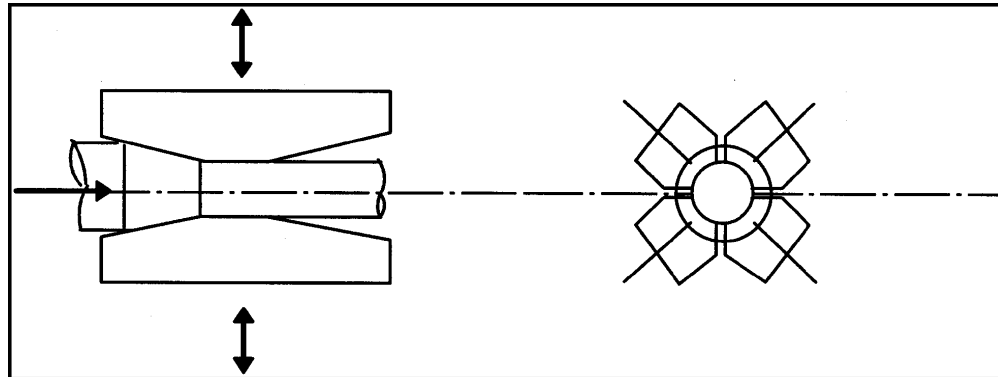


Figure 1.6 A schematic diagram showing the arrangement of the forging dies in the radial forging machine (Ghaei 2005).

There are few studies on parameters affecting the residual stress after radial forging process. In one of these studies, it is shown that the smaller the friction coefficient at the die-workpiece and mandrel workpiece interfaces results in the lower residual stress formation (Tszeng 1987). The smaller die angles make the residual stresses more compressive, hence the surface cracks can be prevented.

1.1.7 Rotary Forging/Orbital Forging

Rotary forging is an incremental bulk metal forming process in which workpiece is formed by a conical die rotating and creating spiral paths. The basic elements of rotary forging are shown in **Figure 1.7** (Standring 2006), the workpiece is fixed on a die sharing same axis, the conical die has a certain angle, and its vertex intersects with the workpiece axis which is called pivot point. The pivot point is an important parameter in machine design; all of the relative motions are defined about this point. There are three operation modes for rotary forging process as shown in **Figure 1.7**. In the first one, there is a rocking die tilted with nutation angle and it is nutated about pivot point. In the second one the die orbits

around the pivot point. In the last one the workpiece is rotated by the die it is positioned on to and the conical die rotates about its axis.

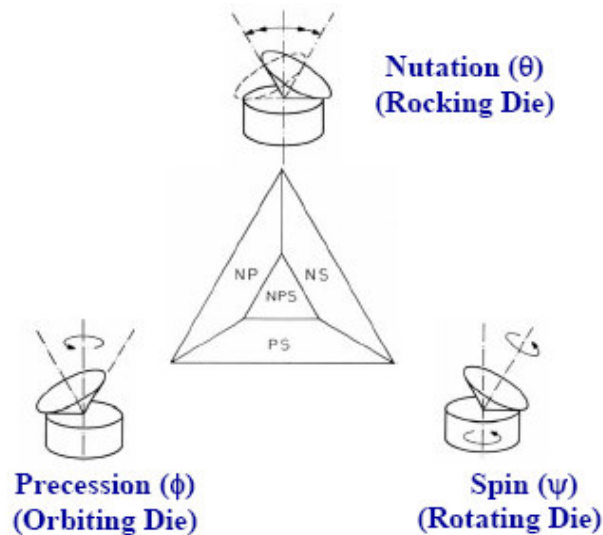


Figure 1.7 Types of rotary forging process (Standring 2006)

To date, rotary forging has been applied widely in practice, but many problems involved in this technology have not yet been solved. The most of the studies on this process is in this technology remains in experimental level (both numerical/physical). Due to the eccentric load of the process and the complicated contact contour and shape between the conical upper die and the workpiece, analytical studies are extremely complex. The related technical problems have to be solved by the trial-and-error method.

Every single step of deformation in other words every incremental stage of rotary forging process can be considered as an open-die forging process. Hence the tooling element is normally a conventional forging set-up where a workpiece is deformed within a standard die cavity. Standring stated the main concerns in design of tools (Standring 2001). The author defined the cavity design as the main

important parameter for stability. In rotary forging, the transition between each incremental stage is a potential phenomenon for occurrence unbalanced loading, hence the instability for any type of operation modes. The cavity must provide stability especially during the initial cycles of spin or precession. The friction in the cavity directly affects the stability, unlike conventional forging process, it is necessary to obtain high friction factors in the cavity to compensate unbalanced loading. In addition to instability, Standing also mentioned about twisting motion of fiber structure in material as an unwanted condition in the process (Standing 2001). This phenomenon can be related to factors like billet aspect ratio, height reduction, the tooling used, the feed rates, the lubrication etc. However, the most dominant parameter affecting degree of twisting motion is the feed rate and the total bite.

The rotary forging is generally used to produce difficult-to-obtain net shape geometries. There are many application areas in the automotive industry: in production of differential gearbox elements, power tools etc. (Bührer 2006).

1.1.8 Rotary Swaging

The German standard DIN 8583 described rotary swaging as "a free forming method for reducing cross sections of metal rod and tube material using two or more tool segments which partially or wholly surround the cross section to be reduced, acting simultaneously in the radial direction and in rotation relative to the workpiece". Simply, rotary swaging is an incremental cold forging method employed to produce axisymmetric parts. In rotary swaging, opposing die segments apply press forces in rapid sequence in the radial direction towards the workpiece axis. During each stroke high specific forming forces are generated. The die segments are guided in slots at the end of the shaft of the swaging head, as shown in **Figure 1.8** (Rathmann 2004). The return movement is derived from the centrifugal forces resulting from the rotation of the shaft. When the base jaw that drives the die is positioned between two pressure rollers, the die is in the open

position; when the highest point of the base jaw is centrally under one of the rollers the dies are closed. The roller cage has a continuous relative movement resulting from the rotation of the swaging shaft. The cam shape on the head of the base jaws is designed for smooth operation and minimum wear in this area.

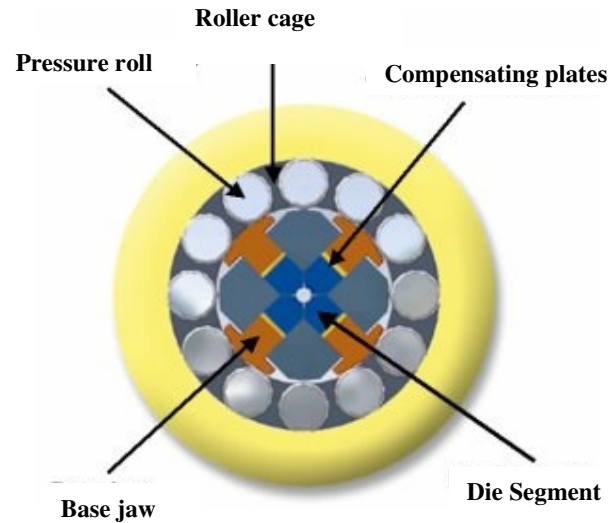


Figure 1.8 A simple representation of components in a conventional rotary swaging (Rathmann 2004).

As a result of radial feed on the workpiece, the final part has smaller diameter than the initial does, therefore this process is generally used in reducing the diameter and in tapering of the tubular or solid workpiece. The major benefits of the process are the repeatability and reliability in production. The process enables the production of parts with tight tolerances and a surface similar to metal cutting (Rathmann 2004). There are many application areas; the process is mostly used in automotive industry, and the process enables the flexible manufacturing of tubular parts which is quite important for lightweight considerations. At present, the correlation between the process-dominating parameters are still unknown, This leads to difficulties in design of rotary swaging machines as well as longer to longer try-out times if component geometries are changed.

1.1.9 Flat/Profile Rolling

The rolling process belongs to the compressive deformation processes, according to DIN 8583 and has been classified based on kinematics, tool geometry and workpiece geometry as shown in **Figure 1.9** (Lange 1985). Rolling can be defined as a compressive deformation process in which there is either a continuous or a stepwise deformation with one or more rotary tools. Additional tools such as mandrels, guide blocks, and support bars may also be used in the rolling process. The force transmission is achieved either by power driven rolls or by the workpiece transport. Based on kinematics, the rolling process can be classified as follows: longitudinal, cross and skewed. In longitudinal rolling the rolled workpiece moves through the rolling gap perpendicular to the axis of the rolls, without rotation about the workpiece axis. The cross rolling is defined as rotary movement of workpiece without any translational motion. In skewed rolling both translational and rotational movements of workpiece occurs. The tool geometry is another characteristic that can be used to classify the rolling process. The process of rolling where the rolls have along their contact surfaces either a cylindrical or a conical form in the rolling gap is termed flat rolling. If the contact surface of the rolls deviates from the cylindrical or conical form, the process is called profile rolling.

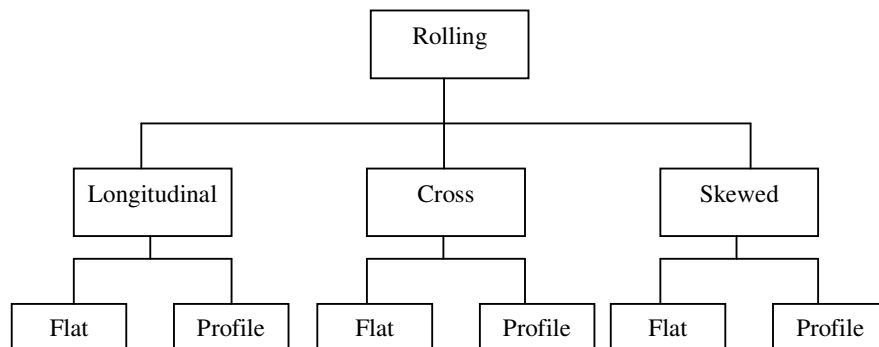


Figure 1.9 Kinematical classification of rolling process, applicable to both hollow and solid workpieces (Lange 1985)

The different rolls in a roll pass usually have the same section along the circumference. However, in reducer rolling operations, the rolls may have variable sections along their circumference. The process consists of two rollers with a certain gap away each other and billet entering through this gap, hence there are there are two groups of parameters. First for rollers: diameter, roller speed, rigidity constant and other material properties, coating. Second one for the billet: initial thickness, material properties and the dimension of the gap through which billet enters are the process parameters. Depending on these parameters many different type problem arises (Hosford 1993). Elastic flattening, due to the high pressure on the roller results in elastic deformation on the rollers and for full plastification, the friction hill can be observed. The friction hill results in elastic flattening. Another effect is roll bending occurs as a result of using wide rollers, using cambered shaped rollers solves this problem. Flat rolling is applicable to any type of formable metal under hot, warm, or cold metal forming conditions.

1.1.10 Ring Rolling

Ring rolling process being widely used in manufacturing ring-type mechanical parts, is mostly employed in bearing, aircraft and automobile industries. The process with has many advantages. There is a little material waste at end of process. The flow of the material tends to align the grains in circumferential direction, which potentially leads to superior fatigue characteristics; if it is cold-formed good surface finish and accuracy with in short production time. Process involves compression and rotation of a ring between two rolls, when the ring is compressed its thickness is reduced while it its diameter grows.

The basic elements of a ring rolling system are shown in ***Figure 1.10***. This system is same as the one used in ring rolling machine in ORS Bearing Company, Ankara.

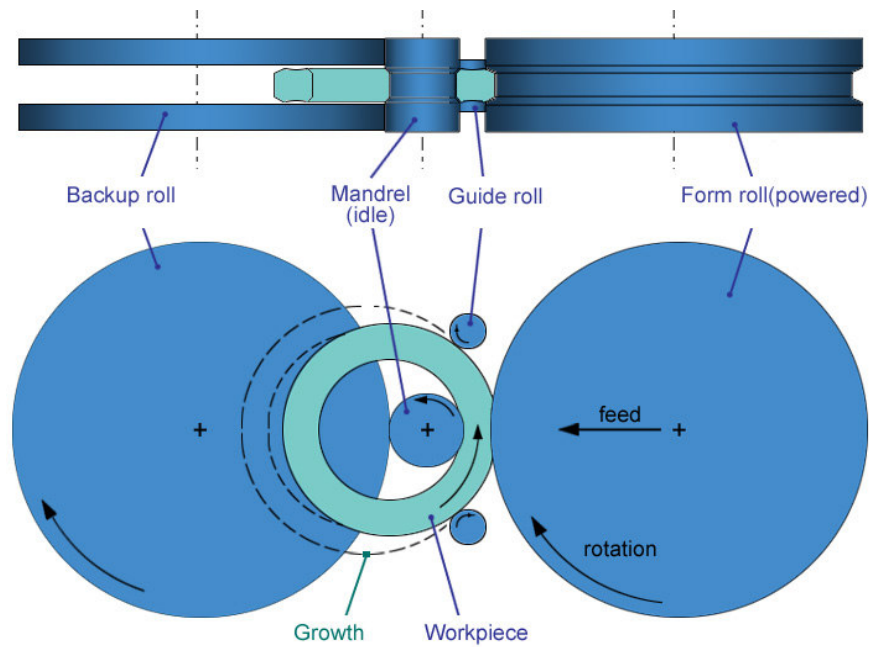


Figure 1.10 Schematic representation of the main parts of the cold ring rolling machine at ORS (Music 2005)

Detailed information about the machine is obtained from Music's thesis study (Music 2005). There is a hydraulic system which provides power to forming roll (also called as king roll), mandrel, guide rolls and the transfer arm. In general driving motor placed at the back of the forming roll powers the roll, rotating it while mandrel is idle, and stationary, supported by a pair of idle backup rolls, it can be vice versa in some cases. The forming roll is not only rotated but also given the required feed rate. The guide rolls, which are idle and moves according to ring diameter are used to stabilize the process and control the ovality of the ring by keeping the ring fixed during initial loading step and preventing oscillatory motion of the ring during rolling step. Loading step consists of transfer of the ring from the loading chute to the rolls. The ring is carried by a hydraulic powered arm, which picks up the ring and places it in between the rolls. As the arm picks up the ring and starts carrying it, forming roll and mandrel move back to allow for the

ring to be loaded. Next, mandrel moves in, passing through the ring, and holds it in place. Finally, guide rolls move in, only touching the ring.

The ring may subject to four main types of forming error. These have been described by Eruc as non-circularity, waviness, dishing (diametric taper) and conicity (Eruc 1992). Allwood et al. (Allwood 2005) in his review paper for ring rolling technology, mentioned about suggestions of Koppers on control procedures by measuring all ring-errors on-line and off-line. Non-circularity is reduced effectively via the radial force component exerted by the axial roll-structure (Koppers 1986). Dishing can be reduced by tilting the inner mandrel. Conical forms are difficult to correct. However, the synchronization of axial torques seems to be effective. Another type of error occurs at the corners of the ring cross section, is the fishtail-out error which is a result of inhomogeneous material spread in thickness direction. As the metal spreads inhomogeneously, a bulge is likely to appear at the edges of the unconstrained faces of a ring rolled in purely radial or axial conditions. This leads to excessive strain in the ring corners, which may cause burrs that can tear off or fold over, and may cause heating or fatigue cracking (Allwood 2005).

Ring rolling had been previously started to produce rings with rectangular cross-sections. However, the need of variable cross sections for many applications require extensive machining which leads to material waste and corruption in alignment of grains. Thus another technology was developed for this challenge; using profiled forming rollers or mandrel depending on the internal and external profile of rings. Despite it is superior to machining, the profile rolling has also disadvantages. Allwood et al. (2005) also mentioned the discussion of Marczinski et al. (1981) about the creation of internal cracks in profile rolling due to the inhomogeneous deformation over the cross-section. Another disadvantage is the difficulty in determining pre-form for complicated profiles, especially when multi-

stage production exists, stability problem occurs during loading and unloading conditions.

Ring rolling can be used for any ductile material, but is most commonly applied to steel products. It is also applied for aluminum and titanium alloys and polymers. There is even example of composite rings produced by ring rolling technology. The ring rolling can be employed under both hot and cold forming conditions. The temperature control is important for hot rolling, Allwood et al.(2005) also mentions about works of Henkel and Koppers on thermo-mechanical treatment of rings, their works show that temperature control and rolling-speed are important to obtain the desired microstructure in the ring.

Incremental Ring Rolling (Flexible)

The conventional ring rolling process has been employed for 150 years and it has been dealt analytically and experimentally for 40 years. However, in this time there have been relatively few developments to process itself (Allwood 2005). In literature, there are some works on alternative designs on process. Two of these include; using multiple mandrels to allow more continuous use of deformation process, increasing degree of freedom of some of the tools that more than one profile of ring can be made with same tool set. Stalker et al. has patented an alternative design, as the latter one, in which some of the axial rolls shifted axially during deformation to control the thin web of the wheel during wheel expansion. As mentioned conventional ring rolling is suitable for producing rings with rectangular cross-sections, and by using profiled forming rolls, variable cross sections can be obtained, however the metal cutting processes are still needed after rolling operations.

The flexible rolling process is still in developing stage, there are few works on going. It was dealt in a collaborative project among four universities; University of

Cambridge-UK, RWTH-Aachen, Germany, Atılım University-Turkey, and Middle East Technical University-Turkey. After a 1,5 years RWTH-Aachen group has started to work separately. The collaboration of other universities is ended by July 2006. The aim of the collaboration was to develop a flexible process that enables rolling wide range of profiles. This thesis study is a part of this collaborative work.

As mentioned before the ring rolling process is used in production of bearings. There are different types of bearings with rings having various inner and outer profiles. In **Figure 1.11** a classification of ring profiles of some bearings are given. The given ring profiles correspond to inner and outer rings of commonly used bearings available in the market. The profiles are classified into two groups: the symmetric and axisymmetric. The symmetric profiles have identical profiles when they are cut from mid axis, they are also axisymmetric. The axisymmetric profiles have unique shape through axial direction there is no repetition.

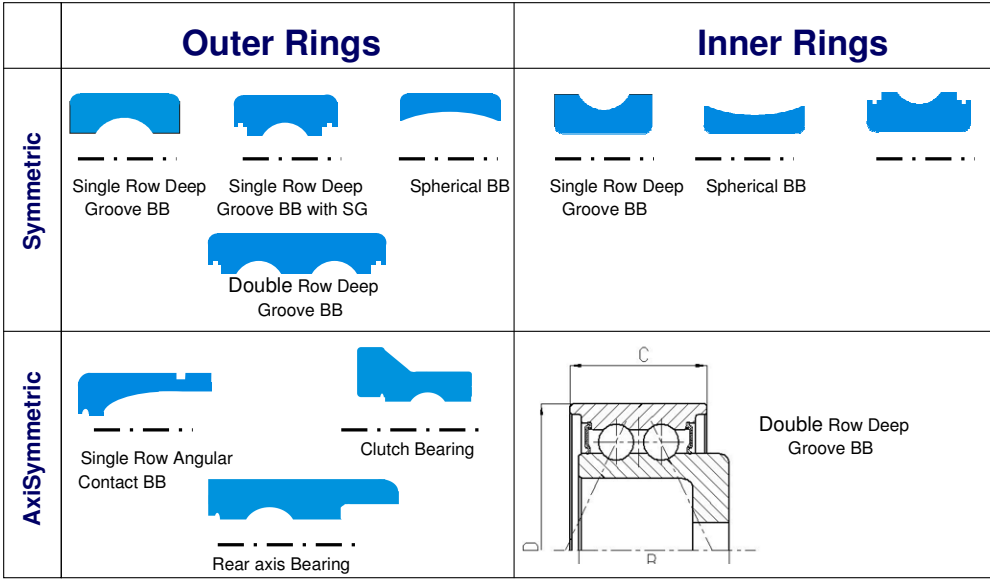


Figure 1.11 Classification of bearing profiles.

The classification of rings is important concern on developing the process. The classification helps to identify the similar constraints that should be provided during the process. For example, for the shapes with similar characteristics, tool penetration position or tool path determination algorithms can show similarities.

The desired process enables production of complex geometries. In many profiles there are difficult to form sections on which machining is costly to attain the desired tolerance range. In **Figure 1.12** the difficult points during production; such as re-entrant shapes, large width changes are shown.

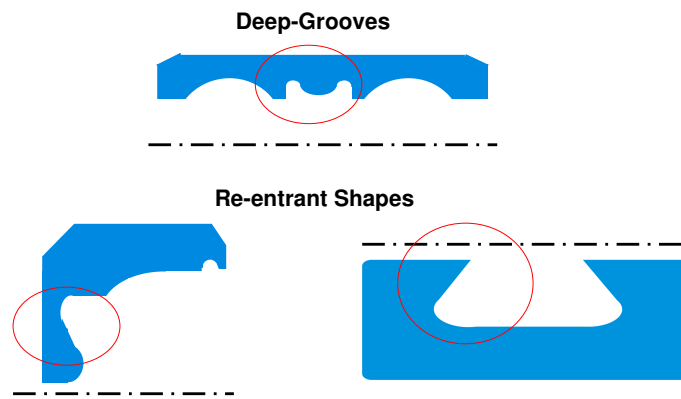


Figure 1.12 Examples of difficult to produce sections in bearings

The evolution of the process is based on near-net shape forming, or in other words reducing the machining. The reduction in machining operations enhances product quality, saves material and improves product quality (fatigue resistance).

The word flexibility does not refer to a single type of tooling and rolling conditions, however it refers to a machine or a system which can be adapted to any type of profile easily. The first step is the identification of similarities on the parts

and finds possible form of rolling conditions. Allwood et al. presented extensive forms of tooling and forming conditions in his periodic table (Allwood 2005). Each form of conditions can have superiorities to others or can have disadvantageous. In other point of view, one of those forms can be optimum process condition for one type of profile while being the worst case for completely different profile. In order to analyze the forms of the process Cambridge group has designed and built a flexible prototyping machine. The machine will be used to examine the possibility of deforming pre-formed rings with rectangular cross-section into any ring shape.

Ease of prototyping is another benefit of flexibility. Prototypes are important in testing the new design, or in improving existing designs. The flexibility in the process enables prototyping without the need of costly tools. Apart from prototyping machines, the feasibility of the process can be investigated by another method: the numerical modeling. The numerical modeling especially FE modeling has been utilized on incremental forming process over 30 years. Despite its attractiveness FE have some challenges on implementation; such as computation time which can make it infeasible. In order to make FE modeling feasible different simplifications and assumptions are considered.

In this study results of the numerical investigations on the incremental ring rolling process will be presented. After brief introduction to some of the incremental forming processes that have similar characteristics, the numerical studies on these processes will be presented in the Chapter 2. In this chapter, the difficulties in implementation and methods to simplify the modeling of the process will be investigated.

The process definition of the incremental ring rolling is broad. In Chapter 3, the process definition will be made in detail and it will be narrowed to a single type of process based on the inferences from the Chapter 2 and on the limitations of

physical experiments. In this chapter, the aim and scope of this study and need for the analysis will be explained in detail.

In Chapter 4, the results of the physical experiments performed by ORS b-Bearing Company will be presented. The experimental methods and measurement techniques will be explained briefly. The limitation on the experimentation will also be discussed.

In Chapter 5, the numerical models will be presented. As a prerequisite, the numerical models for conventional ring rolling will be introduced and studies on this process will be given. Then, the numerical investigations on the incremental ring rolling process that is based on the experience gained by modelling conventional rolling will be presented in detail. The challenges in modelling and the simplification methods will be discussed. The models are developed using commercial programs such as MSC Mentat and MSC Superform, although the programs have many special features for conventional metal forming processes to increase flexibility, user-subroutines is also needed. Therefore in this chapter some information about subroutines and the structure of the subroutine written here is explained.

In Chapter 6, the developed numerical models are discussed and validated with experimental results and compared within each other. The improvements on the models are reasoned and the results are interpreted. Furthermore, parameters that are specific to models are also investigated and presented.

In last two chapters, work done is summarized and recommendations regarding the further work presented respectively.

CHAPTER 2

LITERATURE SURVEY

In this chapter numerical modelling works related to incremental metal forming process having rotational motion features are presented. These processes have already been introduced in Chapter 1. The characteristics of the processes and their applications, some pitfalls have given briefly. However, the numerical modelling issues will be discussed in this chapter. The processes are examined in numerical modelling point of view, and in the most of the examined works, FEM is utilized and different approaches in effective utilization of FEM are discussed. Another subject mentioned in this chapter is the measurement techniques of residual stresses using X-Ray diffractometer, the theory of the X-Ray is explained. These techniques are used in residual stress measurements performed ORS Bearing Company, where the experiments for validating the numerical results were conducted.

As mentioned before, there are few works on flexible rolling and its modelling, however the characteristics of the process can be definitely examined by other incremental forming processes. Among all of these processes, the ring rolling process, which can be considered as a prerequisite for development of flexible rolling, is examined in detail and many different numerical modelling approaches presented in this chapter. There are many numerical models proposed for ring rolling. Both implicit and explicit commercial codes are used, and also there are codes specifically generated for ring rolling process available. Some of these codes are based on analytical models, having significant assumptions to discuss and some involves superposition of the characteristics of the process in to conventional solvers. The critical issues in modelling of ring rolling such as meshing, contact

problems, and computation time, are given and improvements on these topics are presented. For the ring rolling process, commonly used in production of bearings, there are some industrial contributions in terms of modelling, which are validated with experiments. These experiments are also discussed and validations are shown. Before examining the modelling works on incremental forming processes separately and discussing the ring rolling process in detail, the main characteristics of these processes and the challenges during modelling are given. The pitfalls and the current developments are also explained in this chapter.

2.1 General Characteristics of Incremental Forming Process for Numerical Modelling

As it is defined in the Chapter 1, incremental forming processes involves repeated action of tools on an area that is relatively small with respect to whole contact area of workpiece. Hence overall deformation zone is also small compare to the overall deformation domain (Tekkaya 2006). The plastic deformation zones are imbeded in elastic regions. These characteristics result in some challenges in numerical modeling. Just (2006) classified these challenges into six groups: challenges in kinematics, meshing and remeshing, contact and friction, computational costs, number of increments, material parameters. These challenges have direct relations within each other and they are mutually dependent. For example a challenge in kinematic, may cause contact problem, which needs larger number of increment hence longer computation times.

The *challenges in kinematics* are results of the nature of the processes. The challenge in kinematics refers to complexity of the motion of the tools or workpiece during process, such as orbital movement of tools or rotation of the deformable bodies. Modelling these types of motions such as an orbital movement is difficult (Bührer 2006) and yet can not be modelled using commercial software easily. Also complexity in kinematics causes creation of other types of challenges

such as difficulty in contact formation. Such as in the case of rotational motion of a deformable body, at each increment adequate number of nodes on the deformable body should contact with the tools in order to provide continuous rotational motion and to have accurate results (Just 2006). Furthermore, the incremental forming processes have rapidly changing contact conditions, it can be either rotational or translational motion, and cause instability. The instability results in inaccuracy in stress calculations.

The *challenges in meshing and remeshing* are also due to small contact zone and hence the deformation zone. The mesh size should be fine enough to provide adequate contact. Using coarse mesh negatively affects the accuracy of the model, at the same time; convergences can not be satisfied at the large strains. Another problem with coarse mesh is the under filling condition for complex geometries in the die, such as in flow forming of a threaded deformable body (Fritsche 2006). The refinement in the mesh should be reasonable. The finer mesh results in the longer computational time. In addition to direct effect on computation time, making mesh extremely fine causes instability especially in regions of large strain (Music 2005). The calculated strain values are generally greater than it should be; hence the stress calculations are useless. There are many different effective approaches for meshing. Most of them are process dependent; they can be utilized for few types of incremental problems, but not general solutions for all other types. One of these methods is using hybrid mesh -proposed by Hu et al.(1994) incorporating a graded computational mesh and a separate. Another one is non-uniform meshing, used by Music et al. (Music 2005) in ring rolling; it involves meshing the deformable body according to nature of process. These examples will be explained in detail in next sections. Remeshing is vital and generally used tool for modeling incremental processes. However, remeshing is not a remedy for modeling, as large strains induced on localized areas, mesh gets finer which makes computation time longer, hence makes remeshing inefficient. Adaptive remeshing techniques are developed such as non-uniform meshing proposed by FEMUTECH

Company, it involves remeshing the regions in the deformation zone and keeping other regions coarser.

The *challenges in contact and friction* generally arise because of the kinematics of the process. The contact should be sustained according to the constraint: rapidly changing motion. The step size should be selected properly. Contact forms and releases with each deformation cycle, and this deformation cycle should be incremented with sufficient number of increments. Another concern is the friction, determining friction coefficient can be performed by standard test, however friction coefficient can differ during a process or different friction laws can be needed during process (Domani 2006). This is again result of kinematics of the process, the relative motion between tools and workpiece is generally friction dependent.

The *number of increments* affects the computation time severely. Each increment can be defined as single deformation step in cyclic nature of the process. At each increment contact forms and releases, and this needs large number of calculations. Since the overall plastic deformation is achieved in small steps, ideally many deformation steps are necessary. There are approaches for reducing the number of increments, such as similarity approach proposed by Fritsche (2006). This approach is based on similarity rule, and according to studies, each increment has similar deformation histories with the others. All processes can be predicted using periodic functions.

The *material models* can be challenging during modelling. During incremental processes the deformation zone is imbedded in elastic material regions. Furthermore, the elastic neighbourhood of the deformation zone makes the elastic-plastic material laws ideally inevitable (Tekkaya 2006). There is another concern about the material law, which is objected by Meyer et al. (2006). The incremental forming processes are composed of loading and unloading cycles. The material

exposure at a cyclic incremental forming process, the shape changes are not only achieved by monotonic loading but also by alternative loading. Because of this nature simple monotonic constitutive material laws can not be applied to these processes. Another important point is to the hardening characteristics following cyclic paths which should be superimposed to numerical models.

In addition to these challenges, one important characteristic of incremental forming process that makes modelling harder is that they are unsteady processes. Simple steady-state solutions that can be applied to conventional forming processes such as plane rolling are useless (Erunc 1992). This unsteady behaviour causes many problems, such as instability, convergence problems and etc.

2.2 Numerical Modelling of Incremental Forming Processes (IFP)

In this section numerical modelling works on examples for the IFPs are presented.

2.2.1 Roll Forging

There are few numerical studies on roll forging process (Karacaovali 2005). There are some examples of utilization of numerical methods and computer aided design. Biswas and Knight (1976) have developed a computer program for roll-forging die design, which embodies formulated design rules for pre-forms that based on experiences. Another CAD software (VeraCAD) has been developed in Eratz Company by using empirically based forging rules. This software automatically calculates the mass distribution of part and gives optimum number of dies and operations. One of the recent numerical studies on roll-forging is presented by Karacaovali (2005). He modeled 4 staged roll-forging operations in commercial software, MSC. Superform. At each stage, the billet has been rotated by 90° about its centerline. He worked on two models; the first one is a 3D quarter model and in the second one is a full model. The accuracy of the model -in terms of the

geometry- was tested by experiments, and it is found out that the full model agreed with experiments better than it is in the quarter.

2.2.2 Roll Forming (RF)

There are various numerical studies on roll forming. The process is complicated, in terms of kinematics and in many researches the FE models are simplified and they are based on three approaches. The first two approaches are based on simulating strip rolling without friction, while the third approach is based on simulating strip bending between the forming stands. In first approach the initial deformation shape is obtained by pressing the deformed rolls towards the undeformed strip, followed by pulling the strip longitudinally from the strip leading edge through the roll gaps of the forming stands (Senanayaka 1994, Heislitz 1996, Alsamhan 2004).

Kim et al.(1994) presented a numerical tool based on FE called TASKS (Three-dimensional Analysis of Shape forming in Kinematically Steady-state condition). In this program the workpiece is divided by several cross-sections in the rolling direction and the deformed shape at each cross-section is checked with plane strain simulation. The 3D mesh is constructed using sixth order polynomials with undetermined coefficients as streamlines which are calculated by minimizing energy consumed. The shapes and the thickness distributions of strip after roll forming were examined by comparing computation results with experiment and accuracy was satisfying (Kim 1994). Alsamhan et al.(2004) developed FE models to simulated CRF process and predict membrane strain distribution. The model was used to simulate CRF of a trapezoidal channel section, and the simulation results were compared to published experiments. The computation time is decreased by using dual meshes and real time remeshing technique.

Peng et al.(2005) presented a solid shell element model and introduced a co-rotational formulation into the dynamic explicit elastic-plastic finite element method, and a stage of roll forming process is simulated. A co-rotational

formulation is adopted in the stress calculation to remove the effect of rigid-body movement. Deformation gradient F from time t to $t+dt$ can be decomposed as;

$$F = R \cdot U \quad (2.1)$$

where R is the rotation tensor, U is the right stretch tensor. U can be decomposed into the elastic part and the plastic part, then the logarithmic strain increment in the co-rotational configuration is defined as

$$\Delta \hat{\epsilon} = \ln U = \ln(U^e \cdot U^p) = \ln U^e + \ln U^p = \Delta \hat{\epsilon}^e + \Delta \hat{\epsilon}^p \quad (2.2)$$

The constitutive equation in the co-rotational configuration is expressed as

$$\hat{\sigma} = C : \hat{\epsilon}^e = C : (\hat{\epsilon}_o^e + \Delta \hat{\epsilon}) \quad (2.3)$$

where $\hat{\epsilon}^e$ is the total elastic strain in the reference configurations; $\hat{\sigma}$ is the Cauchy stress in the co-rotational configuration, and C is the elasticity tensor. The solid shell element is analogous to the degenerated shell element, but incorporates only displacement degrees of freedom. Using this approach reduced the computation time without sacrificing from accuracy (Peng 2005).

2.2.3 Cross-Wedge Rolling (CWR)

The CWR process has not yet been studied sufficiently, and this is a serious disadvantage for potential industrial applications of this process. Pater (1999) presented a model of CWR process including upsetting, which grounds on upper-bound method. In this model, individual layers of strain area simulated and the state of strain in any layer of the forming zone can be simulated by rotary compression analysis for a plane state of strain, and perfectly rigid plastic material is assumed. With the proposed model, it is possible to determine the rolling force

distributions the material/tool contact surface and the rolling radius during the forming process to calculate the forging dimensions after rolling and to check the process stability conditions (Pater 1999). Another work presented by Pater (2006) is the thermo-mechanical model of CWR using MARC/AutoForge. The kinematics of the process is complex due to non-linear strokes of the tool; hence the simulation should be performed in three-dimensional stress state. This leads to longer computation times and some simplifications imposed into model, such as using rigid tools, assuming isothermal conditions, utilizing symmetry and analyzing the rolling process for simple forged parts. The model forecasts the strain state, calculation of loads values as well as anticipating of phenomena limiting the cross wedge rolling process stability (ovalization and necking conditions can be determined depending on forming angle) (Pater 2006).

Bartnicki and Pater (2005) modeled forming of hollowed shafts with the use of three rolls CWR, and utilized from commercial FE packages, MSC. Superform. In this work they used three dimensional FE model to analyze the stability of the three rolls CWR process of hollow shafts and determining phenomena disturbing the proper course of forming. The model consists of rotary rigid tools and the charge modeled by eight-noded hexagonal elements, because of high deformity in calculations and the remeshing option is available in the software. The remeshing is based on equivalent strain criteria and in case of small holes with small internal diameter, remeshing causes many problems of numerical character.

Fang et al.(2002) presented a model for two-roll CWR using static implicit FEM program, DEFORM-3D, authors utilized the dynamic adaptive remeshing technology for tetrahedral solid elements. The problem with the implicit code that it does not converge easily, hence the solution time increases. However the authors used the enhancements in DEFORM 3D, such as using new method of multiple processors, in which automatic switching between two different deformation solvers (sparse and conjugate gradient solvers) has also implemented.

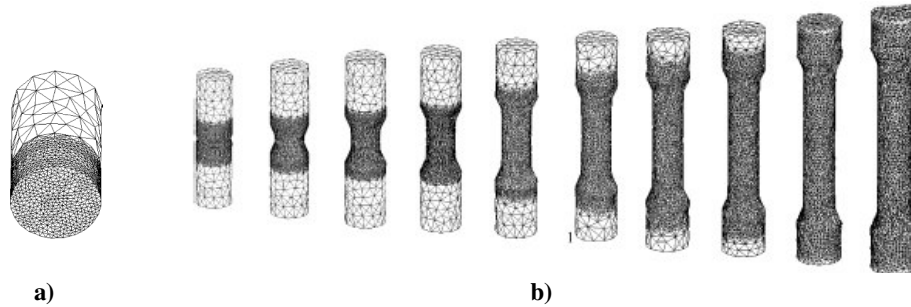


Figure 2.1 a) Non-uniform Mesh for symmetrical model b) deformation sequences for the process (Fang 2002)

The half of the workpiece is modeled using symmetry, with 14235 tetrahedral elements and non-uniform mesh is used (**Figure 2.1a**) Initial deformation regions have finer mesh than the other parts at the first steps, but at final steps using remeshing the mesh topology becomes almost uniform (**Figure 2.1b**).

2.2.4 Spinning

Spinning has one of the most difficultly modelled processes, with high rotational speed of workpiece and small deformation zone which changes more rapidly than the other incremental processes. The finite element modelling of spinning enables the study of parameter that cannot be measured directly; such as transient stresses and strains that occur during (Quigley 2002).

There are similar characteristics of the models, available in the literature. In most of the models mesh is selected fine enough to allow continuity of contact as the nodal forces transfer from one element to the next as the elements pass under the roller. However using extremely fine mesh results in impossibly large computation time. Also using regular meshing of a circular blank will lead to small triangular elements in the center. Several meshing strategies was investigated by Sebastani et al.(2006) and is shown in **Figure 2.2**. Mesh A, the irregular element distribution, is

well suited for deep-drawing simulations it results in local stress peaks due to an inhomogeneous mass distribution in the rotating blank. Mesh B, which is also seen in Quigley's model (2002), neglects the center part of the blank. However, the outer mesh exceeds the aspect ratio requirement of 2/1. The Mesh C, yields better results but inhomogeneous mass distribution in the forming zone, which is not suitable for explicit codes. Mesh D, the partitioned mesh satisfies all demands on mesh quality at the expense of an enlarged model size. This mesh is a compromise of the constraints of the aspect ratio and the homogeneous element distribution and consists of three concentric partitions.

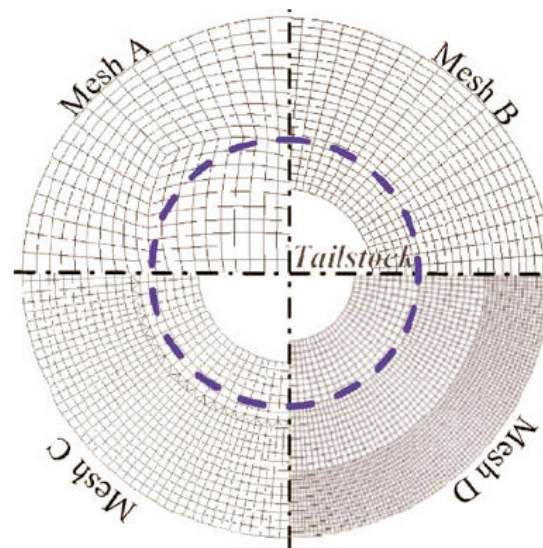


Figure 2.2 Meshing strategies for spinning of a circular blank(Sebastiani, 2006).

Apart from the mesh, the time increment is considered to be important, in terms of the speed of rotation of the workpiece or disk. It can be selected small that each nodes spends many increments as approaching the roller but computation time increases, since number of contact occurrence increases. Quigley et al.(2002) stated three or four increments per element entering the contact region provide a

reasonable compromise. Another characteristic of the models is that only deformable body is the workpiece (Quigley 2002, Xu 2005 and Sebastiani 2006) In most of the mentioned researches, the commercial FEM software with implicit integration schemes is used. However there are few examples such as Sebastiani et al.(2006) presented in which explicit software is used to determine the dynamic effects occurred by the rotation of the blank workpiece.

The spinning, being a cold forming process with high deformation rates, can be modeled using elastic-plastic material model. Yang et al.(2005) presented a 3D finite element model for backward tube spinning process which reflects spinning deformation behavior completely. The simulation catches the complex stress and strain distribution; compressive stress state at contact zones, local tensile stresses around the contact zones on both inner and outer surfaces on the tube. There are models such as presented by Xu et al. (2005) in which rigid plastic material model is selected. This model also predicts the stress strain distribution successfully, however there is no significant comparison with experiments, only characteristics of backward and forward spinning are compared, in this work.

2.2.5 Roll Bending

Although the roll-bending process is one of the very commonly used forming processes in production, there are several problems that prevent this process from being used more widely. For instance; unloading large-size closing parts is difficult; forming super-wide parts is difficult; forming tools are too large and large machine costs are too high. A major problem is the roll inflection caused by the loading force, which seriously affects the forming precision of bending parts (Hu 2001).

These problems also affects the finite element modelling, there are few examples for finite element simulation of the roll bending process. One of the presented by

Hu et al.(2001). In this work a new roll-bending model is proposed which improves upon conventional roll-bending processes. The proposed model not only resolves some inadequacies of conventional roll-bending process, but allows more flexibility in the formation of large bending parts. The authors dealt with upper-bound and lower-bound solutions and also used finite element method to compare the results. The authors used commercial software and used an elastic-plastic material model. The 3D model is assumed to be symmetric and half of the workpiece is analyzed and the results validated with the lower-bound and the upper-bound solutions.

The experience dependency is another problem, the accuracy of roll bending with multiple rolls processes generally depends on the experience of the operator, some reasoning algorithm or a feedback control should be introduced to model. This type of finite element model was proposed by Yang et al(1994). In this model, the motion of rolls for forming a plate into a desired curvature distribution in three roll bending is determined by controlled FEM simulation. In the controlled FEM simulation, the movement of the rolls is adjusted by a feedback control to approach the desired curvature distribution. This movement is iteratively modified on the basis of the fuzzy reasoning by using the calculated curvature distribution during bending in each deformation step (Yang 1994).

2.2.6 Radial Forging

The radial forged part such as hollow shafts are generally used in automobile and aircraft industries, hence residual stresses and the dimensional accuracy are important to be investigated. Tszeng (1987) conducted a study on the residual stresses in the radial forging process and used an axi-symmetric model of the rigid-plastic FEM code ALPID in the simulation of the loading process, followed by an elastic program for the unloading process. In this model dies are modeled as rigid bodies and effect of friction factors on residual stress investigated. In this

code elastic strains are neglected and the stresses below the yield stress not known hence the springback effect could not be predicted.

Jang et al.(1998) worked on stress development in axi-symmetric products processed by radial forging using a 3D non-linear finite element. In this study a 3D FEM model was developed to calculate the residual stresses in a product resulting from the radial forging process. Since the friction factor has important role in determining the forming forces and strain distribution in the forged parts, the lubrication layer in the real process should be reflected properly. In order to handle the contact and friction between the workpiece and the die and the workpiece and the mandrel, a spring-stiffness relationship between two contact areas was established, which is a penalty method. The spring will deflect an amount Δ such that *Eqn. 2.4* is satisfied.

$$F_N = K_s \Delta \quad (2.4)$$

where K_s is the spring stiffness and F_n is the normal force between the contact surfaces. This model has also some assumptions that are generally used within modeling of other incremental forming processes; such as neglecting the deformations in the tools and defining them as rigid surfaces, assuming isothermal conditions, and considering elastic plastic behavior for the workpiece. In addition to these general assumptions, the rotational feed is neglected and the clearance between hammer and the workpiece is neglected.

Another interesting work was presented by Ghaei et al. (2006). In this work, an axi-symmetric model is built using commercial finite element code ABAQUS/Explicit, to analyze the effects of the die shape in the cross-section area on deformation. Additionally, in order to investigate the accuracy of the axi-symmetric model of the radial forging, the results of 3D FEM model were compared with those obtained by axisymmetric FEM model. It is shown that

generally, tubular parts in radial forging are not deformed axisymmetrically and therefore a 3D model is needed to model the process. In this model similar assumptions with previous one are used.

2.2.7 Rotary Forging/Orbital Forging

In spite of the many researchers on incremental rotary forging processes, the finite element analyses are not so much applied to solving the actual rotary forging problems in the related companies; as expected because of the long computation time (Moon 2005). The kinematics of the process makes it difficult to model; the relative movement between workpiece and the conical roller is a spiral feed (Wang 1997). Moon et al.(2005) in his recent work, presented various numerical schemes used for a rigid-plastic finite element method to reduce computational time and minimize volume change during simulation of a rotary forging process. The first scheme is the approximation; the strain rate and the smoothing function (a function reflecting the effect of relative velocity between tool and material on friction) are calculated using the velocity field of the previous time step. This reduces the number of iterations significantly. The second scheme is for controlling the volume change. This model reduced the computation time by one tenth of the computational time consumed in the conventional approaches (Moon 2005).

Munshi et al.(2005) used 3D FEM simulation technique for optimizing parameters in orbital forming of spindle and inner ring assembly investigated by a) measuring the computation time and b) comparing the results of simulations with experiments. Commercial software, DEFORM 3D was used. In this model, workpiece is assumed to be rigid plastic and the tools are modeled as rigid bodies. Rigid Super Element (RSE), which is a recently developed feature of DEFORM 3D, is used. In this method, the equations associated with the nodes in the non-deforming zone are reduced to six representing the rigid body motion. These equations are coupled and solved simultaneously with the equations in the

deforming zones. Therefore, the number of equations and solution time can be reduced significantly. This method decreases the computation time by %91.

Another rigid-plastic model is presented by Kawabe et al. (2003). Also, in this model, the tools are handled as rigid bodies and their shapes are expressed by triangle planes. The relative motion between the die and the workpiece is difficult to model. In this model the upper die is modeled with triangular plane elements and the motion of die is expressed by rotational coordinates of nodal points in these elements. This model is capable of detecting mushroom deformation easily.

2.2.8 Rotary Swaging

There is only one recent work on rotary swaging found, which is still on going in Institute of Production Engineering and Forming Machines in Darmstadt University and Technology. As the other rotary incremental processes, rotary swaging is also difficult to model because of the similar concerns; such as complex kinematics, requirement of 3D modeling, large number of elements, cyclic steps. Rathmann et. al (2004) developed a 3D model using MSC Marc and embedded a subroutine in to the program. In this model, the tools are modeled as rigid bodies, and the workpiece as deformable body with 8-node isoparametric 3D hexahedrons. The workpiece is modeled quarterly to reduce the number of elements, hence the computation time without sacrificing too much from the accuracy (0.04%). In this work they intended to create a technology processor to simplify the input of all necessary data: such as tool parameters, process parameters, to carry out the simulation in background and also to evaluate and represent the results for forces, strains and stress and geometric parameters. It is aimed to make non-FEA user, utilize from FEM without any knowledge on FEM.

2.2.9 Flat/Profile Rolling

The simulation of flat rolling has been studied over 20 years. There are many researches on this process, since this is one of the most commonly used process in the metal forming business, and its kinematics is easier than the others.

The number of elements is large and three dimensional modeling is not practical to decrease the number of variables in the model. Marcal et al.(1978) used line elements for the computation of side spread in plate rolling, however it is not accurate enough for applications

Another simplified model was presented by Li and Kobayashi (1982), in which plain strain assumption is used. This model gives good prediction for large and wide plates however 2D method could not give good predictions for cross section shape of general sections, since it was effectively modeling a 2D ‘forging’ problem. Kobayashi et al. also presented a model using simplified three dimensional elements in which the degree of freedom is reduced by using simplified three dimensional elements.

Mori et al. (1984) presented one of the first models, in which he simulated three dimensional deformations in flat rolling on the basis of the rigid-plastic finite-element method. To analyze the steady-state deformation in rolling in a short computing time, he developed an iterative approach in which from the velocity field, stream lines are constructed and the thickness distribution of the plate is estimated by integrating the velocity of the surface along the stream lines and new finite-element mesh is generated by assuming the stream lines to be element boundaries.

Kim et al.(1990) developed a three-dimensional code for the finite element analysis of plate rolling was, including simulation capabilities of multi-pass

rolling, workpiece rotation between passes, and roll motions of rotation and translation. The program was used for simulation of two-pass rolling under several pass schedules of roll gap control.

Wen et al.(1998) proposed a method that solves the problem inherited in the conventional 2D method by approximating the rolling to an equivalent ‘ring expansion’: the 3D-to axis approximation. This allows realistic elongation to be introduced in the model easily, as displacement boundary conditions. The *Figure 2.3* shows the difference between rolling and the forging apparently.

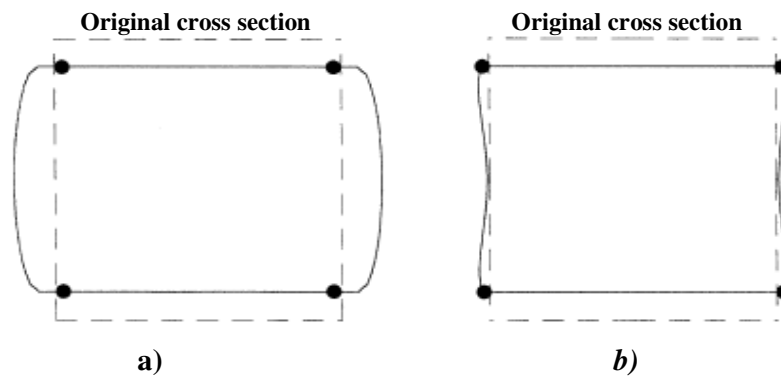


Figure 2.3 Representation of a forged (a) and rolled (b) cross section from the same original dimensions and reduction (Wen 1998)

2.2.10 Ring Rolling

It is mentioned before that the ring rolling process is dealt intensively since it is considered as a prerequisite for flexible rolling process. As the other incremental rotary forming processes, FE simulation of ring rolling is also challenging and the computation time is the one of the major pitfall in utilization of FEM, because of many reasons: its kinematics which involves large number of rotation resulting constantly changing contact conditions in the bite region of the ring, and many

incremental steps, its non-steady behavior, its 3D modeling requirement for the profiled rolling.

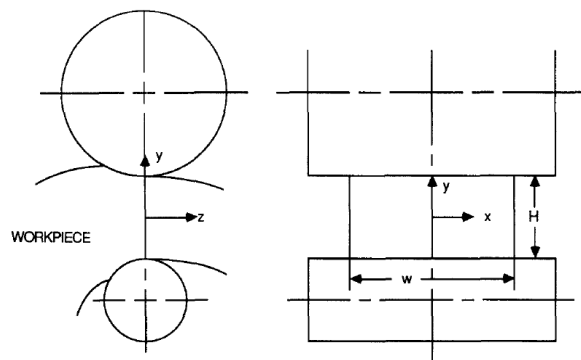
It is obvious that computation time should be shortened to utilize from FEM, there are numerous approaches with this aim in the literature. These approaches can be grouped into two groups: physical simplifications on the process itself and improvements on the modeling. There are various methods using the simplification of the process approach presented, such as plain strain assumption -for non-profiled rolling-, axisymmetric assumption, and partial model assumption. There are also wide ranges of methods on modeling which are solved either using implicit and explicit integration schemes; such as application of different element technologies, innovative meshing and remeshing algorithms, specific to process.

2.2.10.1 Physical simplifications

One of the basic simplifications on the process is the assumption of two-dimensional deformation. Yang et al.(1988), in his early works suggested a 2D implicit rigid plastic FE model. In this work, plain strain assumption that is used in modeling of flat rolling process is considered. Unlike in conventional flat rolling of sheets, the mandrel has smaller diameter, idle and advancing incrementally and continuously toward a form roll of larger diameter in ring rolling process. Hence the thickness change through the bite region has different profile. Yang et.al(1988) proposed a formula for the thickness at exit of the bite region in which the idle rotation of the mandrel is taken into account by introducing it as an unknown. The rigid plastic material model is assumed and the computations are carried out under conditions of steady-state plane strain.

Another approach presented by Tszeng and Altan(1991): pseudo plane strain, in which three-dimensional deformation is decomposed mathematically into a two-dimensional plane flow and a one-dimensional out-plane flow (in rolling

direction). The coordinate system used is shown in the **Figure 2.4** which also represents the approach clearly. For each radial cross-section the coordinate system is so placed that the x-axis is parallel to the roll axes (axial direction), the y-axis is pointed toward the form roll (radial direction), and the z-axis is in the rolling direction (the angular or longitudinal direction). Every point on the ring has three velocity components u_x, u_y, u_z respectively.



(w : width of the ring and H : is the thickness of the ring)

Figure 2.4 The coordinate system for the analysis and the geometrical configurations of rectangular plain ring rolling. (Tszeng and Altan 1991)

The main assumption, which makes the process pseudo-plain strain or in other words defines the out-plane flows, is the following equation.

$$u_z = \left(1 + \frac{y}{R}\right)u_o \tag{2.5}$$

where $u_o = u_z|_{y=0}$ is the velocity at the center of the cross section and R is the instantaneous center radius of the ring at $y=0$, as y increases, the ring diameter

increases hence R changes. The out-plane strain rates $\dot{\epsilon}_{xx}$, $\dot{\epsilon}_{yy}$, $\dot{\epsilon}_{zz}$ are calculated using u_z and imposed into FEM formulation.

The results of this model was compared with; experimental data presented by Mamalis et al. (1976) and theoretical calculations by Yanagimoto and Kiuchi (1990), and three dimensional RING program (Kim 1990). Results for the axial spread of a plain rectangular ring are compared in the following **Figure 2.5**. It is observed that the results strongly agree with the theoretical values; however the calculated results are overestimated when compared to experimental results.

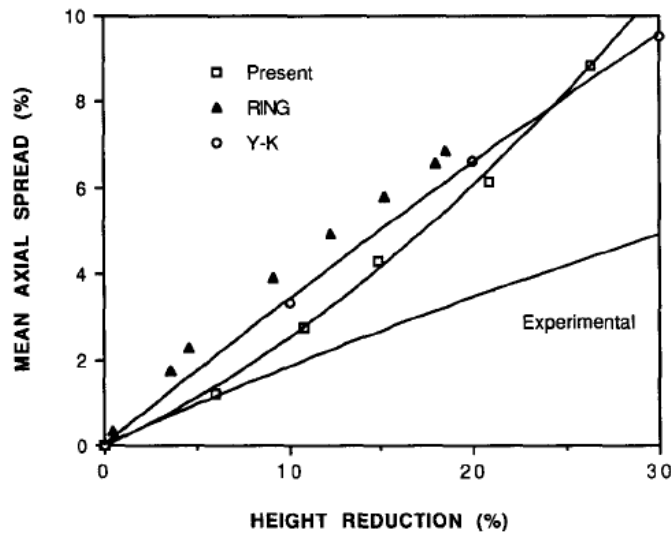


Figure 2.5 Variation of mean axial spread $\Delta w/w_0$ with height reduction $\Delta H/H_0$ for plain ring rolling (Tszeng and Altan 1991).

Another method on modeling simplifications is proposed by Joun et al.(1998). The proposed work is a 2D implicit rigid-plastic FE model. This model is based on the assumption of axisymmetry. The ring is assumed to be formed by an infinite

number of rolls, which is similar to deformation behavior of an axisymmetric forging process as shown in *Figure 2.6*.

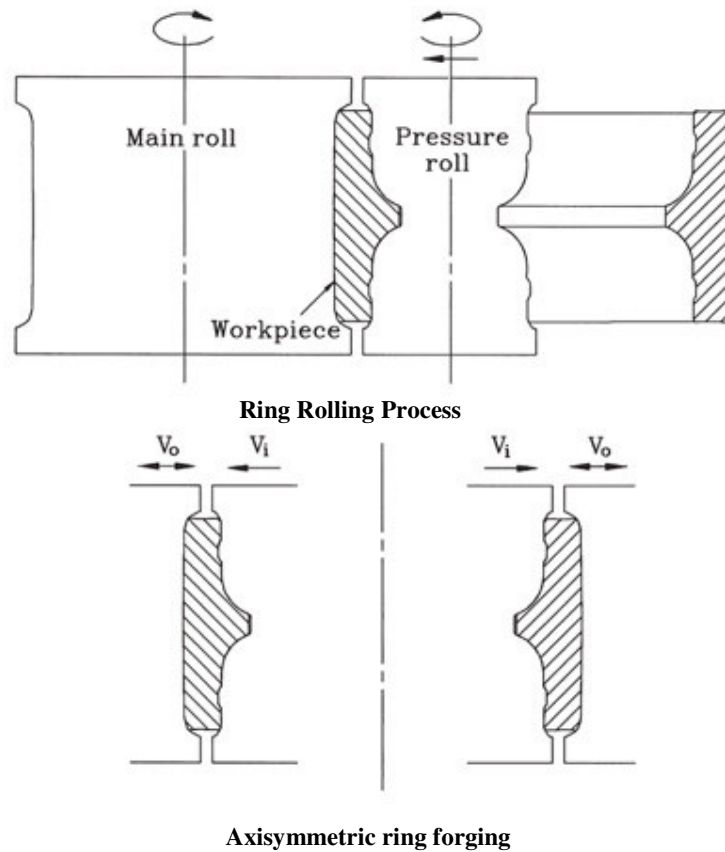


Figure 2.6 Physical modelling of a ring rolling process (Joun 1998)

Different from simulating conventional ring forging process, the main issue here is the calculation of the relative velocities. The velocities are calculated by a force equilibrium requirement. The average circumferential stress on a cross-section of the ring can be defined as;

$$\bar{\sigma}_\theta = F_\theta / A_\theta \quad (2.6)$$

$\bar{\sigma}_\theta$ is unknown but it is known that it is too small compared to average radial stress and it is related to radial forces using axisymmetry;

$$\bar{\sigma}_\theta = \frac{\varepsilon F_{ri}}{A_\theta} \quad (2.7)$$

where ε is called the forge factor, a constant of small absolute value. This factor is specified based on experience, and suggested values are between 0 and 0.02.

A rigid-viscoplastic FEM formulation is used and the one of the tool velocities is specified whereas the other velocity is introduced as an unknown variable, and as mentioned, it is calculated by force equilibrium requirement in a force-balancing iterative scheme. The model was compared with experimental results for ring rolling of a T-profiled section of a bearing ring.

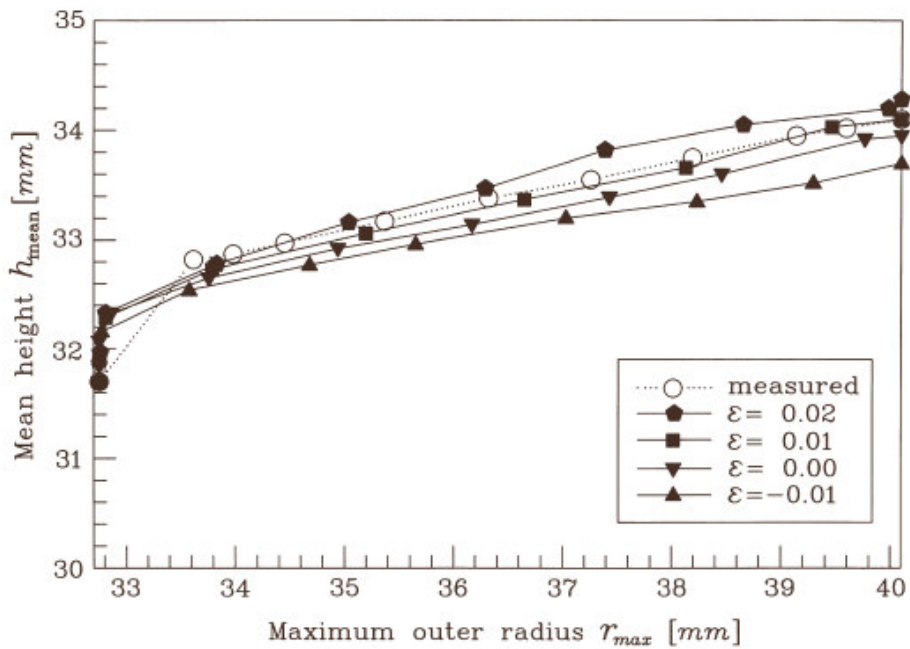


Figure 2.7 Comparison of simulation results for different forging factors.

The authors worked on proper selection of the forging factor and it is seen from **Figure 2.7** that the forging factor with a value of 0.01, is in good agreement with measured values. The solution was observed to converge to experimental results, especially at the end of the simulation, this is due to the assumed circumferential stress on the cross-section of the ring which changes during the process.

Another 2-D study for the non-profiled cold ring rolling process was presented by Utsunomiya et al. (2002). In this work, a method with plane strain assumption was used and an elastic–plastic constitutive equation was used on non-steady-state scheme and solved by implicit formulation.

As the deformation parameters, such as reduction in thickness vs. deformation (**Figure 2.8**) was studied with experiments, it was observed that after a few revolutions of the ring, a pseudo-steady state condition was reached. The reduction in thickness was defined the instantaneous nominal thickness strain caused by passing the roll gap. The reduction increases linearly until 0.3 s, i.e., during the first revolution, and it increases gradually after first revolution.

The reason was explained as follows; at the first revolution ring vibrated and a slope of the thickness along circumferences was formed, thus the reduction was linear as the roll gap decreased. However, from the second revolution, both the materials before and after the roll gap had similar thickness gradients; the draft (i.e., the reducing amount of the thickness) did not change much.

The experimental data was compared with the cumulated data from strain-stress histories of elements in 4 different sections, it was shown that the stress variation outside the bite region was large, suggesting that the elastic behaviour should be considered in the analysis of cold ring rolling process.

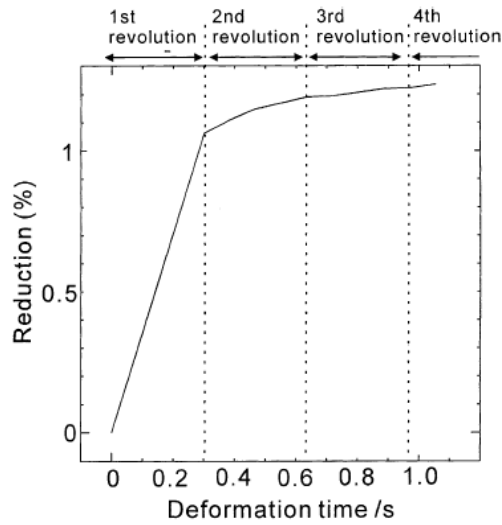


Figure 2.8 Change in thickness reduction (Utsunomiya 2002).

Takizawa et al. (2001), developed an two dimensional approach in which ring was partially modeled and solved using rigid-plastic finite element analysis. In this work, the vicinity of roll gap was partially modeled and new velocity boundary conditions on imaginary planes that cut out the partially modeled part from full model were derived considering some assumptions: the circumferential length of the ring was elongated in the modeled part, the remainder of the ring was considered to be a part of a circle, and the center of the ring laid on the line which links the centers of driving roll and pressure roll.

The **Figure 2.9** shows the deformation model drawn under the three assumptions. The subscription a, b denotes exit and inlet points and the descriptions of variables indicated in the figure is explained as followed.

$$u_{a,b} = \lim_{\Delta t \rightarrow 0} \frac{\Delta x_{a,b}}{\Delta t} = \left[\frac{1}{2} \left(\frac{r_n}{r_o} + \frac{r_o}{r_n} \right) \cos \theta_{a,b} \pm \frac{r_n}{2r_o} (2\pi - \theta_z) \sin \theta_{a,b} \right] r_v - r_n \sin \theta_{a,b} \omega \quad (2.9)$$

$$v_{a,b} = \lim_{\Delta t \rightarrow 0} \frac{\Delta y_{a,b}}{\Delta t} = \left[\frac{1}{2} \left(\frac{r_n}{r_o} + \frac{r_o}{r_n} \right) \sin \theta_{a,b} \mp \frac{r_n}{2r_o} (2\pi - \theta_z) \cos \theta_{a,b} - 1 \right] r_v + r_n \cos \theta_{a,b} \omega + c_v \quad (2.10)$$

With these equations, the velocity vectors of nodes on imaginary cutting planes were represented as rate-variables. The equations were imposed to rigid plastic formulation and the partially modeled finite element mesh was integrated as Eulerian mesh, since the model would flow out from roll gap if the Lagrangian mesh was used.

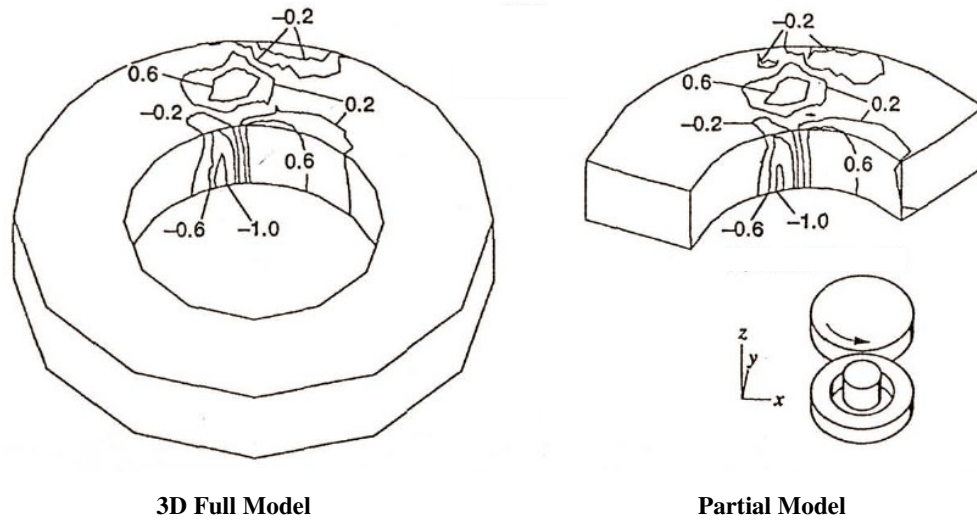


Figure 2.10 Comparison of the partial model with the full model(Takizawa 2001)

Figure 2.10, shows the distribution of normal stress in x-direction that was calculated in full 3D model, when the thickness reduction was 14%. The velocity field was calculated as same as in full model. Hence without sacrificing from the accuracy the computation time was one tenth of that 3D model. The model also detected the fish-tail defect and the results compared with experimental results

found in the literature. Another validation was performed with an industrial application, a profiled ring. The underfill of the material and distribution of plastic strain can be predicted by proposed model.

2.2.10.2 Improvements on the modelling

The 3D ring rolling simulations are preferred especially when profiled rolling is considered and 2D assumptions and axisymmetric assumptions can not be implemented. However, the cost of 3D modelling needs to be decreased somehow. In this part, different works are presented, for reducing the computation time.

The most of the simplifications are related to meshing technology. The non-uniform mesh that is dense in the bite region and coarser in the region outside the bite is one of the basic one. In this way, the number of the elements can be reduced. Davey et al. (2002) suggested a model using similar strategy. The model based on Arbitrary Lagrangian-Eulerian (ALE) formulation and Successive Preconditioned Conjugate Gradient Method (SPCGM) which was iterative solution scheme that mainly exploited the slowly evolving nature of the problem with the effect of reducing the time penalty for each deformation increment (Davey 2000).

In the ALE strategy, there are two meshes used. One for the material, which remains stationary so that keeps the dense region of the non-uniform mesh in the bite region, is used in calculations. The second mesh is uniform and used for storage of data. At each incremental step, information is passed between meshes using interpolation.

The validation of the model was based on experiments conducted by Mamalis et al.(1976). The outer diameter increase rate vs. height reduction graph is given in **Figure 2.11**, which shows good agreement. The implementation of ALE and coupling with SPCGM significantly reduced the computational time as well as obtaining good prediction material flow.

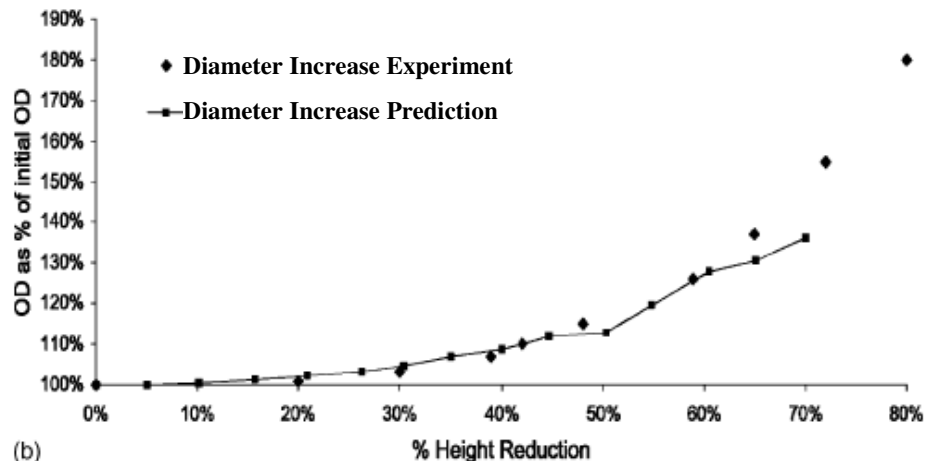


Figure 2.11 Some of the results of ALE model of ring rolling (Davey 2002) compared to results of Mamalis

Kim et al. (2003) investigated prediction of spread, pressure distribution and roll force in ring rolling process using a commercial analyzer SHAPE-RRTM. This program uses 3D rigid-plastic FE formulation and has two mesh system, called, special mesh system (SMS) and actual mesh system (AMS). The mesh systems, previously defined by Kim et. al (1991) are shown in *Figure 2.12*. As it can be observed from figure, SMS was constructed densely in the circumferential direction of the ring workpiece in the deformation region. The shape of the cross section was deformed based on the velocity field found from the rigid plastic FE formulation for SMS, and assuming this field constant for a given time increment, AMS deformed and rotated according to this velocity field.

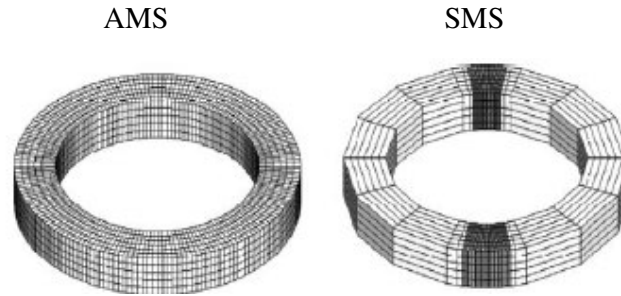


Figure 2.12 Mesh systems defined in the model(Kim 1991)

The material flow patterns calculated from the model for plain ring and shaped ring were well agreed with experiments published in the literature. Especially, the side spread was caught successfully as shown in **Figure 2.13**.

Some important conclusions on the effectiveness of solution tool were obtained: it gave reasonable mechanical predictions, it presented the characteristics pressure distribution for ring rolling which indicated the contact algorithm adopted in the simulation can be regarded as reasonable to simulate ring rolling processes not only for the deformation of the workpiece, but also for the forces and pressures.

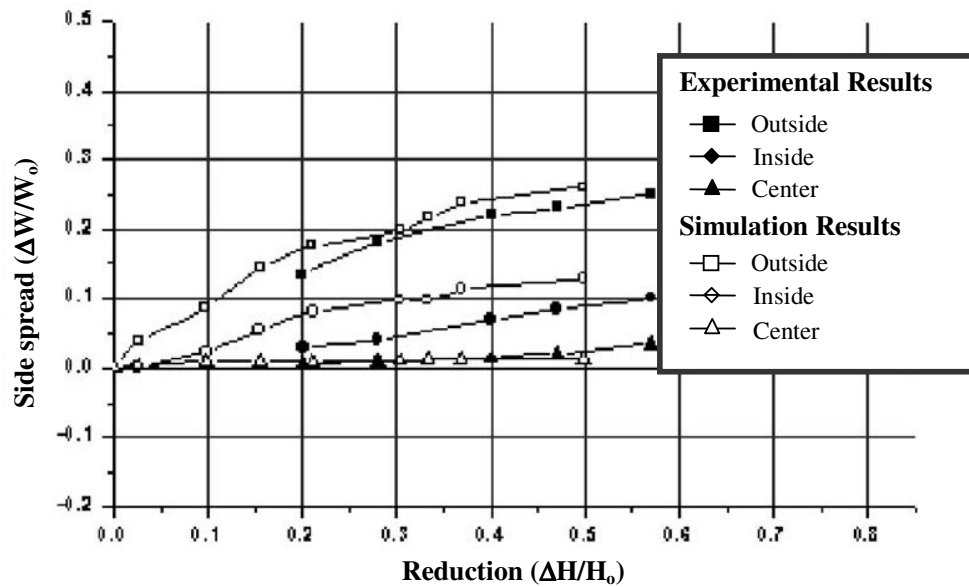


Figure 2.13 Slide spread variation with reduction of height (Kim 1991)

Xie et al. (2000) developed a code called as H-RING, based on rigid-viscoplastic, dynamic explicit formulation. The model was used to simulate the hot ring rolling process, with and without axial rolls. They used the same simplification: the non-uniform meshing. The mesh on the bite region was denser than was on the remaining part. Apart from the basic assumption of considering the tools as rigid bodies, the model had an assumption based on the physics of the process. Since the feed of pressure roll per revolution of the ring is quite small, it could be assumed that every section of the ring deforms under the same condition during one revolution of the ring. As the deformation was calculated in the bite region it was generalized to the whole ring. It means that particles of the ring with the same radius have the same deformation history.

The results were compared with experiments; the diameter increase with respect to the thickness reduction is shown in **Figure 2.14**. The experiment was carried out under real production conditions. The results of the finite element analyses show good agreement with experiment. The simulation results were also used to determine the measures of fishtail defect.

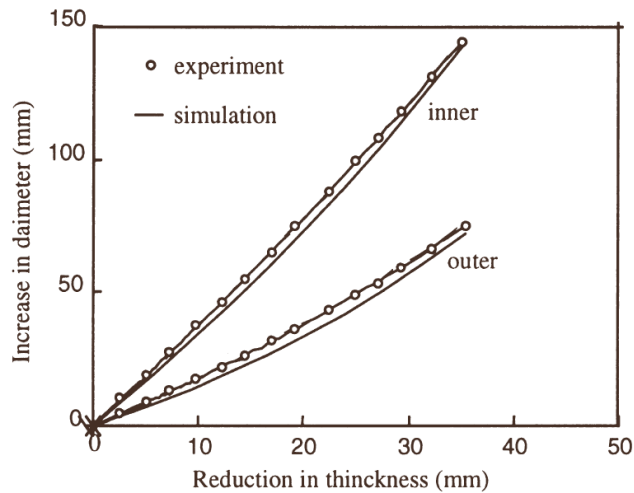


Figure 2.14 The diameter increase with respect to the thickness reduction (Xie 2000)

There is another work proposed by Hu et al.(1994) using same approach; authors called as hybrid mesh model since there are two mesh systems, one is the non-uniform computation mesh dense in bite region and material mesh that was a uniform profile. The information exchanges between the meshes are performed by one to one correspondence at the bite region, whereas are performed by interpolation outside the bite region. Mandrel was taken as frictionless in this model and the results. The authors stated that the computational time was significantly reduced however there was no clear validation.

Although, the implicit codes are preferred in metal forming simulations, explicit codes with their newly developed element technologies have been commonly used. Sawamiphakdi et al. proposed explicit FE model, built in ABAQUS. The major pitfall of the explicit integration schemes is the conditional stability. The stability criteria is defined as follows;

$$\Delta t \leq \Delta t_{\max} = \frac{L}{C_d} \quad (2.11)$$

$$C_d = \sqrt{\frac{E}{\rho}} \quad (2.12)$$

where Δt is the time increment, L is a characteristic element dimension, C_d is the dilatational wave speed of the material, E is Young's Modulus and ρ is the material density. As the cycle time of the ring rolling process is considered, it can be interpreted from the **Eqn 2.11** that stability can be ensured in more than million time increments.

Although the explicit procedure has advantages over implicit procedure, since the mass matrix is diagonal and no iteration is required, the run time is still not

feasible for millions of time increments. However there are some techniques used to decrease the time increments: artificially increasing the speed of the dies reduces cycle time, mass of the workpiece can be increased by a scaling factor to reduce the wave front speed and to increase the stable time. However, making mass scale aggressively results unstable behavior due to inertial effects (Sawamiphakdi 2002)

The model is used for simulating, cold rolling of CV-joint cage, shown in the **Figure 2.15**. In the model, the forming roll, mandrel and support rolls are modeled as rigid analytical surfaces. The ring is modeled using 3D brick elements. The analysis requires 810,000 time increments. **Figure 2.15** shows a comparison between analysis results and actual rolled ring. The geometric difference between the actual and the simulated ring is in the order of half millimeters. The run time 26.1 hours for the full width model on a HP Unix workstation J9000. Despite computation efficiency the explicit methods are not capable of predicting the residual stresses accurately (Tekkaya 2006).

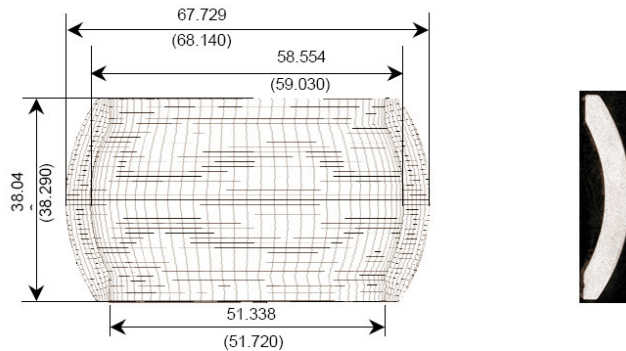


Figure 2.15 Comparison of analysis results and actual rolled dimensions of CV joint cage (actual dimensions are in the parentheses) (Sawamiphakdi 2002)

Another pitfall of the explicit procedure which is not mentioned in the previous work is the volume constancy. The most commonly used codes use linear coordinate system, and when the rotation of a body considered, there are two

components of velocity of any node on the surface of the ring (x,y) . In an explicit procedure these velocities are updated by tangential projection to the next incremental step. This results in growth of the ring in diameter as seen in the **Figure 2.16**. This problem has been handled recently and one of the most important development is performed by DEFORM , they developed new element using cylindrical coordinates (Domani 2006). Another solution for volume constancy problem is proposed by Domani (2006) in which kinematics of the process is changed during modelling i.e. the ring is kept stationary instead the tools are rotated around it.

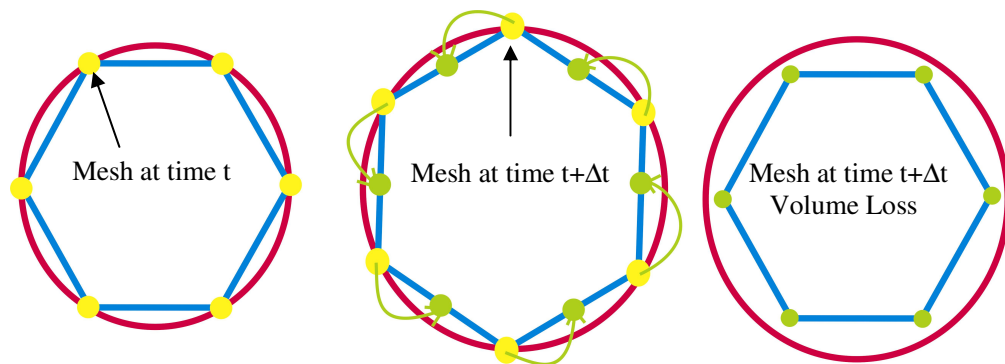


Figure 2.16 Ring growth due to projection of nodal velocities in ring rolling (Montmitonnet 2006)

Another method to prevent volume loss is presented by Montmitonnet (2006) The approach is based on introducing new interpolation scheme. The volume loss is reduced by smoothing the shape after Lagrangian step using cubic splines. And the nodes are replaced at their initial angular position. The **Figure 2.16** shows the volume loss drastically for pure rotation of the mesh and **Figure 2.17** represents the cubic spline approach, in which the mesh return to its initial configuration, hence no volume loss observed.

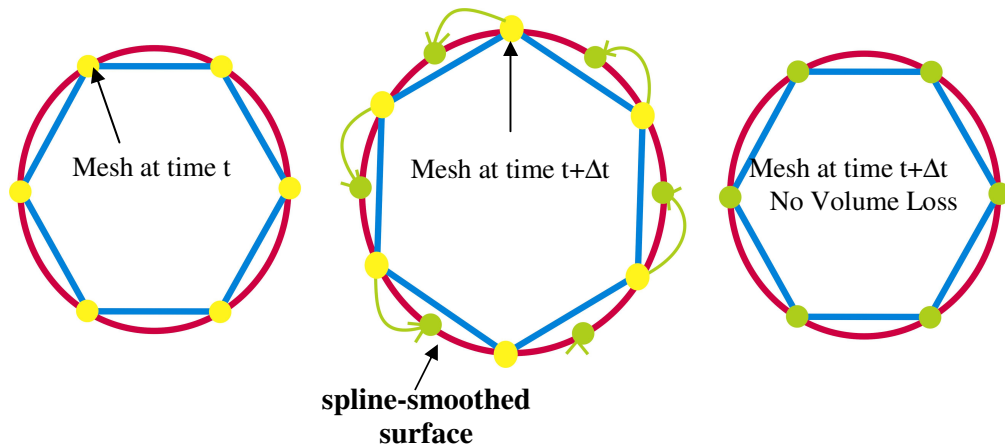


Figure 2.17 Ring growth elimination by cubic spline method (Montmitonnet 2006).

2.2.11 Discussion

The main pitfalls of simulation of incremental deformation processes are mentioned in this chapter. The primary issue in the methods presented is the computation time. Different approaches have been developed for reducing the computation time without sacrificing from accuracy of the prediction. Although there are general purposed models presented, the most of the developments performed are process dependent.

Montmitonnet (2006) discussed whether there are any common treatments that can be used in modeling various incremental processes. He proposed methods, which are also exemplified in many works mentioned before; such as benefiting ALE processes. The other suggestion is dealing the cyclic processes dealt with by algorithms paralleling steady state models.

Just (2006), in his work, evaluated the current status of the FEM and pointed out the inefficiencies, and inadequateness in numerical modeling. He emphasized that the developments on academic side should be in element technologies to obtain a common solution. Enhanced elements with less computation effort should be

developed. He also mentioned about the requirements of enhanced friction laws, which are especially important for residual stress calculations. According to author, the developments on adaptive friction law should be performed, and general purpose algorithms should be worked on.

Even though the models are process-dependent, there are some basic simplifications and assumptions which are considered in many problems. One of the basic simplifications is modeling of the tools as rigid bodies. This reduces the computation time by reducing the number of elements and also reduces the contact occurrence. Defining tools as rigid bodies also enhance the accuracy, especially for circular parts, the rigid bodies are represented analytically, so the discontinuities due to discretization are eliminated. Simplification of physical modeling and assumptions such as plain strain, axi-symmetric are also commonly used. These assumptions are only effective for plain problems, does not work for profiled or complex geometries. The non-uniform meshing method, in which the deformation region is meshed denser than the outer sides is another frequently utilized simplification.

Dynamic explicit methods are extensively used as implicit methods. They are superior in computation time problem, however they are conditionally stable. As mentioned before, in order to satisfy the stability, different methods such as mass scaling, changing cycle time of the process are available. However, these methods can not be used when inertial effects are important in the process. Finally, explicit methods are not capable of computation residual stresses accurately being computationally efficient at the same time (Tekkaya 2006).

Implicit codes, being efficient in calculations of residual stresses, have no stability criteria. The number of incrementation is not limited. However, the numerical model using implicit schemes may not converge to solution. In the implicit

analysis different iterative methods are used so convergence can not be ensured. Convergence is especially problem in simulating process with large deformations. The computation time for the implicit analysis is longer than, the explicit. Pauskar(2006) gave an approximation for the order of the computation time: for implicit analysis the computation time is proportional to N^a , where N is the number of the nodes and a varies between 1.3-2. For the explicit analysis, the computation time is proportional to N . Although there is a big difference in the order of computation time, implicit codes are preferred when stress calculations are vital. The implicit codes are generally utilized with a simplified models rather than full models.

2.3 Theory of X-Ray Defractometer Residual Stress Measurement

In the last section of this chapter, the basic theory of X-Ray Defractometer which is used in the experimental analysis part of the research to measure the residual stresses is presented. The measurements are performed by research engineers at ORS Bearing Company. However it is important to explain the theory behind.

XRD residual stress measurement depends on the fact that the spacing d of the atomic planes in a crystalline material is altered by the stress and that the d can be determined by measuring the angular position of a diffracted X-ray beam. The fractional change in d is a strain from which the stress can be calculated. This method is non-destructive and fast, if only stress at the surface is to be determined.

However, most surfaces of practical interest produced by processes such as grinding, superfinishing, machining, shot peening, etc., require the study of stress distribution beneath the surface. Subsurface measurements are generally necessary because the maximum variation in the stress distribution will typically occur at the surface due to severe plastic deformation, decarburization, etc., and because

fatigue life is found to correlate with the subsurface peak, rather than the surface residual stress (Guley 2004).

In proceeding parts the residual stress measurement is discussed and the equations to evaluate the strain and the stress tensor are given. The sources of errors and corrections, electro-polishing for material removal and correction for the stress value measured at the depth is also investigated

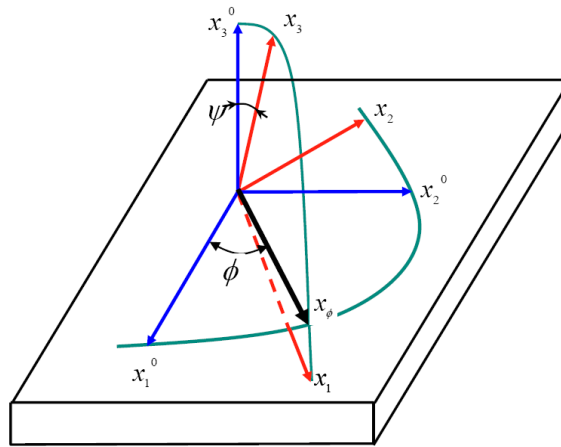


Figure 2.18 Definition of spatial and material coordinate systems (Noyan 1987).

2.3.1 Equations for X-Ray Strain Calculations

In X-ray diffraction (XRD) residual stress measurement, the strain in crystal lattice is measured, and the residual stress producing the strain is calculated, distortion in the crystal lattice is assumed to be linear. Therefore, XRD residual stress measurement is applicable to materials which are crystalline.

The coordinate system is selected as in **Figure 2.18**. The surface of the specimen is represented with axes x_1^o and x_2^o . The laboratory (spatial) system x_i is defined such that x_3 is in the direction of the normal to the family of planes (hkl) the spacing of which are measured by X-Ray deflections. As the lattice spacing

between planes are determined, $d_{\phi\psi}$, is obtained from the position of the diffraction peak for a given reflection hkl , the strain along x_3 is obtained by following f used by SAE (2003) where d_o is the unstressed lattice spacing.

$$(\varepsilon_{33})_{\phi\psi} = \frac{d_{\phi\psi} - d_o}{d_o} \quad (2.13)$$

This strain can be expressed in terms of the strains in the sample coordinate system by the tensor transformation.

$$(\varepsilon_{33})_{\phi\psi} = a_{3i} \cdot a_{3j} \cdot \varepsilon_{ij} \quad (2.14)$$

The direction cosine matrix is in the following form.

$$a_{ij} = \begin{bmatrix} \cos \phi \cdot \sin \psi & \sin \phi \cdot \cos \psi & -\sin \psi \\ -\sin \phi & \cos \phi & 0 \\ \cos \phi \cdot \sin \psi & \sin \phi \cdot \sin \psi & \cos \psi \end{bmatrix} \quad (2.15)$$

Using direction cosine matrix the the **Eqn. 2.13** becomes

$$\begin{aligned} (\varepsilon_{33})_{\phi\psi} = & \varepsilon_{11} \cdot \cos^2 \phi \cdot \sin^2 \psi + \varepsilon_{12} \cdot \sin 2\phi \cdot \sin^2 \psi + \varepsilon_{22} \cdot \sin^2 \phi \cdot \sin^2 \psi + \varepsilon_{33} \cos^2 \psi \\ & + \varepsilon_{13} \cdot \cos \phi \cdot \sin 2\psi + \varepsilon_{23} \cdot \sin \phi \cdot \sin 2\psi \end{aligned} \quad (2.16)$$

This equation is called the fundamental equation of X-ray strain determination. This equation can be simplified by considering the conditions for the polycrystalline materials. In the polycrystalline materials, it is possible to obtain three basic type of $d_{\phi\psi}$ vs. $\sin^2 \psi$ behavior (Noyan 1987). In **Figure 2.19**, these are shown and with the corresponding conditions.

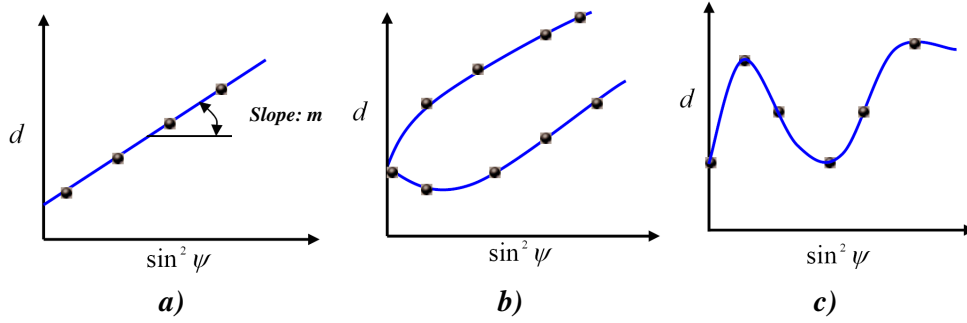


Figure 2.19 $d_{\phi\psi}$ vs. $\sin^2 \psi$ behaviors **a)** Regular, $\varepsilon_{13} = \varepsilon_{23} = 0$;
b) Regular, $\varepsilon_{13}, \varepsilon_{23} \neq 0$ **c)** Irregular, no condition

In **Figure 2.19a**, the ε_{13} and ε_{23} are zero, hence the **Eqn .2.16**, can be simplified to **Eqn.2.17**. This formula predicts a linear behavior as is seen from the graph, and also from the equation which indicates that $\sin 2\psi$ is cancel out.

$$(\varepsilon_{33})_{\phi\psi} = \underbrace{(\varepsilon_{11} \cdot \cos^2 \phi \cdot \sin^2 \psi + \varepsilon_{12} \cdot \sin 2\phi \cdot \sin^2 \psi + \varepsilon_{22} \cdot \sin^2 \phi \cdot \sin^2 \psi - \varepsilon_{33})}_{m = \text{the slope of the linear curve}} \cdot \sin^2 \psi + \varepsilon_{33} \quad (2.17)$$

In **Figure 2.19b**, a regular behavior is observed. Either ε_{13} or ε_{23} is non-zero, d measured at positive and negative ψ will be different due to argument “ $\sin 2\psi$ ” associated with other terms, causing ψ -splitting

In the **Figure 2.19-c)**, the behavior is irregular and cannot be treated without further modification. In the particular case, steep stress gradient causes non-linearity due to effective depth of penetration. Thus the average strain state being sampled by the X-ray beam is different for each ψ tilt.

2.3.2 Equations for X-Ray Stress Calculations

Each element just under the surface is subjected to deformation; hence the three principal stress states are induced. At the surface, to which the X-ray diffraction

measurements are confined, plane stress conditions are assumed to exist so σ_{33} is considered to be zero. However due to lateral contractions and Poisson's ratio, there will be a component of strain ϵ_{33} in the direction of surface normal. In the following parts equations for both zero and non-zero cases for σ_{33} are given. Considering isotropic material the stress strain relation can be defined as:

$$\epsilon_{ij} = \frac{1+\nu}{E} \sigma_{ij} - \delta_{ij} \frac{\nu}{E} \sigma_{kk} \quad (2.18)$$

Then, substituting this equation into fundamental equation of X-ray strain determination (*Eqn. 2.16*) yields *Eqn. 2.19*

$$\begin{aligned} (\epsilon_{33})_{\phi\psi} = & \frac{1+\nu}{E} (\sigma_{11} \cos^2 \phi + \sigma_{12} \cdot \sin 2\phi + \sigma_{22} \cdot \sin^2 \phi - \sigma_{33}) \cdot \sin^2 \psi + \frac{1+\nu}{E} \cdot \sigma_{33} \\ & - \frac{\nu}{E} (\sigma_{11} + \sigma_{22} + \sigma_{33}) + \frac{1+\nu}{E} (\sigma_{13} \cdot \cos \phi + \sigma_{23} \cdot \sin \phi) \cdot \sin 2\psi \end{aligned} \quad (2.19)$$

The above equation is used to derive the equations given in *Table 2.1*. In the table the equations are derived according to different cases. In the first case, ($\sigma_{13} = \sigma_{23} = 0$). The formula *Eqn. 2.20* predicts a linear variation of d vs. $\sin^2 \psi$ as indicated by *Figure 2.19a*. The stress in the x_ϕ direction can be obtained directly from the slope of a least squares line fitted to the experimental data, measured at multiple ψ , if the elastic constants E , ν and the unstressed lattice spacing, d_o are known. If d_o is not readily available the lattice spacing measured at $\psi = 0$ is substituted for d_o . Such substitution is based on the fact that, for most materials, elastic strains may introduce at most, 0.1 % difference between the true d_o and d at any ψ . Since d_o is a multiplier to the slope, the total error introduced by this assumption in the final stress value is less than 0.1 %, which is negligible compared to the error introduced by other sources (Guley 2004).

Table 2.1 Summary of X-ray stress determination equations

	$\sigma_{13} = \sigma_{23} = 0$	$\sigma_{\phi} = \sigma_{11} \cos^2 \phi + \sigma_{12} \cdot \sin 2\phi + \sigma_{22} \cdot \sin^2 \phi \quad (2.20)$ $(\varepsilon_{33})_{\phi\psi} = \frac{d_{\phi\psi} - d_o}{d_o} = \frac{1+\nu}{E} \sigma_{\phi} \cdot \sin^2 \psi - \frac{\nu}{E} \cdot (\sigma_{11} + \sigma_{22}) \quad (2.21)$
$\sigma_{33} = 0$	$\sigma_{13}, \sigma_{23} \neq 0$	$a_1 = \frac{1+\nu}{E} (\sigma_{11} \cos^2 \phi + \sigma_{12} \cdot \sin 2\phi + \sigma_{22} \cdot \sin^2 \phi \cdot \sin^2 \psi) - \frac{\nu}{E} \cdot (\sigma_{11} + \sigma_{22}) \quad (2.22)$ $a_2 = \frac{1+\nu}{E} (\sigma_{13} \cos \phi + \sigma_{23} \cdot \sin \phi) \cdot \sin 2\psi \quad (2.23)$
	$\frac{\partial \sigma_{3j}}{\partial z} \neq 0$	$\zeta = \frac{\sin^2 \theta - \sin^2 \psi}{2 \cdot \mu \cdot \sin \theta \cdot \cos \psi} \quad (2.24)$ $(\sigma_{ij})_{\psi} = (\sigma_{ij})_{z=0} + K_{ij} \zeta_{\psi}^{n_{ij}} \quad (2.25)$
$\sigma_{33} \neq 0$		$a_1 = \frac{1+\nu}{E} (\sigma_{11} \cos^2 \phi + \sigma_{12} \cdot \sin 2\phi + \sigma_{22} \cdot \sin^2 \phi - \sigma_{33}) \cdot \sin^2 \psi + \frac{1+\nu}{E} \cdot \sigma_{33} - \frac{\nu}{E} \cdot (\sigma_{11} + \sigma_{22} + \sigma_{33}) \quad (2.26)$ $a_2 = \frac{1+\nu}{E} (\sigma_{13} \cos \phi + \sigma_{23} \cdot \sin \phi) \cdot \sin 2\psi \quad (2.27)$

In the second case a_1, a_2 are defined in *Eqn. 2.22* and *Eqn. 2.23* respectively. The slope and the intercept of the a_1 vs. $\sin^2 \psi$, and a_2 vs. $\sin|2\psi|$ are found. Thus, if $d_{\phi\psi}$ is obtained for three ϕ tilts (for ex. $0^\circ, 45^\circ, 90^\circ$). The slope and the intercept equations can be solved for all the unknowns.

The third case is also represented by *Figure 2.19c*; the oscillatory behavior in d vs. $\sin^2 \psi$ curve is observed. This behavior indicates presence of gradients in σ_{3j} , as well as variation of σ_{11}, σ_{22} or σ_{12} . This non-linearity occurs due to the changing effective depth of penetration of X-rays with ψ tilt, i.e. the average strain state being sampled by the X-ray beam is different for each ψ tilt. In this case, the d spacing thus the strain obtained by the X-ray beam will be the average of this gradient over the effective penetration distance of X-rays, ζ . This distance is limited by absorption and depends on $2\theta, \psi$. The effective penetration depth equation is given by *Eqn. 2.24* and the average stress determined by X-rays at any ψ tilt is *Eqn. 2.25*. The stress gradients can also be estimated using *Eqns. 2.24-2.25*.

Another case is for $\sigma_{33} \neq 0$, the estimation procedure is similar with the second case. The slope and the intercept of the a_1 vs. $\sin^2 \psi$ for $\phi = 0^\circ, 45^\circ, 90^\circ$, and slope and the intercept of a_2 vs. $\sin|2\psi|$ for $\phi = 0^\circ, 90^\circ$ are found. The estimated results yields the shear stresses σ_{13}, σ_{23} respectively.

2.3.3 Layer Removal by Electro Polishing and Correction of Layers

The material removal should be performed without inducing any stress on the surface. The only stress free methods are appear to be electrolyric and chemical polishing (Noyan 1987). In electropolishing, the electrolyte and operating

conditions used depend on the material or alloy. Solutions in most extensive use are based on phosphoric or perchloric acids. Perchloric acids produce better surface finish than phosphoric; however, the temperature of the perchloric acid should be maintained below a certain level due to the explosive hazard (Guley 2004). A thin oxide layer is easily removed by electropolishing but a thick scale should be removed by pickling or by mechanical means prior to electropolishing.

When stressed layers are removed, the successively measured stresses at depths below the surface must be corrected by an amount related to the relaxation created by the removed layers. This means that all determinations except the initial surface value must be corrected to obtain the true stress that existed before the layers were removed [Moore 1958]. These corrections can be determined by the theory of elasticity and are expressed as functions of the successively measured stresses.

CHAPTER 3

PROBLEM DEFINITION

In this chapter, the problem investigated in the thesis is defined. The incremental ring rolling process has been defined but a concrete definition of the process has not been presented yet. The incremental processes involving rotary motion have been investigated and numerical studies have been presented in the literature review. On the base of these investigations, the problem solving approaches are developed and the extent of the thesis is determined. The elements of the problem such as raw material, process conditions are also indicated. Finally the aim of the analysis and need of this work are explained.

3.1 Definition of the process

The process has various alternatives, but basically in the process; a narrow mandrel, which could have any profile, is used to deform part of the ring cross-section, and may be controlled to move both radially and axially during the forming cycle. This definition is made by Allwood et al. (2005). The physical representation is shown in *Figure 3.1*.

This process configuration has potential to be used in either hot or cold ring-rolling, and the narrow mandrel could be applied to either radial or axial faces. With this configuration, it is aimed to obtain many ring profiles with the same tooling, without set-up times between products. The major advantage overseen is the reduction of proceeding machining operations. This reduction is important to keep the material characteristics of the rolled workpiece, by maintaining the fiber

structure uninterrupted. A seamless product with uncorrupted grain structure will have better mechanical characteristics. Another outcome of reduction in machining is the material saving.

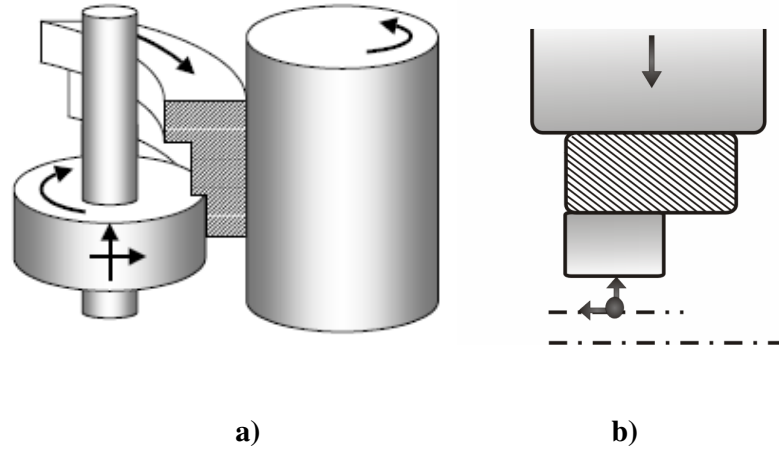


Figure 3.1 a) Representation of incremental ring rolling process (Allwood 2005)
b) Cross-section view of part

The process has a broad definition, as an initial start it should be simplified for investigation. In this work, the process is simplified and a narrow mandrel is positioned from the edge of the ring and the ring cold formed by means of the feed and rotational motion given by a form roll. The process analyzed using different mandrels and positioning them from edge with a certain distance. The mandrel is kept stationary during rolling; the schematic view is similar with **Figure 3.1b**. The simplification depends on some restrictions due to the experiments that are performed to verify the model and observe the material flow in ORS Bearings Company. Detailed procedure of the experiments is explained in the proceeding chapter. The process is simplified, also due to other verification method: the secure numerical models which have very long computation time to finish. Investigations are based on similar conditions of the real process some elements of the process are explained are raw material, boundary conditions.

The raw material is selected as 100Cr6 and which is widely used in bearings industry and it is also called as “bearing steel”. It is a high carbon, low-alloyed steel 100Cr6. Mechanical and metallurgical properties of bearing steel are given in **Table 3.1** below. This is the material which ORS bearing company uses and data are obtained from an academic work supported by ORS (Music 2005)

Table 3.1 Mechanical and metallurgical properties of bearing steel (Music 2005)

MATERIAL		1.3505 (100Cr6, SAE 52100)					
COMPOSITION							
C	Si	Mn	P	S	Cr	Ni	Cu
%	%	%	≤ %	≤ %	%	≤ %	≤ %
0.90 - 1.05	0.15 - 0.35	0.25 - 0.45	0.030	0.025	1.35 - 1.65	0.30	0.30
MECHANICAL PROPERTIES							
Brinell Hardness HB 30 (as annealed)						≤ 207	
Hardness when hardening in water						66 HRC	
Hardness when hardening in oil						65 HRC	
HRC hardness at tempering temperature 100°C						64	
HRC hardness at tempering temperature 150°C						63	
HRC hardness at tempering temperature 200°C						62	
HRC hardness at tempering temperature 250°C						59	
HEAT TREATMENT							
Hot working (°C)						1150 - 850	
Soft annealing (°C)						780 - 800	
Normalizing (°C)						870-900 / 600-650	
Hardening temperature for quenching in water (°C)						800 - 830	
Hardening temperature for quenching in oil (°C)						830 - 870	
Temper (°C)						150 - 170	

The flow curve of the material is also obtained from ORS bearing company. They used the flow curve data from the torsion tests performed at the Institute of Virtual Production of Eidgenössische Technische Hochschule in Zürich / Switzerland (ETH / IVP). Music presented comparison of the flow curve data, found in literature and experimental data and it is shown in **Figure 3.2**. The graph basically shows a strain-stress relation for different tests using same materials with small differences in composition. The material composition can differ among various suppliers and even can change among different batches from a single supplier. All of the flow curves shown were measured at temperature of 20 °C. Strain rate changes from 1 to 1.6 s⁻¹ for the given flow curves.

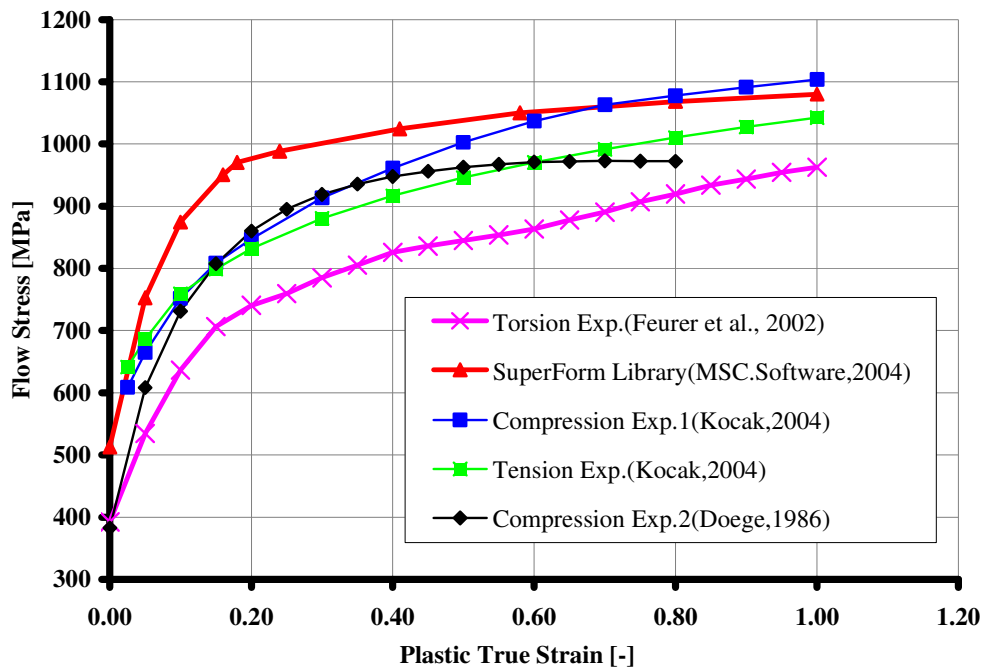


Figure 3.2 Bearing steel flow curves from various sources (Music 2005)

The flow curves agree with each other, there are differences up to %15 percent, which is a result of the mechanical properties differs by chemical composition.

The flow curves obtained by the simple tension and compression tests vary about 100 MPa flow curves from torsion tests. This is a result of Bauschinger Effect occurring in torsion. In torsion of thin walled tubes, change in direction of straining occurs, which results in lower measured flow stress due to Bauschinger effect. Hence difference is observed as in *Figure 3.2*.

The process conditions and the boundary conditions are explained in the next chapter. However another parameter which is used in analysis is the friction. The friction factor in the ring rolling process at ORS bearing company is used. In previous studies they had performed ring compression tests and used a semi - analytical model. In these studies the friction between ring and the mandrel and the form roll is analyzed using Coulomb friction law. As a result, the friction factor is found to be 0.08 based on Coulomb's Law.

The material properties and the friction factor is temperature dependent, the temperature for conventional cold ring rolling process is about 40°C (Music 2005). The process assumed to be isothermal with constant temperature of 40°C.

3.2 Need for Analysis

The incremental ring rolling process is a newly developing process; there are neither analytical nor numerical studies on this process in the literature. Like all other incremental forming processes, the incremental ring rolling has also complex nature which makes analytical modelling almost impossible. The process has complex material flow characteristics of which has not been dealt either experimentally. The slip-line field solutions that were firstly proposed by Johnson and Mamalis were study of conventional ring rolling process which was successful in predicting velocity fields are useless for incremental ring rolling. Also the experimental studies on conventional ring rolling, that were performed to predict

the rolling force and torque can not be utilized, the material flow characteristics differ since a narrower mandrel is indented to workpiece.

There are various types of defects in conventional ring rolling process due to its instable nature; such as fish tail defect, ovalization and etc. In order to prevent these, many different control strategies are developed and additional tools are installed on machines which enable closed loop control. However, defects in incremental ring rolling process have not been identified yet. It is aimed to obtain near-net shaped parts, hence the defects should be identified and control strategies should be developed. Hence identifying the geometry is important.

The residual stresses are another matter of subject. At the end of the metal forming processes, residual stresses are induced in the workpiece. The residual stresses are important for both intermediate part and final part. For intermediate parts, the residual stresses are important in the proceeding operations. Ease of machining and failure such as fracture due to highly induced residual tensile stresses are some expected results of residual stresses. For the final parts, the residual stresses are important for the performance. Especially for the parts under dynamic loading the fatigue resistance is important and residual stresses have direct influence on fatigue resistance. There is not any important contribution in the literature on the computational and experimental basis even for the conventional ring rolling. Thus investigating the residual stresses induced in the incrementally rolled ring is a valuable task to perform.

In the previous chapter, numerical studies on ring rolling process are presented in detail. It is shown that the major problem is the computational time. Different approaches such as plain strain simplification or axi-symmetry assumptions are used in modelling to reduce the computation time. These types of assumptions are not valid for the incremental ring rolling. The incremental ring rolling process has more complex stress state during the deformation and also there are more contact

release occurrences which make the computational time longer than it is in conventional ring rolling. For a process in a developing stage, models with low computation times will be efficient and provide faster developments.

3.3 Aim and Scope of the Study

The main aim of this study is to develop an efficient numerical model that can be used to predict the material flow (i.e. geometry) and stress state in the incrementally rolled-ring accurately. The model should base on some simplification which reflects the process perfectly. The simplified model must be compared with the experimental results and reliable numerical models in the literature. This comparison should be both for the material flow and the stress state after deformation.

Another aim of the study is to emphasize the flexibility of the incremental forming processes with rotary motion, to introduce the application areas and to present current status in numerical modelling of these processes. These studies are also important on the developing stage of flexible rolling process. Especially the study on conventional ring rolling having a similar process nature is a prerequisite for incremental ring rolling.

This study is starting point for the detailed characterization of the new process and gives basic idea about the feasibility of the process. The characterization includes, determining the flow behaviour, investigating the process window, finding the defects, the optimum tool design, the optimum tool path and etc. These will be further studies on this process.

CHAPTER 4

EXPERIMENTAL STUDIES

In this chapter the experiments performed at ORS Bearings Company are presented. The aim of the experiments is to judge the feasibility of the incremental ring rolling process and to examine the stability of the incremental ring rolling process. Since the process has not been tried before the material flow is questionable. Therefore the experiments can provide some clues about material flow; by the observing the shapes and measuring dimensions. The observation such as oscillations that causes in stability and tool wear were also concerns of the experiments performed. The residual stresses measured from some samples are also helpful in comparing the incremental ring rolling with the conventional one. Another important need for the experimental analysis is due to validation requirements of the numerical models, thus one of the experiment was analyzed in detailed and used for validation.

All of the tools for experiments were designed and all of the experiments were conducted by research engineer Omer Music using utilities of ORS bearing company. The experiments were conducted with some limitations in tool design and the machine adaptation. The experiments require flexible machines in which tools can be moved independently, however the conventional ring rolling machines which were adopted to produce single type of profile in a mass production were not flexible enough. The tool design alternatives were restricted to rigid machine construction, which must not be harmed anyhow. Another limitation was the time spent for experiments. The experimental studies involves: the plan for the experiments, designing tools and adopting them to machines, experimentation, measurements. All of these steps require extensive time and labour work.

In this chapter the steps of the experimental studies are explained, including the detailed information about tool design, measurement techniques and the results of the experiments are presented. Some information about the nature of the process obtained by the experiments is discussed here. The experiment which is used to validate the model is also discussed and results are presented.

4.1 Plan of the Experiments

The incremental ring rolling process involves stepwise forming, and the effect of the mandrel offset from the center is not determined. In the experiments, these effects were aimed to be determined. The mandrels in different widths were penetrated to the rings from different positions. The position of the mandrel was defined as the distance from the edge of the ring or offset from the center of the ring.

In the first series of the experiments, the offset was given to the mandrel and the effect of the offset on the material flow is investigated. In the second series of the experiments, the set-up and the tooling were updated according to results of the first set and more than the effect of the offset, the stability of the rings were examined. In the third series, the effects of rolling parameters (the width of the mandrel and the amount of penetration) on the final profile, stability and the residual stress were examined. In the proceeding parts the series of the experiments will be explained and the tooling of the experiments is introduced.

4.2 Machine and tooling

Conventional ring rolling machine used at ORS factory was used in experiments. The machine set-up is given in **Figure 4.1**. A conventional ring rolling machine was introduced in the first chapter. The machine consists of 4 basic elements. The form roll (king roll), which provides the feed and the rolling force by rotation about its

axis, can have different profiles according to external shape of the ring. The two different types of form roll were used for the experiments. The guide rolls, stabilize the process by controlling the diameter variation it hydraulic system; however the guide rolls were not used in all experiments since they were adapted for conventional ring rolling. The back up rolls control the thickness variation and it was not used in the experiments. The mandrel, which was idle and had same width with the ring in conventional rolling, can be in different sizes and be positioned from the edge of the ring. The idea of the incremental forming involves simultaneous motion of the mandrel during, rotational motion of the ring. However this necessitates a special drive system which was almost impossible to install on the machine without causing deformation.

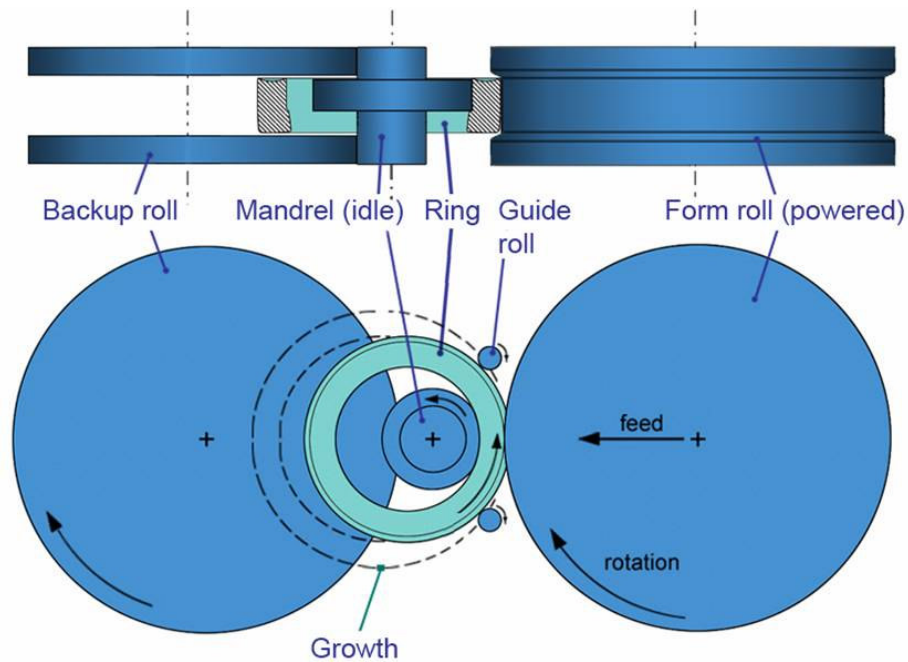


Figure 4.1 Machine set-up for the experiment

The only changeable parts of the machine are the mandrel and the form roll. The form roll has two different profiles. The profiles of the form rolls and the mandrels are shown in detailed in proceeding parts. The specification for the machine is given in **Table 4.1**.

Table 4.1 Ring rolling machine specifications

Capacity	<i>Max. rolling force</i>		70 KN
	<i>Max. rolled outside ring diameter</i>		85 mm
	<i>Min. rolled inside ring diameter</i>		40 mm
	<i>Max. rolled ring width</i>		Depends on ring inside diameter before rolling
Tools	<i>Forming roll</i>	<i>Max. outside diameter</i>	160 mm
		<i>Min. outside diameter</i>	150 mm (also dependent on the mandrel diameter)
		<i>Max. width</i>	60 mm
	<i>Backup roll</i>	<i>Max. outside diameter</i>	248 mm
		<i>Min. outside diameter</i>	220 mm
		<i>Width</i>	19-30 mm
	<i>Mandrel</i>	<i>Max. forming diameter</i>	45 mm (also dependent on forming roll diameter)
		<i>Min. forming diameter</i>	15 mm
	Speed	<i>Forming roll</i>	
<i>Forming roll feed rate</i>		0 – 10 mm/s	

4.3 Measurement Equipments and Methodology

The results of the experiments were measured in two ways, the geometry of the results were measured using compass and numerically controlled profile measurement tool by Omer Music and the residual stresses are measured by

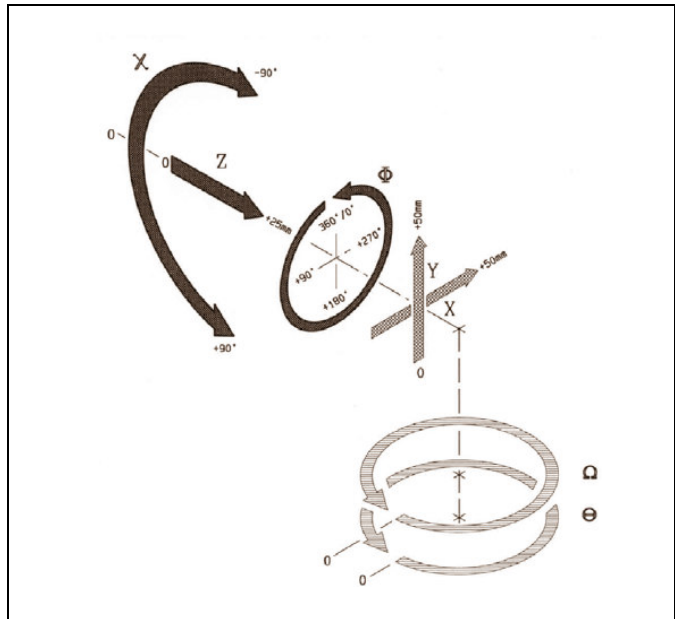
research engineer Volkan Güley using X-ray diffractometer (XRD) at facilities of ORS Company . The XRD system basically consists of three parts

1. X-ray tube
2. Goniometer, Texture-Stress Attachment and X-Y stage
3. Detector

X-ray tube is the source of X-rays and X-rays produced is guided with a collimator pointing the measurement point. Electrically charged particles are accelerated by applying a potential difference and creating an electrical field. Then they are decelerated by hitting the target material.

Goniometer, TSA and X-Y Stage are the parts of the XRD system that provides all the necessary movements for the measurements. In **Figure 4.3** Goniometer, TSA and X-Y Stage are shown with the corresponding movements. **Table 4.2** shows and lists the axis movements with the related hardware limitations.

Table 4.2 Axis movements with hardware limitations

 <p>The diagram illustrates the various movements of the XRD system components. It shows a coordinate system with X, Y, and Z axes. A large curved arrow indicates rotation around the Z-axis, with angles of -90°, 0°, and +90°. A smaller circular arrow indicates rotation around the X-axis, with angles of +90°, 0°, +180°, +270°, and 360°. A vertical arrow indicates translation along the Y-axis, with a range of 0 to +50 mm. A horizontal arrow indicates translation along the X-axis, with a range of 0 to +50 mm. A vertical arrow indicates translation along the Z-axis, with a range of 0 to +25 mm. A circular arrow indicates rotation around the X-axis, with a range of 0 to 180 degrees.</p>	Symbol	Movement
	Ω	-3° to 182°
	θ	-5° to 163°
	χ	$\pm 90^\circ$
	ϕ	infinite rotation
	X	0 to 50 mm
	Y	0 to 50 mm
	Z	0 to 25 mm

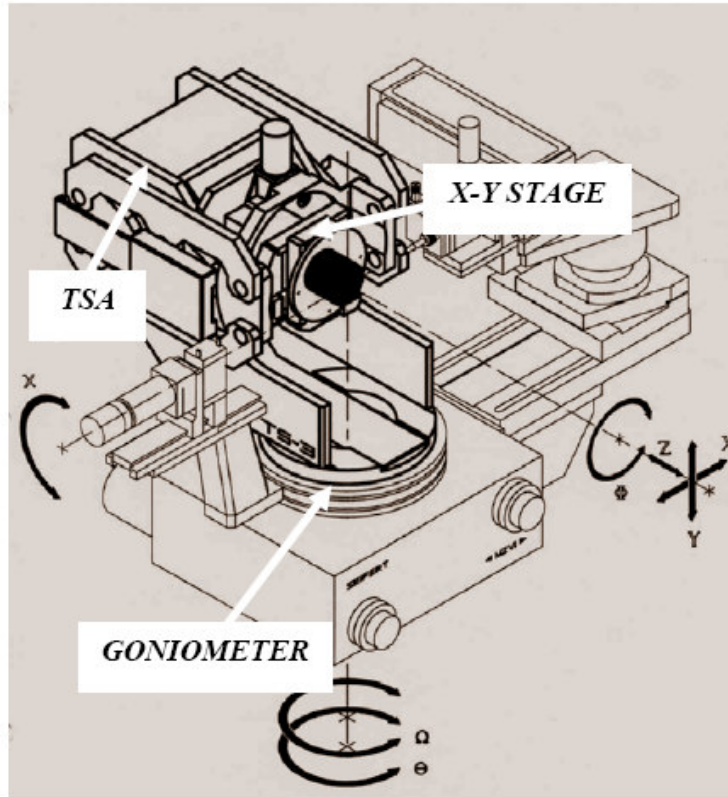


Figure 4.2 Goniometer, TSA and X-Y Stage

The detector in the system is a Position Sensitive Detector (PSD). PSD is capable of counting 50000 pulses per second. It has a 10 degree window span with a $70 \mu\text{m}$ position resolution. There are $212 = 4096$ channels on the PSD. 10 % Methane + 90 % Argon mixture (P10 Gas) is used as the gas flowing through the channels at a flow rate of approximately one liter per hour.

The methodology of the measurements can be summarized in three stages. The first one is the preparation, in which the surface layers are to be removed by a stress-free method. Electropolishing is applied to remove layers. Etching is followed by polishing of the surface to get rid of surface irregularities created by polishing. The second step is the mounting; the specimen is mounted on the sample holder of TS.

The final step is the determination of the full stress tensor. The diffraction curves must be obtained at least three independent ϕ tilts. $0^\circ, 45^\circ, 90^\circ$ are angles used for the tilts in the measurements (as explained in **Section 2.3.2**). ψ axis is an axis on the sample coordinate system which is the corresponding axis of χ . The angle up to 90° can be used for the evaluation; however, intensity is lost as the angle is increased. 45° is the maximum angle used in this analysis. The angles which the measurements taken were not recorded. But generally the data is taken for

Residual stress measurement by X-ray diffraction is based on evaluation of the diffraction data. The position of diffraction peaks is to be determined for stress measurement. At a defined ϕ angle, three diffraction curve is recorded .X-ray data is corrected and then peak points can be determined by several methods. Such as parabola fitting above a threshold value, center of gravity-mean value determination.

After determining the peak points, d vs. $\sin^2 \psi$ graph is drawn. The diffraction data obtained in residual stress measurement on ball bearing rings shows splitting ψ , thus $\sigma_{13}, \sigma_{23} \neq 0$. It is also assumed that $\sigma_{33} = 0$. Hence the procedure explained in **Section 2.3.2** is used to determine and the correction methods are applied

Error associated with the residual stress measurement depends on various factors: ϕ , ψ and θ angles, measurement time, condition of the surface and material etc. In the case of Cr-K α radiation incident on 100Cr6 material and one hour measurement time, error in residual stress values in the stress tensor is maximum ± 20 MPa independent of its value (Guley 2004). The measurement time is the main drawback of the experimental procedure. For each point more than 2 hours is spent.

4.4 Series of Experiments

The experiments are completed in three different series. The measurements were taken for some spaces.

4.4.1 First Series of Experiments

In this series, a narrow mandrel was aligned from the edge of the ring, which was formed by a profiled roll as shown in **Figure 4.3**. The figure is a section view of the real process. The ring with 16 mm width was positioned to the machine and a mandrel in 8 mm width was fixed such that its half contacted with the ring. The ring was placed into the form roll with narrow shoulders. The guide rolls are shown in **Figure 4.1**, used in as similar fashion. The back-up rolls which prevent the axial movements of the rings were not used in this experiment, thus the form roll with narrow shoulders kept the ring in the deformation zone. The form roll and the mandrel were rigid tools (low elastic deflection) and made of tool steel.

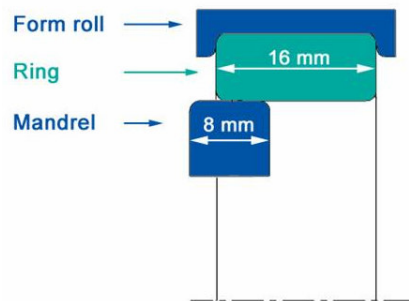


Figure 4.3 The schematic representation of first series of experiments

The rings were rolled under constant rotational speed of 150 rpm. The amount of the penetration, in other words “the bite”, was between 0.15-3 mm (The bite was the half of the difference between the initial and the final diameter of the ring). The experiments were performed for different bites in order to observe the effect of

deformation amount on material flow direction. A non-uniform deformation scheme was expected to be observed, since the force applied was localized.

The results are evaluated qualitatively, no measurements are taken. The material flow for the ring is indicated in *Figure 4.4*.

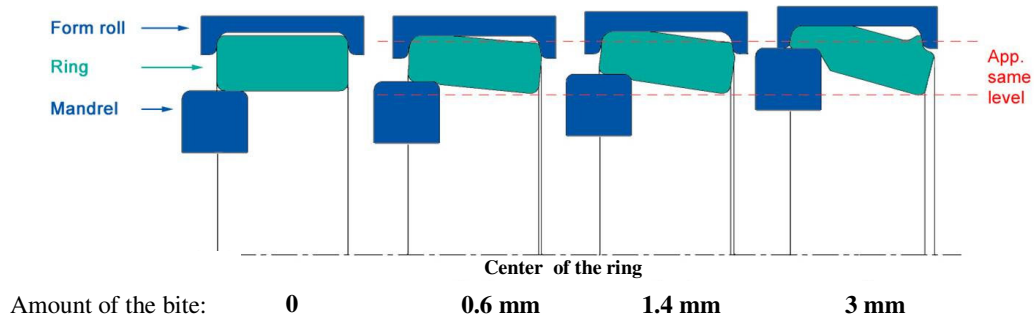


Figure 4.4 Sketch of the ring shape at different stages of the experiment

In this series, it was observed that it was not possible to control the amount of bite into the ring with this configuration, so the experiments were performed by timing process. The bite amounts shown in figure are approximate values. The ring started to tilt towards mandrel, starting from a deformation of 0.6 mm, however its movement was restricted by the shoulder of form roll. As the deformation was increased to 1.4 mm the tilting motion continued and irregular cross-section was observed. These tilting also caused rings to slide, and this sliding motion made the contact length between the mandrel and the ring shorter.

The diameter of the ring increased and also the width of the ring elongated. As the contact length decreased and the ring grew in width direction, the moment arm of the deformation force exerted by action of form roll on mandrel also became longer, which increased the tilting motion with deformation. When the bite was about 3 mm, the ring is stuck to form roll and stopped rotating, as the process continued diameter stops increasing however amount of tilting continued to increase.

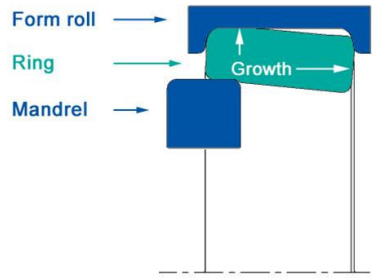


Figure 4.5 Sketch of the ring shape at different stages of the experiment

The material flow on the ring is shown in **Figure 4.5**. The material flow was in two directions; in radial and axial. The radial flow increased the diameter whereas the axial flow cause tilting of the ring. However it was also observed that the diameter increase is only on the left side where the mandrel and the ring was in contact. The diameter of the right side was almost same; this directly showed that the deformation force is diverted to axial direction which caused broadening in width. With the restricting effect of the shoulder of the rollers, and with the axial material flow, the right side of the ring became conical.

4.4.2 Second Series of Experiments

The aim of this series was to examine the stability and observe the shapes resulting from straight paths. It was also to examine the residual stresses distribution in this configuration and to compare it with the conventional ring rolling. The comparisons were based measured data in XRD machine, which is presented in this section.

Different than the first series, in this study the shoulders on the form roll were wider and the guide rolls are not used. Two mandrels were manufactured with 5 and 10 mm in widths. The mandrels with different widths were positioned in four configurations, which are shown in **Figure 4.6**. In the first and third configurations, mandrels with 5 mm and 10 mm were aligned to right edge of the ring with 16 mm width. In the other two configurations the same mandrels were positioned to center of the ring.

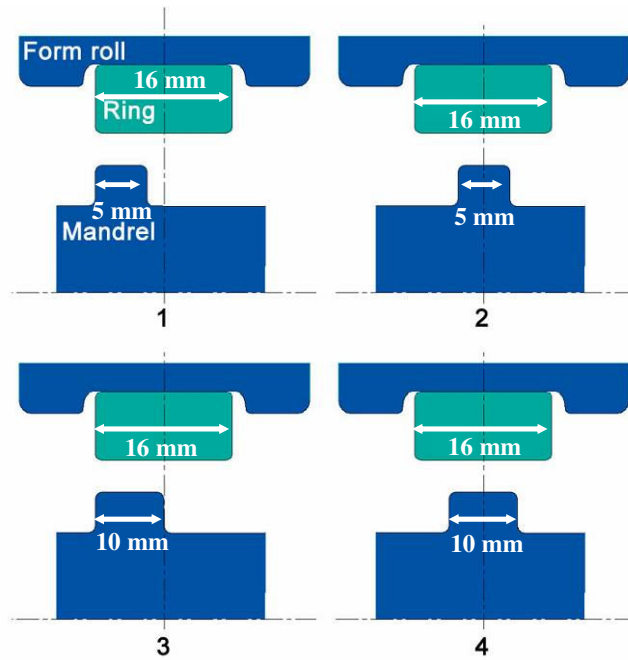


Figure 4.6 Sketch of the ring shape at different stages of the experiment

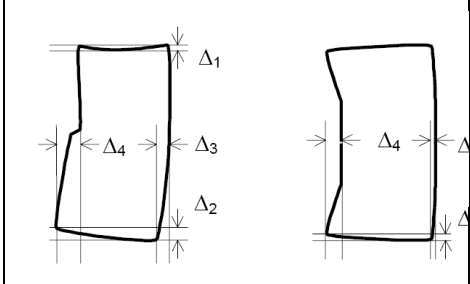
The bite could not be controlled with the configuration of the machine; the bite amount was also based on timing. Initially the bite of 2.5 mm was tried however for the wider mandrel the bite was 1.1 and 1.3 mm into the ring and for the narrow mandrel the bite was 1.2 and 1.8 mm.

Totally 40 pieces were tried; and during the experiments, the most important problem was the quick sliding motion of the ring, which was caused by the oscillations due to high order of instability. Since the ring was not squeezed within narrow die shoulder or back-up rolls, sliding motion made the experiment impossible to be completed, and it was also a potential danger for both machine and the operator. Many of the trials failed and become scraps.

In the **Table 4.3**, the geometric analyses of the some samples are shown. The deflection amounts are given. These samples were selected from the trials which

are conducted precisely in terms of accuracy of bite amount and alignment. The values shown are the averages.

Table 4.3 Dimensions of deformed ring

	Config. No:	Bite	Δ_1	Δ_2	Δ_3	Δ_4
	Edge Aligned (5 mm)	1.8	0.46	0.81	1.05	3.72
Center Aligned (5 mm)	1.2	–	0.46	0.10	1.72	
Edge Aligned (10 mm)	1.1	0.17	1.35	1.40	1.74	
Center Aligned (10 mm)	1.3	–	0.71	0.25	0.97	

In the figure given in **Table 4.3**, it is observed that rings remained planar, however when the workpieces were investigated it was seen that there was a high conicity on its faces. In general for the center aligned configurations; it was observed that the process was more stable.

In the produced parts climbing towards to ring hence tilting from the form roll was observed. The amount of climbing differed depending on the configurations. When 1st and 3rd configurations are compared (narrow and wide mandrel aligned from edge) it is observed that Δ_4 , which can be consider as order or climbing, is more in 1st configuration. Although the amount of the bite for 3rd configuration is approximately 70% of the 1st one, the Δ_4 differs more than 100%. It was observed in the first series that the material flow was in axial direction; and as the contact length decreased, the moment causing the climbing or tilting motion increased. Therefore, in these experiments, it was observed that narrow mandrel causes more tilting. Another reason for this difference was the high oscillatory motion of ring when it was rolled by narrower mandrels. The same comparison was also valid for 2nd and the 4th configurations; however order of tilt was more in edge aligned mandrel than it was in center aligned ones. For the edge aligned mandrels fishtailing can be observed and amount of the fishtailing was more for narrow mandrels.

Another investigation on these experiments was based on residual stresses. The residual stresses induced in the workpiece after incremental and conventional ring rolling were compared. However for this time; the rings with same initial and final dimensions were rolled in one step by conventional ring rolling and in three axial steps by incremental ring rolling. The schematic view is shown in **Figure 4.7**

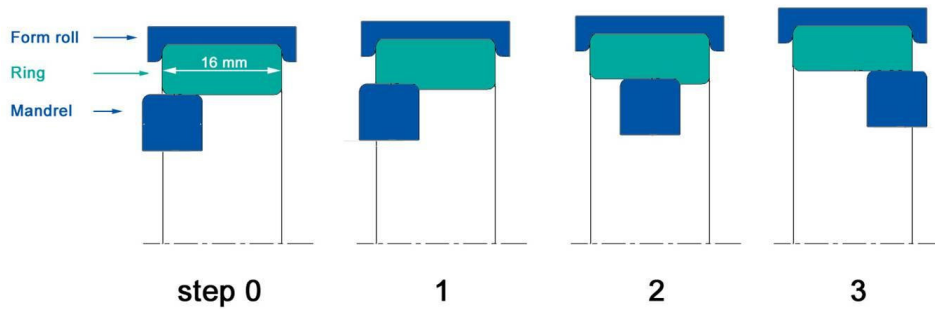


Figure 4.7 a) The schematic view of the process

Residual stresses were measured in XRD along the inner and outer face of these two rolled rings. The results of tangential residual and axial stresses for inner and outer face are given in **Figure 4.8-11**. It is observed that the axial variation in the residual stresses along the surface of the ring is more than it is in conventional ring rolling. The axial variation in the stresses in incremental ring rolling is due to slight variations of the penetration of each increment. Also the rate of instability is higher in incremental ring rolling, the back-up rolls used to reduce the oscillations hence the instability is induced.

The graphs are given in **Figure 4.8-4.11** show that the residual stresses were more tensile in incremental than it was in conventional ring rolling. The trend of the distributions were similar, however there were big differences in magnitudes. The difference was biggest in tangential stress on the inner surface of the ring and lowest for the axial stresses on the outer surface. The errors for these measurements are ± 0.5 mm and ± 20 Mpa.

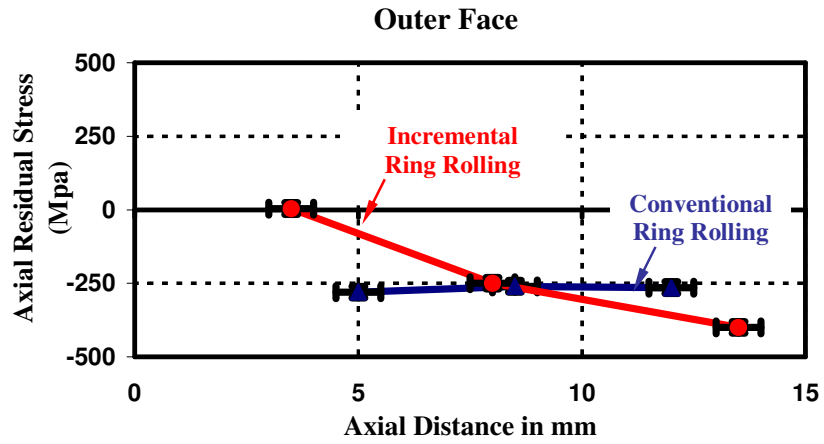


Figure 4.8 Axial residual stress distribution on outer face

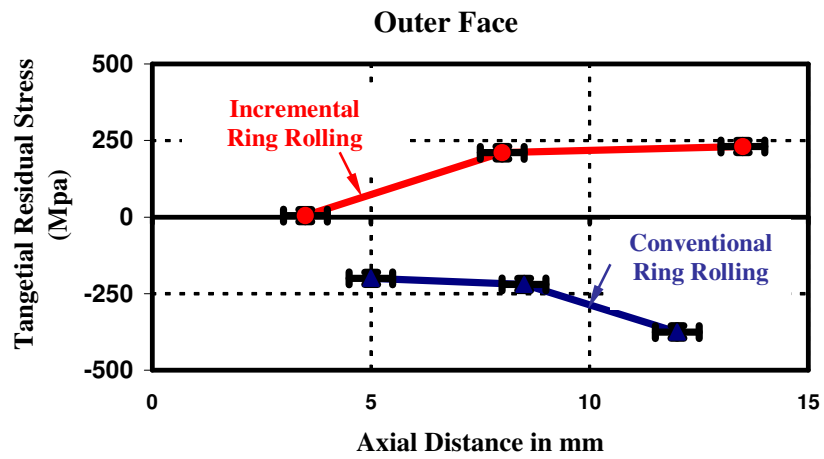


Figure 4.9 Tangential residual stress distribution on outer face

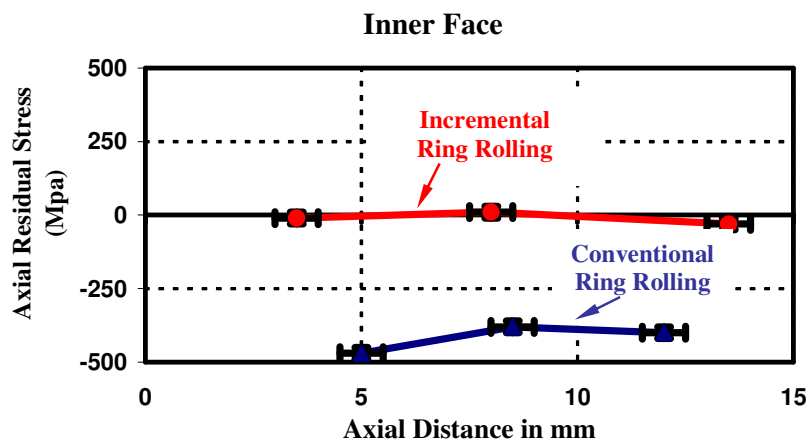


Figure 4.10 Axial residual stress distribution on inner face

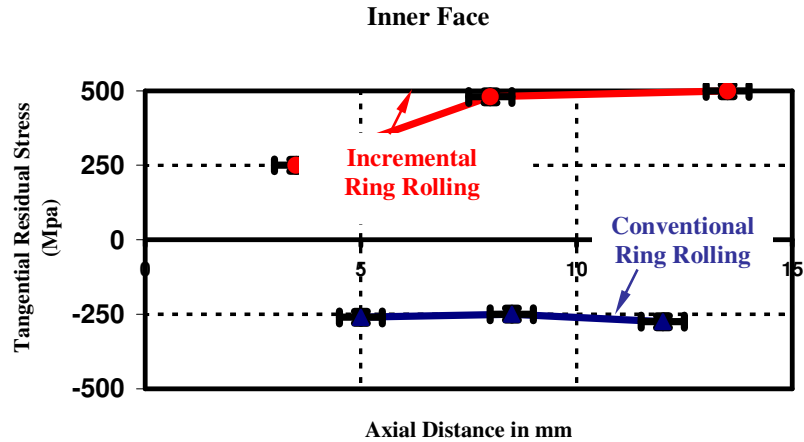


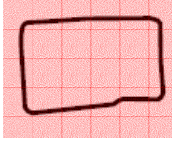
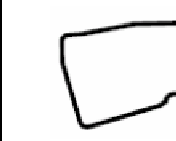
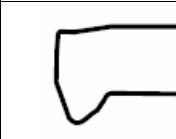
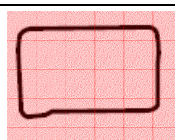
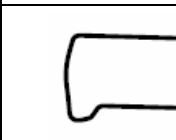
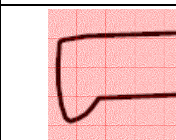
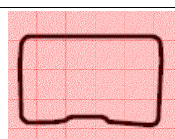
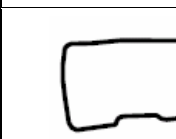
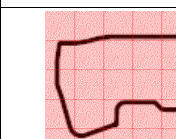
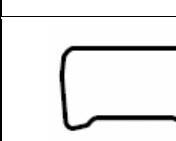
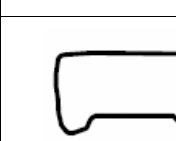
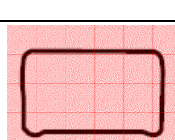
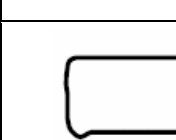
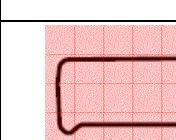
Figure 4.11 Tangential residual stress distribution on inner face

4.4.3 Third Series of Experiments

The aim of this series was to investigate the effect of rolling parameters on the profile, the residual stresses and stability. These experiments were continuation of second series however the approach was more systematic. The ring was formed using four mandrels with different widths (5, 7.5, 10 and 12.5 mm) and positioned from the edge and center of the ring respectively. The configuration was similar with the one in **Figure 4.6**. The experiments were conducted with 1, 2 and 3 mm penetrations. Totally 24 experiments were performed, and the final shapes were observed and compared. Also, the residual stresses were measured using XRD.

The experiments were performed under constant forming speed (150 rpm) and feed (0.4 mm/sec). The tools were made of the same material. The experiments were performed under same conditions, however some variations occurred due to oscillations which highly depended on the width of the mandrels; the amount of desired penetration could not be reached in some of the samples, and many trials failed. However results shown here are from the trials which were conducted with less failure. In **Table 4.4**, the profiles of the rings are shown.

Table 4.4 The final profiles of the rings

		Penetration [mm]	1	2	3	
		Width of the mandrels (mm)		Edge Aligned Mandrel	5	
7.5						
10						
12.5						
Center Aligned Mandrel	5					
	7.5					
	10					
	12.5					

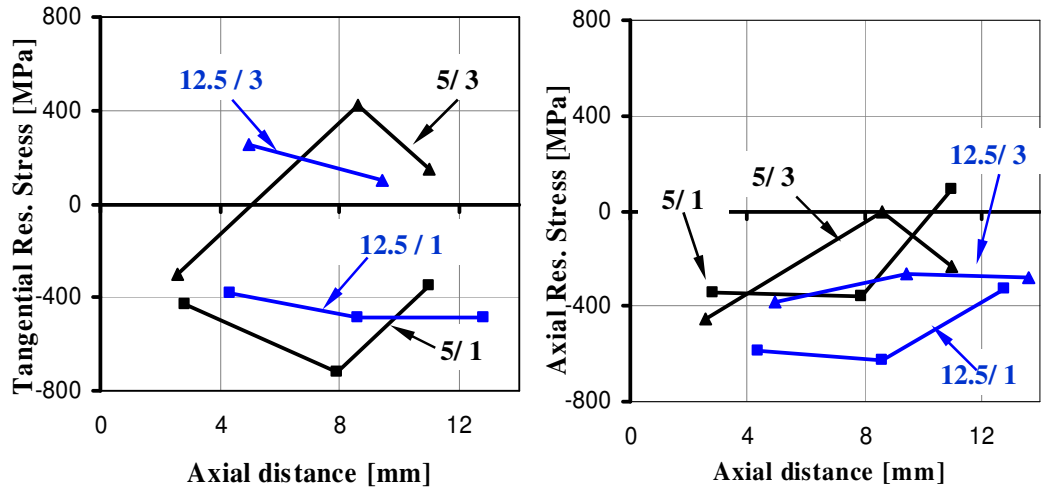
In the given table, the final profiles of the rings give important information about the material flow during the process and the effect of mandrel width and penetration on the stability of the process. For 1 mm bite, almost in all configurations the rates of irregularities in the profile, which are indicators of instability, are low when the first column is observed. During experiment, the amount of the bite was controlled more easily than it was in others. However as the amount of the bite was increased, it was examined that the irregularities increases. This means that the stability was not reached, the characteristic of the process is a obviously non-steady state. Another observation for bite of 2 and 3 mm, which was also examined in the first and second series, was related to mandrel width. It was systematically shown that as the mandrel width was increased, the rate of irregularity decreased hence this means that the process with wider mandrels was steadier.

The fishtailing out defect was observed in the edge aligned mandrel configuration and as the amount of the bite increased the order of this defect also increased. The faces of the rings were conical and in the center aligned case the cambering was observed. The material flow out to the surface creates cambers on the surface.

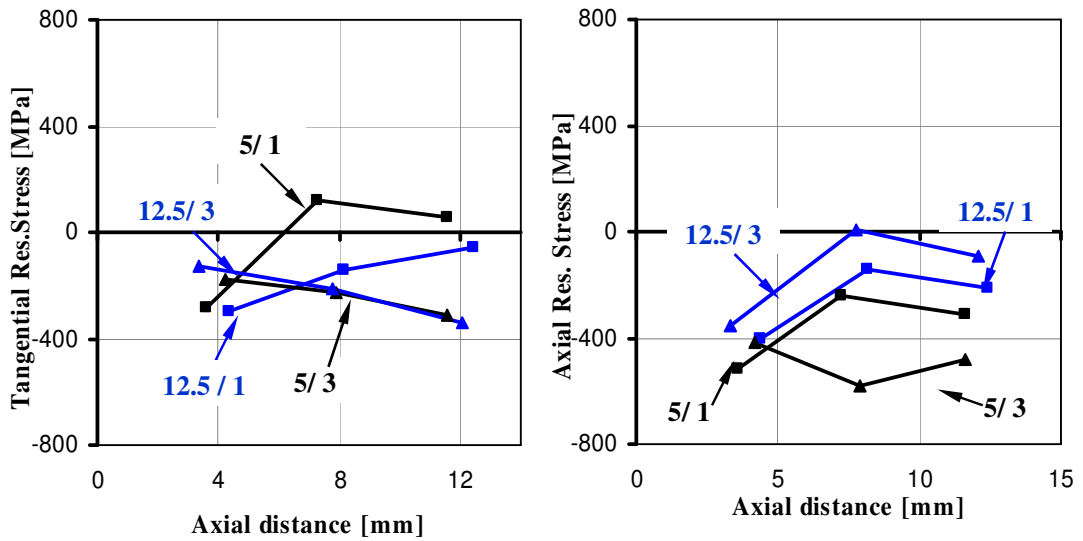
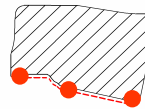
The process with the center aligned mandrel approached to conventional ring rolling process as the width of the mandrel was broadened. Hence the irregular profiles were not extensively observed for center aligned cases. The most irregular shape for this configuration observed in the process with 5 mm mandrel. This also indicated that regardless of position of the mandrel, the narrower mandrels caused instability which brought irregular deformation

The residual stress measurements were also taken for this series using XRD. It takes long to get measurements, as it is stated in *Section 2.3*. It takes approximately 100 minutes to obtain the stress components at a point either on inner or outer surfaces of the ring. If the measurements had been taken from three points for each of inner and outer surface of the 24 pieces, it lasted about 120 hrs

which was approximately 15 working days of the operator. Because of this reason, the measurements are not taken from all samples; only 8 of the samples were chosen which are indicated by red highlights in *Table 4.4*. The residual stress graph of the samples are given in *Figure 4.12-13*.



a) Inner face measurements



b) Outer face measurements

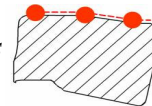
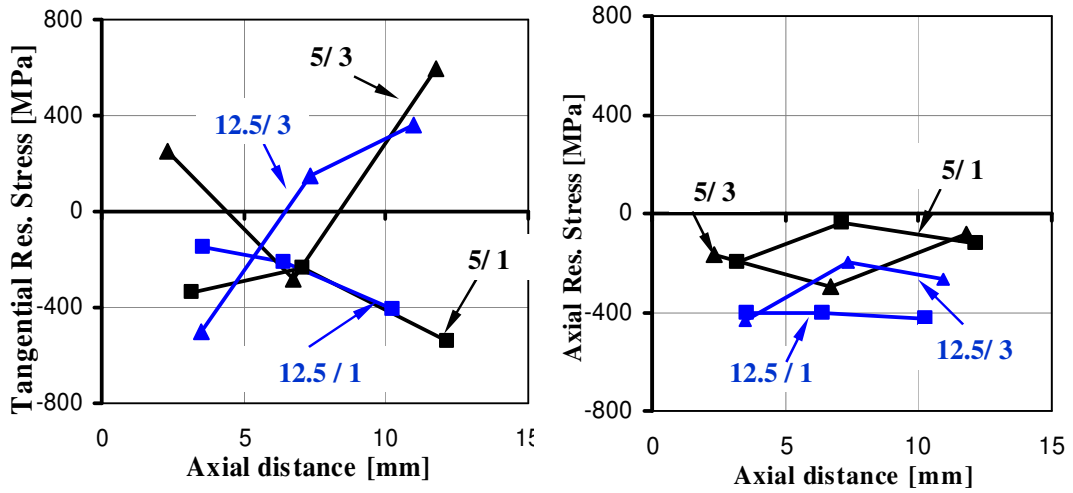


Figure 4.12 Tangential and axial residual stress distribution on **a)** inner face; **b)** outer face of the ring in edge aligned mandrel configuration.

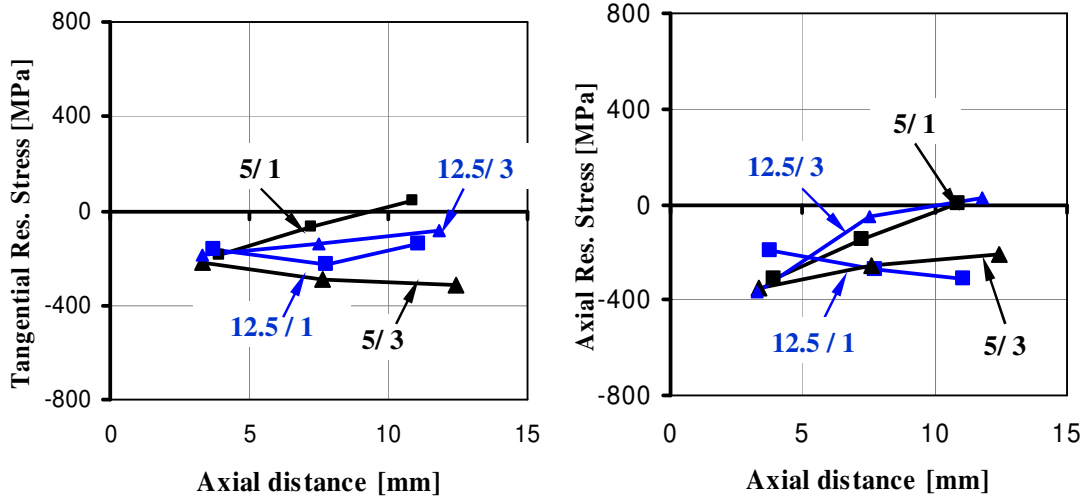
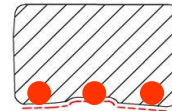
In the **Figure 4.12**, the stress values are given for the edge aligned configuration with the mandrels having 5 and 12.5 mm respectively. On the graphs, 5 and 12.5 designates the mandrel width and the 1 and 3 indicates the amount of the bite. The measured points vary since the measurements were taken according to points that are marked before experiments were performed.

In the **Figure 4.12a** it is observed that tangential residual stress variation for 1 and 3 mm bite differs extremely. The difference at the second data point is about 1000 MPa with 5 mm mandrel, which is extremely high. This difference is smaller in process with the 12.5 mm. It indicates that the smaller mandrels induce more residual stress on the workpiece at high deformations. It was also observed in the first and second experiments that narrower mandrel caused more tilting and conicity at high bite rates, which causes high tangential residual stresses. The axial residual stress variation is less than it is in tangential stresses. The ring was axially free during the experiments, however it there is an extensive ring elongation in width direction, this induce residual stresses after release of loads.

The measurements on the outer faces (**Figure 4.12b**) shows that the residual stresses for 5 mm and 12.5 mm widths differ at 1 mm bite although having similar trends. However as the bite is increased to 3 mm, the results converge after about 8 mm axial distance. At high deformations, the tilting cause contact release, on the side near mandrel (after about 8 mm axial distance), so that no friction force on tangential direction is exerted on this side. The circumferential stress on outer face changes in a steady-state trend. The residual axial stresses vary for process with 5 mm mandrel width significantly however the difference is not high for 12.5 mm width case. The oscillations are more in narrow mandrel case than they are in wider ones, the excessive oscillations cause sliding motion on the ring hence irregular deformation as it can also be seen from **Table 4.4**.



a) Inner face measurements



b) Outer face measurements

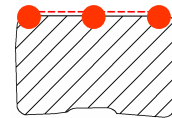


Figure 4.13 Tangential and axial the residual stress distribution on *a) inner face;*
b) outer face of the ring in center aligned mandrel configuration.

The residual stresses distribution shown in *Figure 4.13* for center aligned mandrel configuration. The tangential residual stress variation between the outer and inner surfaces is higher in center aligned case than it is in edge aligned. This variation can be defined as the difference between the maximum and the minimum of the three stress values measured. The outer and inner residual stress variations are given in *Table 4.5*.

Table 4.5 Variation in residual stresses for different configurations

Mandrel position	Mandrel width	Measured Surface	Tangential Residual Stress Variation		Axial Residual Stress Variation	
			1 mm	3 mm	1 mm	3 mm
Edge Aligned	5	inner	370	450	450	450
		outer	345	345	280	160
	12.5	inner	110	150	300	115
		outer	240	215	264	360
Center Aligned	5	inner	305	880	165	130
		outer	235	100	315	140
	12.5	inner	260	860	30	233
		outer	85	110	120	400

The tangential stress variation is maximum in the center aligned case for both type of mandrels at high deformation rates (5/3 and 12.5/3). However when the axial stress variations for these configurations are checked it is observed that they attain lower values. When the table is examined it is observed that the effect of amount of bite on variation is more significantly seen at center aligned case. For example, amount of variations for 5/1 and 5/3 edge aligned configuration are 370 and 450 MPa respectively, which means 20% increase. However these variations for 5/1 and 5/3 center aligned configuration are 305 and 860 MPa, which means more than % 200 increases.

The tangential stresses are higher for center aligned case, in the edge aligned configuration the stresses are reduced with tilting action; however tilting is less in center aligned case which induces higher residual stresses on workpiece.

Another outcome of the experiments was the detection of tool wear. During the experiments, same forming loads exerted by form roll, however the mandrels which countered the load, varied in dimensions. The narrower mandrels carry approximately the same load as the wider carry, thus high stress was exerted on the narrow mandrels. The abrasion was detected especially at the edge of the mandrels, and the amount of the abrasion was excessive on mandrel with 5 mm width whereas there was no visible damage on the one in 12.5 widths.

4.4.4 The Experiment conducted for numerical modeling

Many experiments were performed to investigate the material flow and stability of the process and also to examine the residual stresses. However, it needs extensive labor, material, tooling and time, in other words it is expensive. Especially time for measurements are extremely long, just for determining stress state on a single point approximately 2 hours spent. As it was stated in previous chapter, the aim of this thesis is to find an efficient numerical model to investigate all of the parameters mentioned. However it is important to verify the model with experiments. Therefore, an accurate experiment should be conducted to model the process.

The experiment which was used to verify the numerical models was 3rd configuration in the second series of experiments shown in **Figure 4.6** in second series. The amount of the bite was 1.1 mm. The reason for choosing this experiment is explained in the numerical modeling part.

The conducted experiment was analyzed in more detail than the other experiments. The aim of numerical modeling is to obtain accurate results in terms of geometry and residual stresses. Therefore in the analysis of the experiment, the final profile

of the ring is measured by profile measuring machine, and the residual stress data are taken on XRD precisely. In the stress measurements, the stress state at 9 points on outer face and 8 points on inner face is used, which takes approximately 5 working days.

The geometry of the final shape is given in *Table 4.3* before, and it will also be compared with numerical models in proceeding chapters. The tangential and the axial residual stress distributions on inner and outer surfaces are shown in the *Figure 4.14-17*. The data points were selected considering the irregular geometry of the specimen. The data measurements were more difficult at the edges of inner and outer surfaces and at the region where tilting starts on the inner face. The errors of the stress measurements are taken as ± 50 MPa and ± 0.5 mm for each data point.

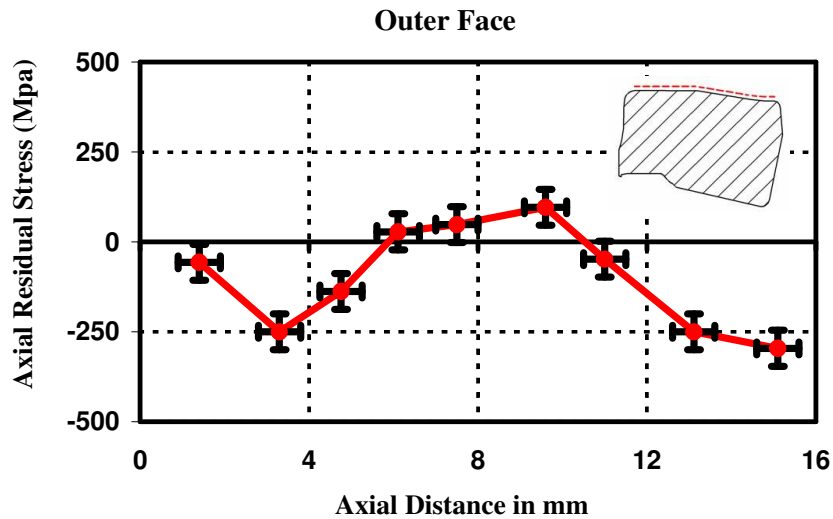


Figure 4.14 Axial residual stress distribution on outer face in the experiment for validation.

In *Figure 4.14*, it can be observed that there is a non-uniform stress distribution on outer surface. The axial residual stresses are compressive in regions close to edge whereas tensile in mid regions. The magnitudes of the compressive residual stresses are high.

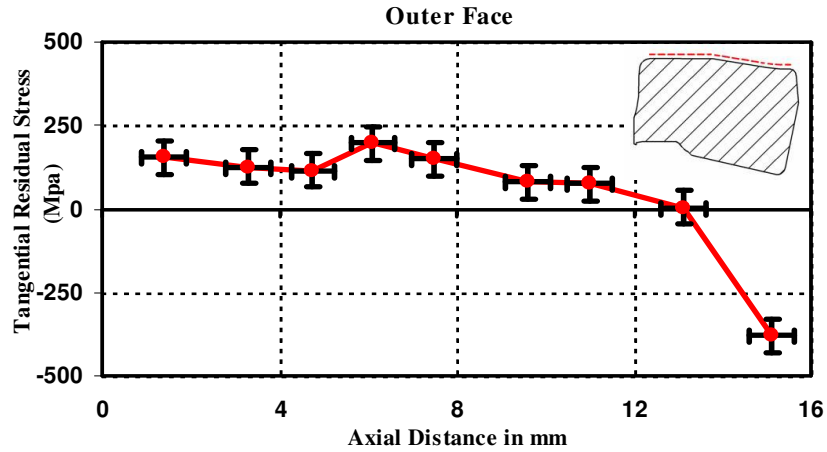


Figure 4.15 Tangential residual stress distribution on outer face in the experiment for validation.

In *Figure 4.15*, it is seen that the tangential stress distribution is more uniform when compared with the axial residual stresses. The stresses are tensile except for the region close the edge of the ring. The magnitudes of the tensile stresses are low.

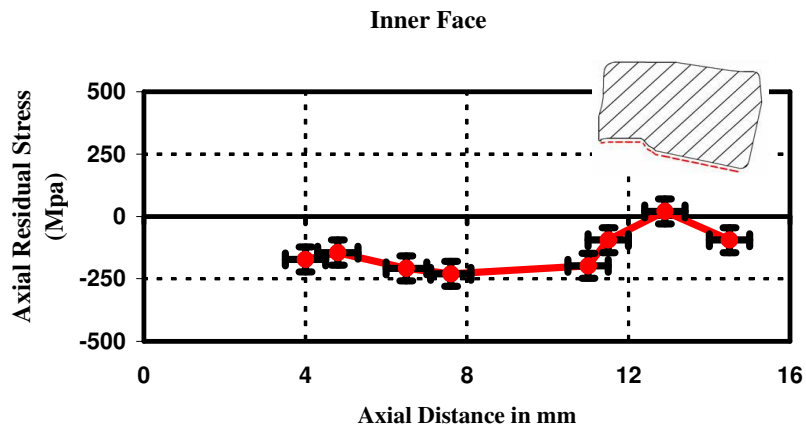


Figure 4.16 Axial residual stress distribution on inner face in the experiment for validation.

In *Figure 4.16*, it is seen that the axial stress distribution is more uniform on inner face when compared with outer face. The stresses are compressive except for a small region close the edge of the ring.

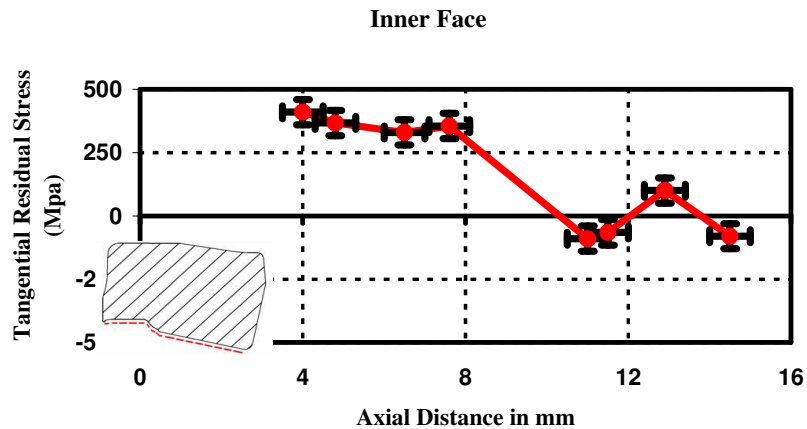


Figure 4.17 Tangential residual stress distribution on inner face in the experiment for validation.

The tangential stress distribution on inner face is not uniform, tensile at the regions where there is a surface to surface contact with the mandrel; however it is compressive on the region where the contact can be assumed as point to point because of the edge of the mandrel. Although it has small fillet, the stress induced is high at that region. The measurements at this region are not reliable as the others.

In summary, systematic experiments were conducted and material flow characteristics was observed, the effect of process parameters on stability and residual stresses are analyzed. The analyses were performed in one of the configurations in detail, which was used to validate the experiments.

CHAPTER 5

NUMERICAL MODELS

In this chapter, the finite element (FE) models developed for simulation of the incremental ring rolling process will be presented. The parameters affecting the models will be introduced. The boundary conditions, basic assumptions will be explained. The procedures followed in modeling will be mentioned and need of some additional requirements such as utilizing from user-subroutine and algorithm developing will also explained. In modeling, commercial packages MSC. Superform and MSC Mentat were used.

In this study, the models were developed systematically. The analyses were started from simple models that were prerequisites of the proceeding ones. First of all, previous models for conventional ring rolling- 2D Full Model, 2D Rigid Segment Model and 3D Full Model- were examined and modeling parameters were studied. The numerical investigation was started using the experience gained from analyses of these models; a simplified model was developed for conventional ring rolling and was called as *3D Segment Model*. Secondly, based on the experiences on conventional ring rolling process, a reliable 3D Full Model of incremental ring rolling process was simulated, which had deficiency of long computing time. Finally, the simplified model developed for conventional ring rolling (*3D Segment Model*) was adapted to incremental ring rolling process using special boundary conditions and user-subroutines. Three types of segment models were developed, 3D Segment Model, 3D Segment Model with Soft Elastic Region and 3D Velocity Coupling model. All of these models will be presented in proceeding parts. In **Table 5.1** a summary of models presented in this chapter is given. In the table, the needs of developments and analyses of the models are stated.

Table 5.1 Summary of presented models

<i>Conventional Ring Rolling</i>	
<i>Two-Dimensional (2D) Full Models</i>	Investigated to understand the nature of the numerical modeling. Finding optimum numerical parameters mesh topology, step size, relative force tolerance, contact parameters etc.
<i>Two-Dimensional (2D) Segment Model</i>	The model was examined to understand the simplification method for implementing it to 3D models.
<i>3D Full Model</i>	The model was analyzed to be used as a reference model for simplified models.
<i>3D Segment Model</i>	It was developed on the basis of 2D segment model and 3D full model. This model became a prerequisite for other simplified models
<i>Incremental Ring Rolling</i>	
<i>3D Full Model</i>	This model was developed to be used as a reference model for simplified models.
<i>3D Segment Model</i>	This was direct implementation of 3D segment model used for conventional ring rolling. However some improvements were needed.
<i>3D Segment Model with Soft Elastic Region</i>	This is the improved version of 3D segment model.
<i>Velocity Coupling Model</i>	This model was supported by user subroutines to apply the special boundary conditions and constraints. Based on the assumption of coupling velocities of boundary planes of a partially modeled ring segment.

5.1 Numerical Models for Conventional Ring Rolling

All numerical models presented here are based on some basic assumptions and characteristics in modeling, these are valid for all of them unless otherwise is stated. The basic assumptions and the characteristics of the process are given as follows

- 1) The modeled process consists of two main stages: initial squeeze that provides adequate initial contact between the ring and the tools, and the rolling step in which form roll is rotated with a constant rotational speed as well as being translated with a constant feed.
- 2) To start the rolling initial contact is needed and at the initial squeeze step, the ring should be squeezed such that it is contacted with the forming roll and the mandrel with at least three nodes. This is important for accurate shear stress distribution along the surfaces in contact. And if the contact occurs within less than three nodes, the slipping condition of the ring on the tools, and instability is observed in the rolling step.
- 3) The elastic deformations on the tools are neglected and the tools are assumed to be rigid.
- 4) The mandrel is idle, and this characteristic can be given by using *load control option*, which models the mandrel as a rigid, rotational tool. This will be explained in next sections.
- 5) The rigid tools are modeled using NURBS (Non Uniform Rational B-spline) option, provided by the program. This enables modeling the tools analytically, which provides more accurate calculations of the surface normal and a smooth continuous surface with high accuracy in contact formation.
- 6) The effect of the supplementary tools such as guide rolls and back-up rolls are neglected.
- 7) The material model is selected as elastic-plastic and the flow curves data is obtained from torsion tests of ORS Bearing Company.

- 8) The friction factor is selected as 0.08 and Coulomb friction law is used
- 9) As it was stated in Chapter 3 the process is isothermal. The temperature is kept 40°C during whole process.
- 10) Eight-node brick element is used in the 3D analyses.

5.1.1 Two-Dimensional (2D) Full Models

The 2D models mainly based on the plain strain assumption. This assumption can not be used for incremental rolling process since the plain strain is assumed for width direction and the process is based on forming in incremental steps. However this model was used to analyze the nature of the process and control of numerical parameters. In the *Figure 5.1* the model is shown. The strains; ε_z , γ_{yz} and γ_{xz} are zero.

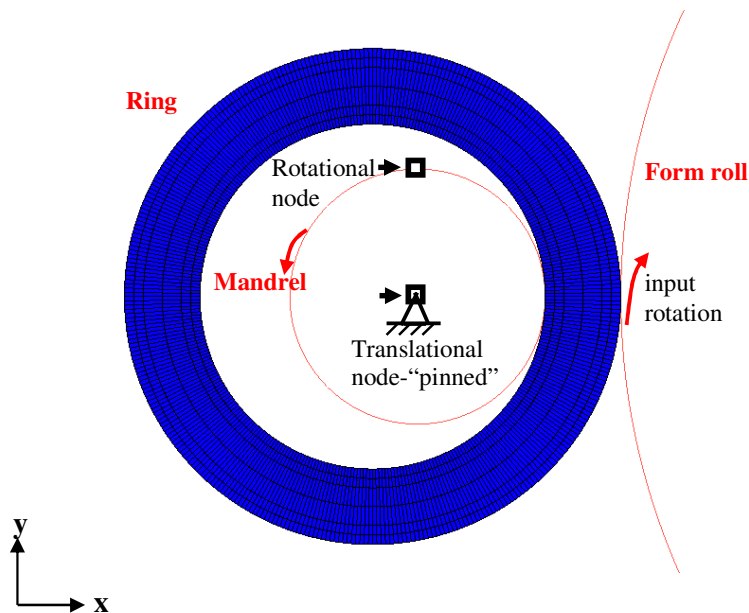


Figure 5.1 Plane strain model with load control option

The mandrel modeling is an important issue in numerical modeling; there are two ways of modeling the mandrel. First one is modeling mandrel as a deformable body. This approach makes the rigid body assumption waived, however increases

the computation time. Another approach is the “load controlled body” option which is available in MSC.Superform and MSC.Mentat. This was used in modeling all of the proceeding models. In this option, two nodes are attached to rigid body and these nodes control the translational and rotational motions of the body. This enables assigning boundary conditions to the rigid body to control the motion of the body. The *Figure 5.1* also shows the translational and rotational nodes attached on the body. The translational node was attached to center of the mandrel and the rotational one was on the outer rim. The rotational node stores the angle of rotation of the rigid body, in this case mandrel.

The model consists of two basic steps of the process; the initial squeezing, which provides adequate contact formation for the next step and the main rolling step. In the plain strain model no displacement boundary condition is applied to rotational node, this leaves the mandrel free to rotate. However, the translational node is fixed in x- and y- directions by a displacement boundary condition, thus the mandrel rotates as it is fixed in a pin joint.

5.1.1.1 Numerical Parameters

The numerical parameters were studied using the models developed in previous studies. In previous studies, the convergence testing had been performed (Music 2005). This test is used to check the validity of the model. It consists of modeling the same process with different mesh topologies and comparing the stress distributions.

The converging testing performed in this study involved simulating the process with five different meshes, as shown in *Figure 5.2*. The topology of the mesh directly affects the results of the simulation. Increasing the number of elements provides more accurate results, however the computation time increases approximately in order of square. In the convergence testing, the circumferential and the axial stresses along the radial direction were compared, since in the ring

rolling process the gradients occur in radial direction. The results of these studies showed that there were high stress gradients both in the inner and the outer surface of the ring, these gradients converged to certain values in inner part whereas failed to converge at the outer parts. In this thesis, this gradient was investigated by changing purely numerical parameter related to convergence: convergence criteria and the tolerances.

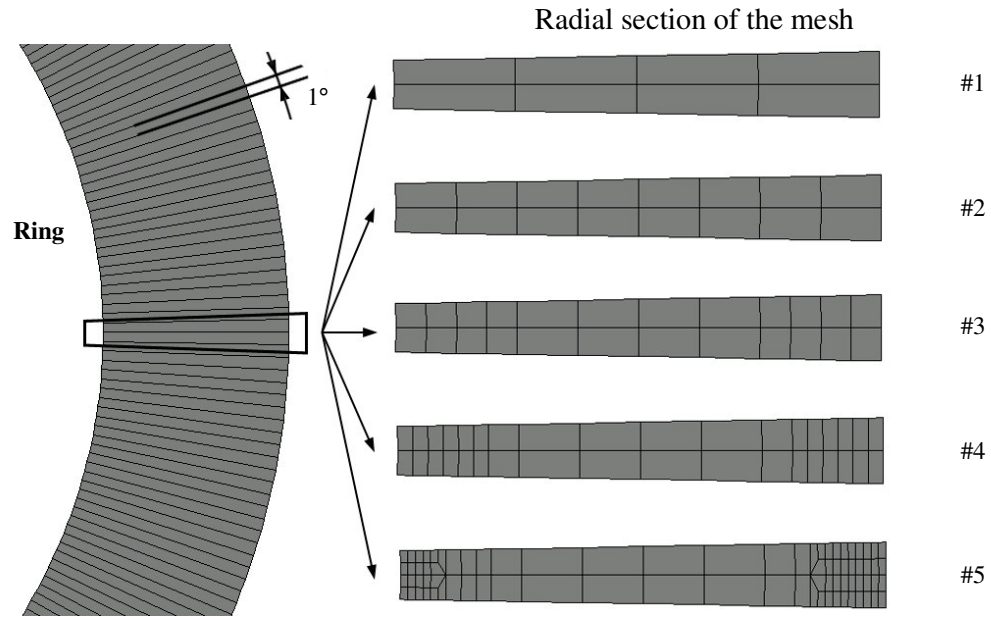


Figure 5.2 Mesh topologies used in the analyses (Music 2005)

An important aspect of nonlinear analysis is the selecting of the convergence criteria and the tolerances. The convergence criterion selected in the model is based on converging to a solution when the ratio of the maximum residual load to maximum residual (out-of-equilibrium) force is less than or equal to a specified value, which can be defined by the user with a parameter; the *relative force tolerance* (ξ). The default value for ξ is 0.1 in the program. As the ξ is decreased, the accuracy will increase with a cost of increase in computation time. The analyses were performed with ξ values of 0.1 in previous studies (Music 2005). In this thesis the convergence testing repeated for the ξ value 0.01. The results of the analyses are shown in **Figure 5.3**. The mesh no.1 is coarse and there are only 4

elements in radial direction which is inadequate, and the mesh 2 has two times more elements than mesh no. 1. The stress distributions along the ring section for mesh no.1 and mesh no. 2 show high stress gradients in the inner and outer sections of the ring. The differences between the stress values are high for these models. These differences are lower for more refined meshes, the number 3 and 4, which is an indication of converging to a certain value. Similarly the difference is less for mesh 3 and 5.

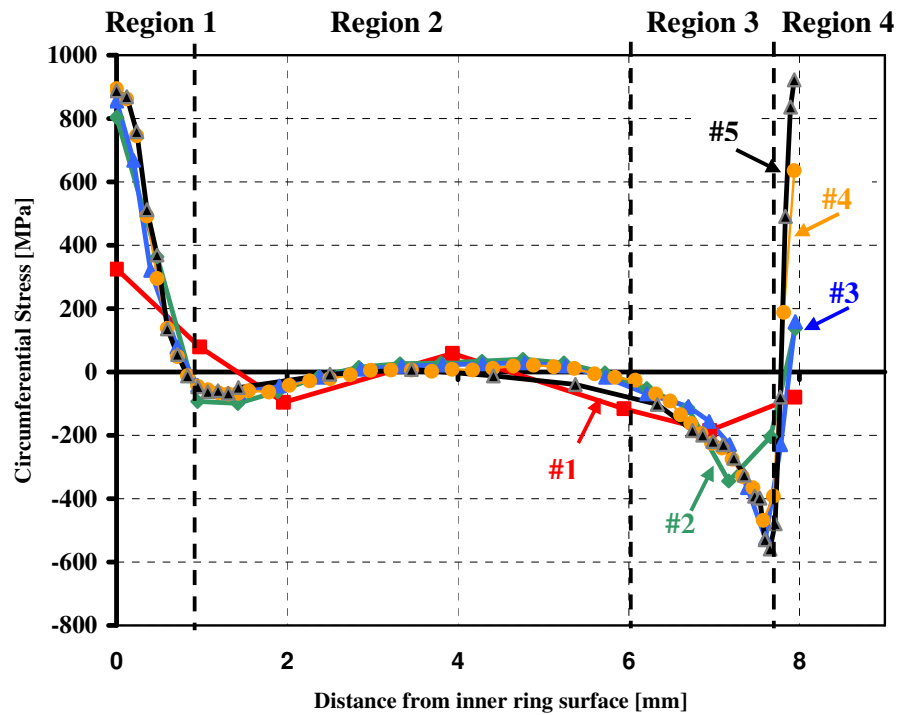


Figure 5.3 Circumferential stress distribution in radial direction for different mesh topologies and for $\xi=0.01$

The aim of this analysis was to investigate the effect of relative force tolerance (ξ) on the gradient at the inner and outer parts of the ring. There is a gradient in the inner surface which converges to certain values, for both $\xi=0.1$ and $\xi =0.01$. However, in the outer surface it does not converge the for both cases, hence the residual stresses on the outer part of the ring, can not be predicted accurately with these models. In the inner part, the contact between the mandrel and the ring is

outer-inner contact which is easier in terms of contact formation than the outer-outer contact condition between the form roll and the ring. The convergence difference between the inner and the outer side is due to distinct contact conditions of on each sides. However as mesh gets finer the difference reduces as shown in the figure. It is difficult to catch this gradient.

The stress variations between the results of models with different meshes exist for both $\xi=0.1$ and $\xi=0.01$ cases. These variations converge to certain values and they are lower for the $\xi=0.01$ condition. In order to examine the variations, the graph in the *Figure 5.3* is divided to four different regions, because taking average will not directly shows the converged values.

Table 5.2 Comparison of variations in stress for different relative force tolerances

	Mesh #3 and #4		Mesh #4 and #5	
	Axial Residual Stress (MPa)	Circumferential Residual Stress (MPa)	Axial Residual Stress (MPa)	Circumferential Residual stress (MPa)
$\xi = 0.1$				
<i>Region 1</i>	9.70	39.80	4.20	0.90
<i>Region 2</i>	30.43	16.04	52.05	20.46
<i>Region 3</i>	32.30	25.50	104.74	101.86
<i>Region 4</i>	19.00	182.25	74.50	192.92
$\xi = 0.01$				
<i>Region 1</i>	3.45	39.90	3.25	2.90
<i>Region 2</i>	29.18	14.61	53.92	20.39
<i>Region 3</i>	25.80	23.20	96.82	96.64
<i>Region 4</i>	9.00	182.58	58.67	192.08

The average residual stresses values were calculated for each model at each region. The model with mesh no. 1 and 2 were eliminated for comparison. The difference between the average stress results of the models with mesh no.3 and 4, also mesh

no.4-5 were calculated. In the *Table 5.2*, the calculated results are shown. It can be observed from the *Table 5.2* that the, residual stress variations for different types of meshes decrease as the relative force tolerance parameter decreases. However, the amount of decrease is not significant when increase in computation time of the analysis is considered. The computation time increases by 2 times for the most refined model.

Apart from the relative tolerance other numerical parameters such as the step size, contact tolerance, contact distance bias, penetration check and the node separation were also investigated. In the previous works these parameters were worked extensively and reliable results were obtained. During the research step of the thesis these parameters were also investigated, and combination of these parameters were found. In these analyses the mesh number 3 was used.

Two of most important numerical parameters that were dealt the *step size*, which is the size in seconds of each incremental step in the analysis and the *contact distance tolerance* which is the distance below which a node is considered to be in contact with another body with a default value of 5% of minimum edge length of the element. These two parameters have great interaction between each other, because of the nature of the ring rolling process. The combination of these parameters is important for computation time, since they have direct effect on it. As the step size the contact distance tolerances are decreased, the computation time will increases. There will be an ideal step size for each contact distance to give minimum computational time. For each contact distance value, there will be an ideal step size that will allow nodes to contact and separate from the tools in a minimum number of iterations. In addition to computation time constraint, node sticking is another important problem related to these parameters. For high and low step size values, the node sticking on tools can be seen. The solution of this problem requires comprising of the parameters. There is a band of parameters in which node sticking is not observed and computation time is minimum. It was concluded that for default value of the contact distance tolerance (5% of minimum

element length) and for 0.1 sec of step size, the minimum computational time without node sticking can be obtained (Music 2005).

Contact distance bias, which is used to position the contact tolerance around the surface, is another examined parameter. The default value of the parameter is used in the analyses. It can take values from 0 to 1. In the analyses, this 0.95 is used. In the previous works the 0.45 was found to be optimum value for the distance bias (Music 2005). This value also tried and computation time decreased only by 4% hence 0.95 is also admissible.

The *node separation* is another parameter investigated. This is also important for node sticking problem. This parameter can be defined as the tensile force, stress or fraction of flow stress acting on the node, at which a node will be allowed to separate from the contact body. The stress options are used in the modelling since they are independent of element size, which is preferred in analyses including remeshing. The values should not be large, otherwise the node will not be able to separate from the body and the analysis may not converge to a solution. Large values also results in long computation time (MSC. Software, 2004). The values were determined according to contact stresses for this analysis 10 MPa is used.

The last parameter investigated is the *penetration check*, which defines the procedure applied to a node when it penetrates a contact body. There are three options available; increment splitting, iterative and none. In the analyses, “iterative” option, which applies Newton-Raphson type procedure to determine the solution, was used. This is the most efficient and recommended option. In the none option no penetration checking procedure applied and this is not recommended for a rolling analysis. The Increment splitting has the advantage of being robust, but it requires higher computational time as compared to the iterative procedure, which is more efficient but not as robust (MSC.Software, 2004). Thus, the more efficient and recommended option “iterative” has been used in all the analyses performed.

5.1.2 Two-Dimensional (2D) Segment Model

The full models are satisfying in accuracy, however the computation time for full models are long. The aim of the model presented here is reducing the computation time for the analysis with reasonable accuracy. This model was also developed in previous work (Music 2005), and in next sections the improved versions of this model will be presented. In this model, the plane strain assumption is also valid. The mandrel is modelled as a load controlled body and the defined boundary conditions for mandrel in full model are also applicable.

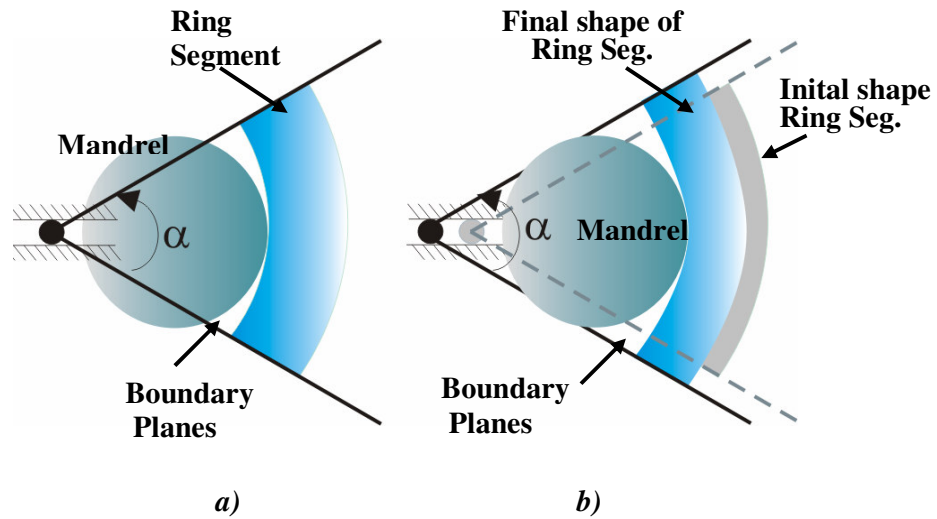


Figure 5.4 The 2D segment model; a) initial b) final configuration

In this approach, the ring is modelled partially assuming that remaining part as rigid. The rigidity of the remaining part is provided by two frictionless boundary planes with high separation stresses as shown in **Figure 5.4a**. These planes are modelled as a single rigid load controlled body; therefore the translation and rotation control nodes are attached onto the body. The planes have no relative motion with respect to each other thus the angle remains same. The motion of the planes is similar to motion of a bar moving in a cylinder in slot joint; they rotate about a common center of rotation point and fixed only in the vertical direction (translational node is fixed in horizontal direction), this enables sliding in

horizontal direction as in a slot. These motions of the planes let the ring slide in reverse direction and grow its diameter as shown in *Figure 5.4b*.

The model has a cyclic scheme different than the full model. Each cycle represents one single rotation of ring and consists of steps: approach, initial squeeze, rolling, tool release and moving the ring to its initial position. As the whole part of the ring is deformed and ring rotates, in order to continue analysis, the ring is brought to its initial configuration by tool release and rotation operations. During this cyclic analysis, many errors are observed especially at the rotation of the ring step. After completion of each cycle new analysis is performed using results of previous cycle. This leads interruptions in the analysis. An alternative method will be presented in order to prevent this problem in the next section.

In this model the computation time decreases however the results deviate from the full model with a maximum error of %7. As the reduction in the computation time which is almost one fiftieth of full model, is concerned, this error amount is reasonable. The main modelling parameter affecting accuracy is the segment angle. As the segment angle increases the model gives better results (Music 2005).

In this research the numerical analyses, performed in previous work for this model, were repeated in order to understand the approach and to validate the results for numerical parameters. The numerical parameters investigated in the full model are applicable in this model. The effect of relative force tolerance is also investigated for this model, in order to increase the accuracy. However it is found out that the increase in accuracy is in the order of 2.5%.

5.1.3 3D Full Model

In this thesis 3D Full model for conventional ring rolling was not investigated extensively, however the results obtained from the previous works presented for comparison with the developed models. This model is the straight forward

representation of the real process. The plane strain assumption is not used in these models. The only simplification used is the utilization of symmetry; in the width direction, ring is uniformly rolled using a mandrel having same width, thus dividing the ring in two from the middle will represent the process exactly. This simplification directly reduces the number of elements, then the computation time. The all assumptions mentioned at the beginning of this chapter are valid for this model.

The symmetry simplification is utilized by defining symmetry body option in the MSC. Superform; this treats the body as symmetry surface. The mandrel is modelled as load controlled body. However different boundary conditions are applied on the translation and the rotation nodes. The translation node is fixed in all directions, and the rotation node is fixed in two directions and it is left free in axis of rotation. As mentioned before the rotation node stores the angle of rotation of the body (if it is fixed in axis of rotation, the body will not rotate).

Numerical Parameters

Similar numerical parameters were investigated for this model. The convergence testing with different mesh topologies was also performed. However the analyses were performed for 3 meshes only, since the computation time was extremely longer (almost 15 times) than 2D models. This restricts the extent of refinement in the mesh. The stress distribution for three different mesh topologies was investigated. The results are shown in *Figure 5.5* and the stress values are collected in radial direction which is indicated on the mesh topology figures with red arrows.

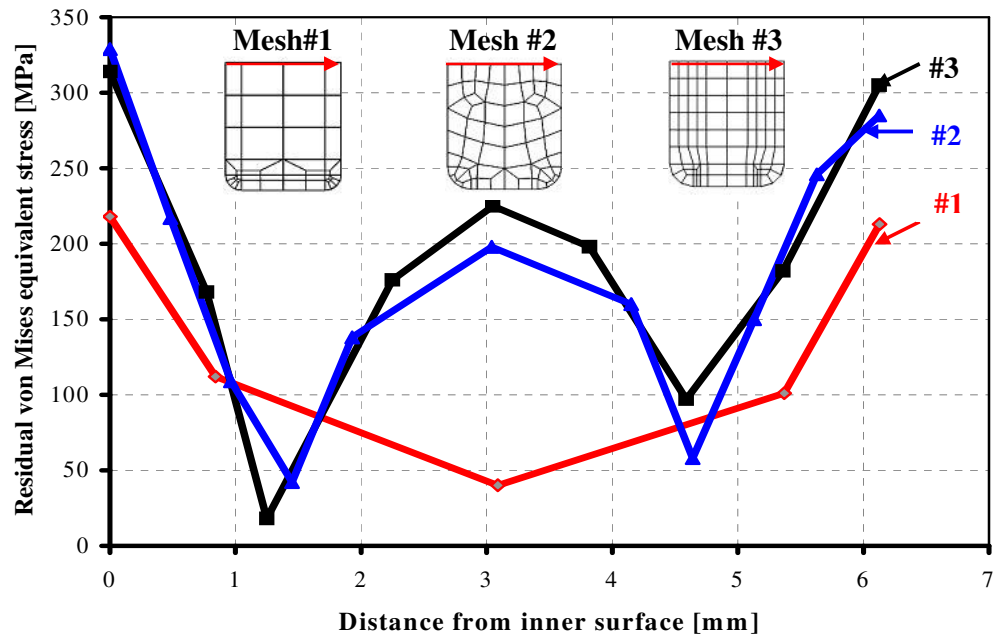


Figure 5.5 Residual Von Mises equivalent stress distribution for different mesh topologies (Music 2005)

The mesh number 1 is coarser and the results are completely different from two refined meshes. The distribution trends for two refined meshes -the number 2 and 3- are similar and there is an indication of convergence. If the mesh is refined further, it is expected to have similar trend with a reduction in variation. The stress gradient in the outer surface is also observed in this analysis. Independent of mesh topology the gradient does not converge to certain value. However as mesh gets finer the difference reduces. This investigation validates the outcome of previous convergence testing analysis for 2D model; the residuals stress at the outer surface can not be predicted by using these models accurately, the reason can be solved by special contact algorithms and further refinement, which is out of scope of this thesis.

The geometry of the tools and the ring differs in two- and three-dimensional analysis. The axial direction exists in the 3D modelling this increase the degree of

contact. However in the analyses it was shown that there was no significant difference in contact conditions and hence in the numerical parameters.

The step size and contact tolerance analyses showed that the minimum computation time was observed in a similar band with of the two-dimensional model (Music 2005). The computation time is minimal at the same contact tolerance (default value of the program) with small different step size (around 0.1).

The all numerical parameters investigated were found to be same or very close to ones mentioned in two-dimensional numerical modelling part.

5.1.4 3D Segment Model

In the previous sections, the analyses on previously built models were explained, as it was mentioned that these analyses were performed to understand the basic numerical parameters and the nature of the process modelling. This examining part was the most important step in this study to develop new models for incremental ring rolling process on the basis of this examination. Before going through incremental rolling analysis, a new model was developed for conventional ring rolling, which made easier to go the next step. This model is a 3D segment model, which is purely based on the assumptions in the 2D segment model and the 3D full model with some minor inclusions.

The model is shown schematically in the *Figure 5.6*. In this model the ring is also modelled partially with a constant angle, and the remaining part of the ring is assumed to be rigid by using rigid boundary planes. The boundary planes are modelled as load controlled body. Different from the 2D Segment model; in this model, the rotation node is fixed in two directions (in x-, y- directions in *Figure 5.6*) while keeping free in direction of rotation. The symmetry is also utilized in this model and symmetry body is used. The mandrel is modelled as in 3D model.

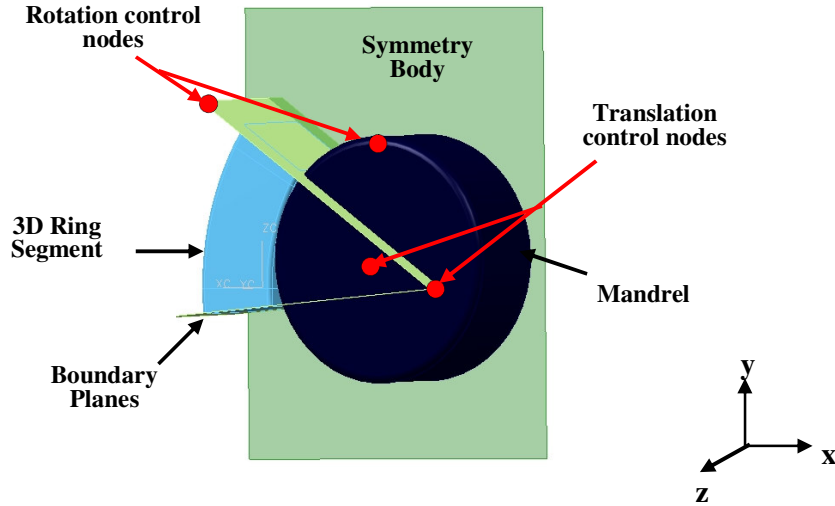
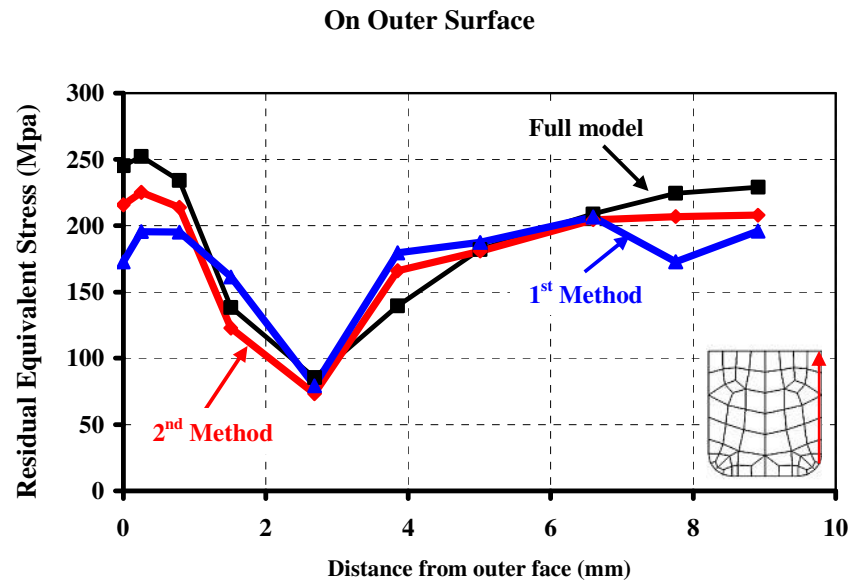


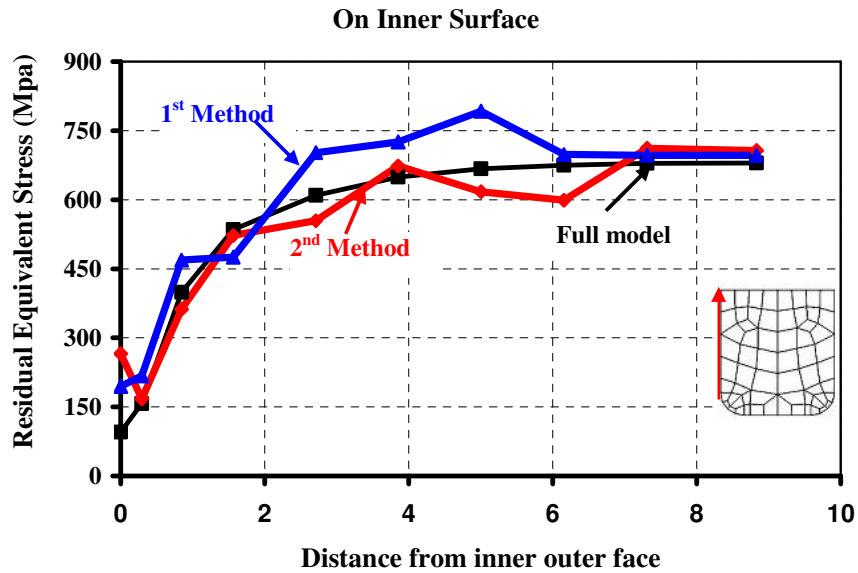
Figure 5.6 The elements of 3D segment model

As mentioned before, the segment model has a cyclic scheme consists of number of steps. Each cycle consist of approach, initial squeeze, rolling, tool release and moving the ring to its initial position, which represents one single rotation of ring. As the whole part of the ring is deformed and ring rotates, in order to continue analysis, the ring is brought to its initial configuration by tool release and rotation operations (called as 1st method in proceeding parts). However this method creates problems in terms of computation time and contact formation problems after the rotation step of the ring to its original position. An alternative method (called as 2nd method in proceeding parts) is proposed to eliminate these problems. This method reduces the steps of a cycle to initial squeeze and the rolling. After whole part of the ring is rolled, one cycle is completed and the second cycle starts without interruption just by rolling the form roll in reverse direction. This method reduced the computation time and it was found out that it enhances the accuracy.

The equivalent stress distributions for both methods are compared in **Figure 5.7a-b**. The results are compared with the full model results. In this analysis mesh number 2 in **Figure 5.5** was used and the data was collected from the points on the red arrow line.



a)



b)

Figure 5.7 The residual stress distribution on a) outer surface b) inner surface of the rings for two different methods of cycle

The error accumulated for both models are calculated with respect to full model results: the error of on the outer surface of the ring is 13.1% and 6.9%, on the inner surface it is 9.4% and 5.8% for the first and the second models respectively. The

computation time is 7.5 hours for the first model where as 5.5 for the second model. Hence the modelled is improved for both in accuracy and computation time. This shows the efficiency of the second method.

The computation time decreases with this model depending on the segment angle used. The accuracy of the model also depends on the segment angle. The analyses were performed to observe this dependency, will be presented in the next chapter. This model is efficient in terms of computation time and the accuracy level is reasonable. Therefore, this model will be a based model for the models presented in proceeding sections.

5.2 Numerical Models for Incremental Ring Rolling

The models presented in this section are developed on the basis of the analysis performed in the previous sections. Four different models are presented in this section. The main aim is to find a simplified model that is verified with experiments and with reliable numerical model. The previous studies showed that the 3D full models provide the most accurate results; hence the simplified models will be compared with the 3D full model. However it is not easy to obtain an accurate model. Although near-optimum numerical parameters studied in the previous section reduce the modeling time and the trial and error procedure reasonably, the time spent for computation is extremely long.

One way of reducing the computation time is to choose a simple process to model. Thus, the process investigated becomes the main issue; in this sense, the process was selected as the 3rd configuration as shown in ***Figure 4.6***. As mentioned before, this configuration does not involve any axial or radial movement of the mandrel. The narrow mandrel is aligned from the edge of the ring and it is free to rotate while being stationary in axial and radial directions, this configuration helps to reduce the computation time by reducing the degree of freedom of contact formation. Another reason to select this process is easiness of the experimentation

in the process. At the end of the process, non-uniform deformation and tilting occurs, hence it will also be possible to investigate these behaviors with numerical models.

Various configurations were modeled and analyzed during this study however in this thesis only verified models are presented

5.2.1 3D Full Models

These models are also straight forward representations of the process. There are no basic simplifications that differ from the original process. The characteristics of the models are same with the conventional ring rolling models. The process also consists of two stages: the initial squeezing and the rolling. There are few differences in boundary conditions and meshing topologies and the numerical parameters used.

The mandrel was also modeled as a load controlled body and the boundary conditions applied on the mandrel were same. The main difference with the previously studied model was the lack of symmetricity in the current one. The schematic representation of the process is shown in the *Figure 5.8*. The narrow mandrel was aligned to edge of the ring, so the symmetricity simplification and modeling half part of the ring in width direction is not applicable. This extremely increases the computation time. However the contact length can be smaller in the incremental case, this reduces the computation time. (The computation time for a model with reasonable accuracy is about 14 days)

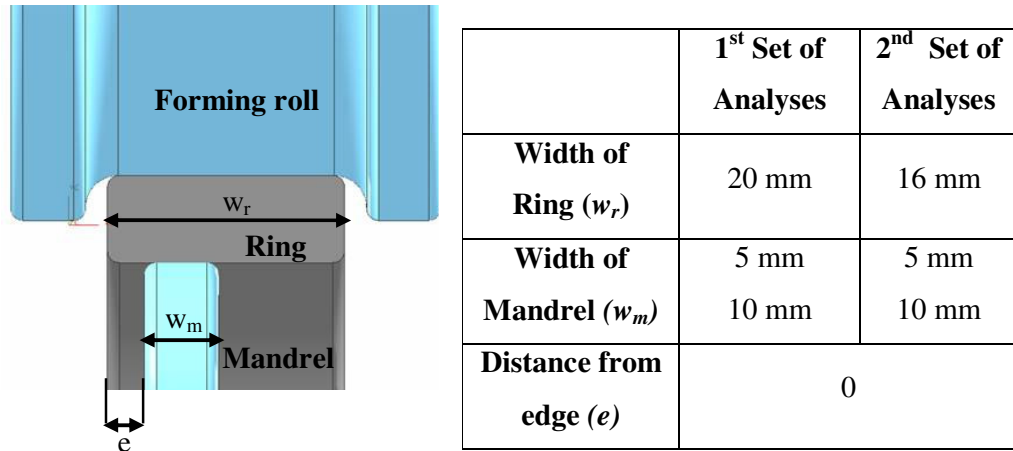


Figure 5.8 Schematic representation of the model and the set of analysis

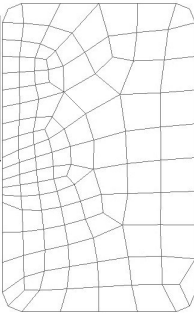
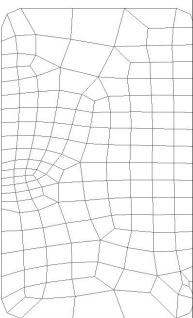
At the first studies on numerical modeling, it was observed that the ring oscillates in the axial direction, at the initial squeezing step and the early stages of the rolling step. The main reason was thought to be wrong selection of contact parameters, then contact tolerance and distance bias parameters were decreased, however the oscillations could not be prevented. It was also observed in the experiments that the ring oscillated at early stages, especially for narrower mandrels. The reason for the oscillations was explained in the previous chapter. With these oscillations, analysis failed to converge. In order to solve this problem, the ring was fixed in axial direction from three points, till stability was reached.

The numerical modeling was performed in two sets, as given in **Figure 5.8**. The analyses were conducted for two rings differ in width, and these rings were formed with 5 mm and 10 mm mandrels. The results of these models will be given in next chapter. However among four models, one model was investigated in detail: the process in which ring 16 mm in width was formed by 10 mm mandrel was investigated. The main reason of selecting this model was related to the stability of the process. The models with 5 mm mandrel were not reliable since even later stages of the rolling, oscillations were observed and at the inner part the large stress gradients were observed. Another reason was the ease of measurement of

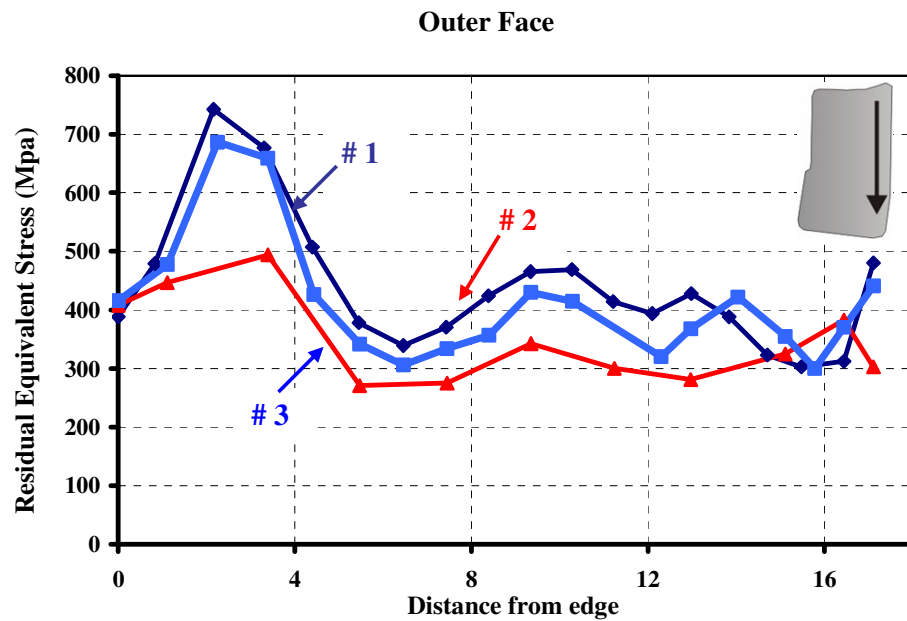
the final products for this model. The numerical investigation in the proceeding parts, will be based this model.

Three different meshes were investigated in the numerical modeling; the topologies are shown in **Table 5.3**. In the figures, the cross section of the ring is given (such as **Figure 5.8**). All of the topologies have non-uniform configurations, the mesh is fine at the regions where the mandrel touches ring, in other words on the bite region. The first mesh is the coarsest, especially on the outer surface. The finest mesh is the 3rd one; not only the bite region but also the outer face has finer topology. The total numbers of elements are given for each mesh configurations. The elements are expanded about the center of the ring with 1.5° differences.

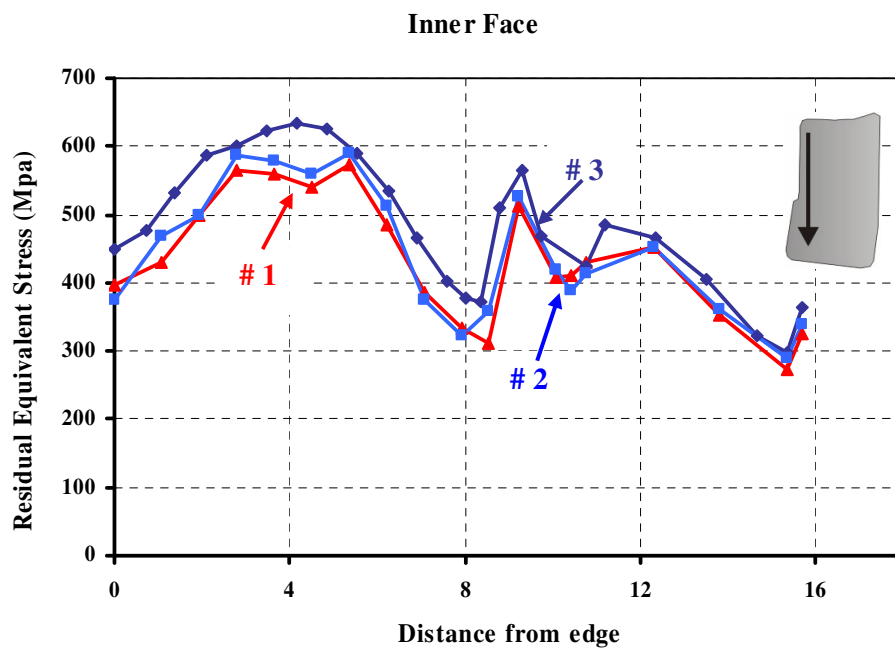
Table 5.3 Mesh topologies used in model

Mesh #1		Mesh #2		Mesh #3	
Mandrel		Forming Roll	Mandrel		Forming Roll
Total Number of Elements					
	26,880		39,600		51,600

The effect of the mesh on the equivalent stress is given in **Figure 5.9a-b** for the outer and inner surfaces of the ring respectively. **Figure 5.9a** shows that the maximum difference between the results of first mesh and the third is about 250 MPa (35.8% of corresponding value), and the maximum difference between the third and the second is about 90 MPa which is approximately 11.3%.



a)



b)

Figure 5.9 Equivalent residual stress distribution on the a) outer b) inner surface of the ring, for different mesh topologies

On outer surface *Figure 5.9a*), the convergence is better for second and third meshes since the mesh topologies on this side are similar. The variations in the results are smaller on the inner side, because the difference between the mesh topologies are less than it is on the outer side. The convergence for the first and the second mesh is observable. The variations on the inner surface are high on the regions where mandrel touches the ring (bite region) and lower for the remaining part. The maximum variation between the first and the third mesh is a 20 % difference at the bite region, which is acceptable for this region. The stress distribution in circumferential direction and the axial direction will be given in next chapter. There is a better convergence in the inner side.

The numerical parameters such as contact tolerance, distance bias were selected based on previous discussion. The converging ratio which increases the computation time as it is reduced was chosen 0.01. These parameters are also used in the further studies.

5.2.2 3D Segment Model

The segment model developed for conventional ring rolling process was implemented on the incremental ring rolling without changing any assumption except for the ones related to process characteristics; such as symmetry which has already been mentioned in full model case. Another difference is the boundary condition which is temporarily placed in order to prevent the oscillations.

The angle analyses were performed for the segment model and the effect of the angle on accuracy of the results were investigated. These results were compared with the full model and the experiments. The comparisons showed that the accuracy of the 3D segment model for incremental ring rolling was not as good as it is for conventional ring rolling (The analyses were performed with third mesh topology and the numerical results will be given in next chapter). The comparisons

also showed there is no significant change in accuracy with angle; hence 30° segment will be used in further studies.

The main crude assumption of this model is fixing the boundary surfaces as planes. This assumption is absolutely valid for a conventional ring rolling process, although the regions that are close to boundary planes can not be deformed as it is in real process. The growth in circumferential direction is uniform in conventional ring rolling. However as it was also observed in the experiments, the material flow is non-uniform in radial and axial and thus in circumferential direction in the incremental case. The tilting motion, which is an outcome of non-uniform flow, creates bending moment on the boundary surfaces. Therefore, the boundary surfaces can not remain plane in the real process. The planes start to warp. It can be concluded that this model can not reflect the real process perfectly. However its computation time is nearly one thirteenth of the full model, so it is attractive to improve this model instead of leaving at this stage.

5.2.3 3D Segment Model with Soft Elastic Region

As discussed in the previous section, the 3D Segment model can not reflect the real process perfectly because of the warping at the boundaries. The non-uniform deformation in the circumferential direction induces extra stresses on the boundaries, which results in loss in accuracy. The boundaries should be relieved somehow, in order to utilize from this model.

In this model the boundaries of the ring are relaxed with soft elastic deformable regions. The schematic representation of the process is shown in *Figure 5.10*. These regions are soft enough to allow warping, and they suspend the warping at the boundaries of elastic-plastic ring segment. The boundary surfaces of these elastic regions are fixed with rigid surfaces as in the previous model.

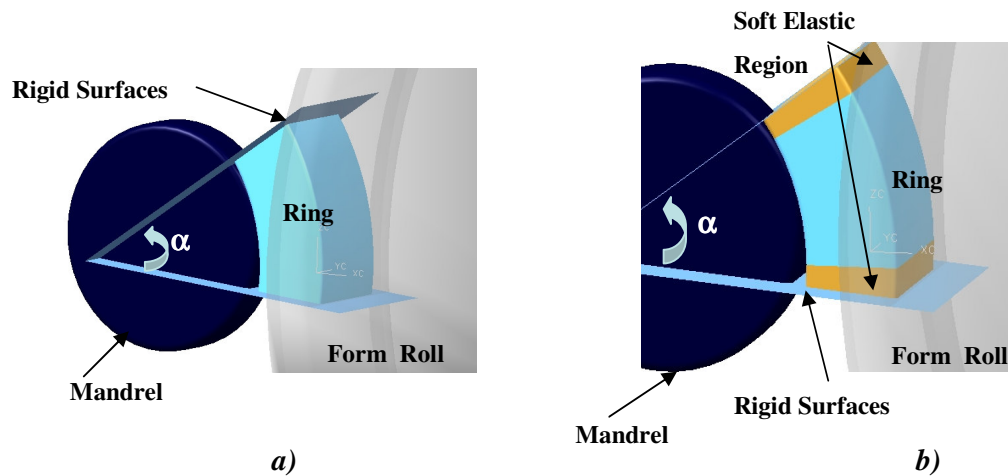


Figure 5.9 a) 3D Segment Model b) 3D Segment model with soft elastic region

There are two main parameters to investigate in this model. The first one is the material used and the second is the thickness of the region. The elastic region should be soft enough to compensate the stresses and it should remain in elastic state during the process. Therefore its modulus of elasticity should be low and its yield stress must be high. There is no need to investigate the yield stress, since the order of stress can be predicted from previous model. The yield stress is selected as 2 GPa.

The main material parameter for the elastic region, the modulus of elasticity, was analyzed using a 3D segment model. In the **Table 5.4**, the results of 3D segment analyses with 50 MPa, 1,000 MPa and 50,000 MPa of elastic modulus are compared with 3D Full Model. The table shows the error in equivalent strain distribution along radial direction. In the table, it can be observed that as the stiffness of the region decreases the error also decreases. The error in equivalent strain for the modulus of 50 MPa is less compare to error for the modulus is 50,000 MPa. and 50,000 MPa is stiff for warping. A modulus value of 1,000 MPa gives moderate results and also soft enough. Thus, the analyzed numerical models presented in next chapter, modulus of elasticity is selected as 1000 MPa.

Table 5.4 Error in total equivalent strain for different modulus of elasticity values.

Modulus of Elasticity (MPa)	Error in Total Equivalent Strain (%)
50,000	3.8
10,000	1.1
1,000	0.97
50	0.99

Another parameter investigated was for the thickness of the elastic regions. In the study for the modulus of elasticity, the thickness was as selected as three element length. The results were satisfying, however further analysis was performed with thickness of 2,3,4 and 6 element length. The **Table 5.5** shows the error induced for each. The error increases with increasing the thickness of elastic region. If the warping of planes and computation time are considered, the thickness was selected as 4 element length. This was checked on using 2D Model since computation time increases with increasing the length significantly.

The segment model with the elastic region provides better results compared to the plain segment model. However, at large strains, it can not give accurate results. It will still be powerful in determining the geometries, but not for residual stresses.

Table 5.5 Error in total equivalent strain for different thickness of elastic region

Thickness (# element length)	Error in Total Equivalent Strain (%)	Computation time for 2D Model (min)
2	0.81	~14
3	0.97	~16
4	0.99	~18
6	0.89	~20

5.2.4 3D Velocity Coupling Model

The segmentation is an efficient simplification method in analyzing the incremental ring rolling process, and the accuracy of the previous models especially in geometry is reasonable. However the residual stress results need some improvements when compared to full model results. The stress induced on the boundaries was relieved with the elastic region, however in order to reflect the problem more accurately the boundaries should completely relieved. If the boundary surfaces are removed without adding any boundary condition, the process will be roll bending process; the segmented ring will be deformed as billet flowing through two dies, reducing in thickness. Therefore, some additional boundary conditions should be applied on the boundaries.

If the two symmetric boundary planes are thought to be a control volume and the remaining part of the ring is assumed to be rigid, the normal velocity of the particle enters will be equal to exit velocity ($\bar{V}_{n_{inlet}} = \bar{V}_{n_{exit}}$, in **Figure 5.10**). However the remaining part of the ring elastically deforms due to rolling forces and this leads a slight difference between the inlet and the exit velocities of a particle travels through a control volume. This difference is shown in the **Figure 5.11** for two symmetric planes $\pm 90^\circ$. In the figure, normal velocities of the nodes on the mid of the planes are given. The data collected in the radial direction starting from inner face of the ring. The velocity profile on different planes; $\pm 10^\circ$, $\pm 20^\circ$, $\pm 30^\circ$, $\pm 45^\circ$, 60° and $\pm 75^\circ$ were also investigated. They have also small variations between the inlet and the exit velocities however are not presented.

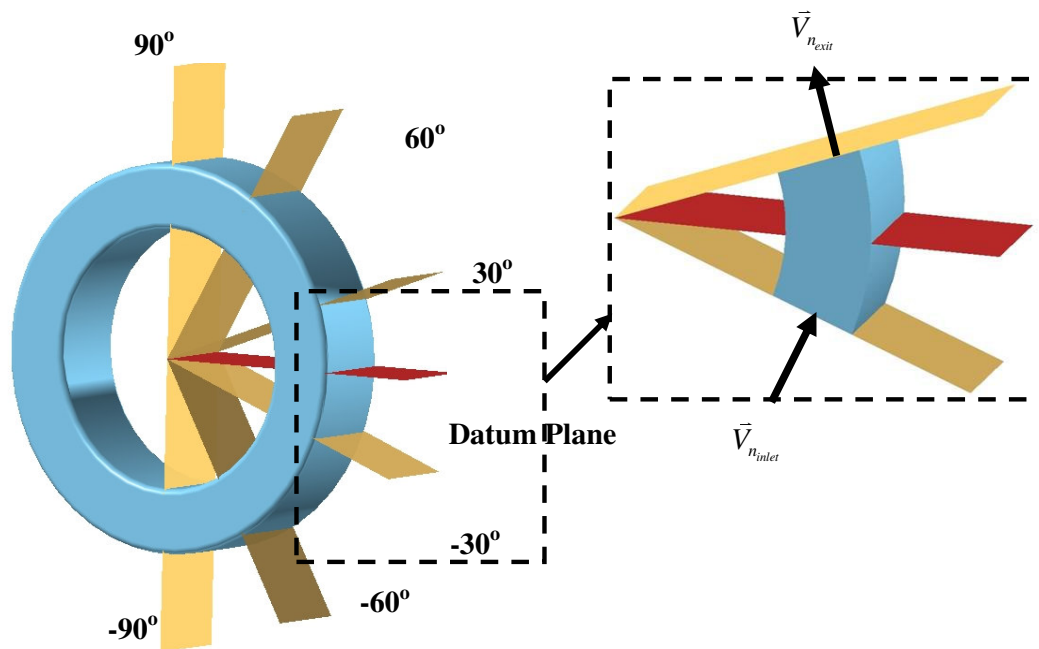


Figure 5.10 The imaginary boundary planes, cut for velocity profile analysis.

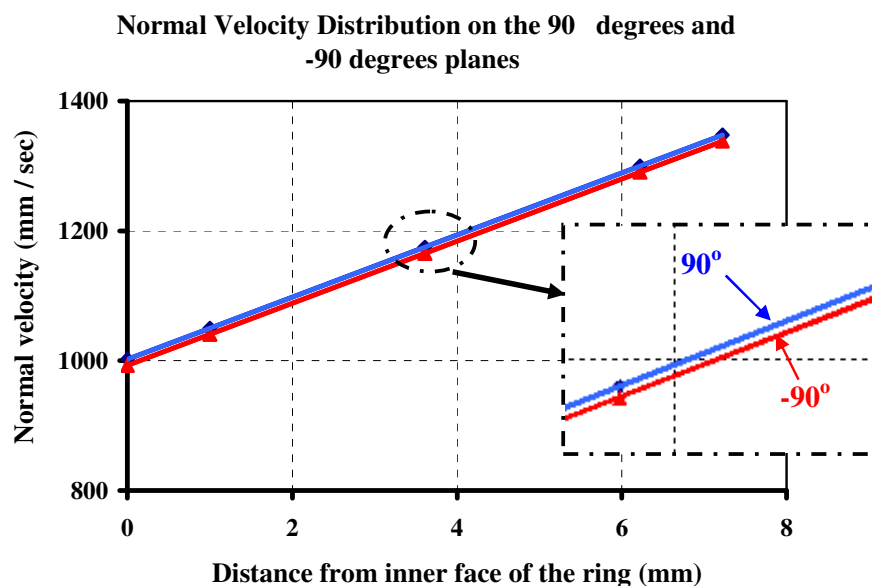


Figure 5.11 Normal velocities of the nodes on the mid of the planes are given.

The result of investigation of the velocity planes can be used as a boundary condition in the modeling. The normal velocities of these two symmetric planes can be coupled. However, this boundary condition is not enough to represent the real process. The ring is a circular body and introducing this boundary condition

does not help to maintain the circularity. This can be provided by an additional constraint, which enables ring to rotate about a single point or a curve. The nodes on the boundaries should be restricted with this constraint. The ring rotates about its center for conventional ring rolling process and every node on the boundaries of the segment rotates about this center. However in the incremental ring rolling, as mentioned before, the surfaces on the boundaries do not remain planar, warpage on the surface are observed, hence the rotation axes of the nodes change. This is a continuous change due to ring growth and tilting motion.

Implementation of boundary condition and the constraints on the program

The main challenge is the implementation of this constraint and the boundary condition on to the model. The previous analysis MSC.Superform had been used, and the utilities in the program were adequate for modeling. However, this pre-processor of this program is not flexible for more complicated boundary conditions and additional constraints. Therefore, a more powerful and flexible pre-processor was needed, and MSC. Mentat with its high number of pre-processing utilities was selected. The models prepared in MSC. Mentat and the MSC. Superform are solved by same numerical solver and the numerical parameters determined are same for two of the programs. Hence the comparison of the models can be performed without any doubt. Although the MSC. Mentat is flexible, it is not possible to directly implement the constraints; additional support is needed. This is provided by user subroutines which are supported by the features in the program. The most important features of the program are; the tying option and the user subroutine UFORMS, which makes tying more flexible to use.

Tying

One useful features of MSC.Mentat is the *tying*. The program contains a generalized tying (constraint) condition option. Any constraint involving linear dependence of nodal degrees of freedom can be included in the stiffness equations.

A tying constraint involves one tied node and one or more retained nodes, and a tying (constraint) condition between the tied and retained nodes. The degrees of freedom (for example, displacements, temperatures) of the tied node are dependent on the degrees of freedom of the retained nodes through the tying condition. In some special tying conditions, the tied node can also be a retained node. The tying condition can be represented by a tying (constraint) matrix. (MSC. MARC Manual Vol. A, 2005)

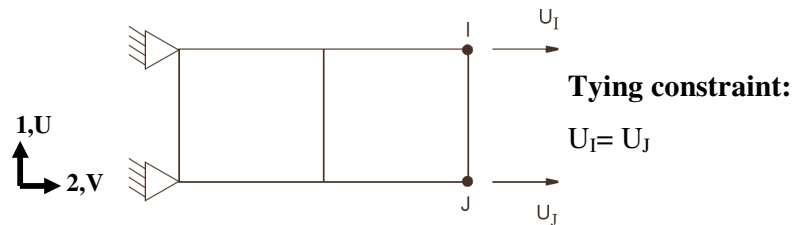


Figure 5.12. Simple tying constraint (MSC. MARC VOLUME A, 2005)

A simple example of the tying can be shown in the **Figure 5.12**. In the figure the tying constraint imposes the constraint that the first degree of freedom of node *I* will be equal to that of node *J* at all times. In the program, there are tying codes which represent the tying constraint defined by the program, in addition to these the user subroutine UFORMS is a powerful method to specify a user-defined constraint equation. This constraint can be nonlinear; for example, it can be dependent on time or previous deformation. In the modeling this option was used, however it is not straight a forward task. It involves algorithm development and programming.

UFORMS user subroutine

In MSC.Marc (The commercial name of the solver of MSC.Mentat and MSC. Superform), the user subroutine feature constitutes one of the real strengths of the program, allowing the user to substitute his own subroutines for several existing in MSC.Marc. The user can write the program in FORTRAN environment. The user-

subroutines have their own variables that can be called from the *common blocks*, it is also possible to define user defined common blocks and store the variables. There are also utility routines that are defined in the program these are ELMVAR and NODVAR. The ELMVAR utility routine allows the user to retrieve element data from the MSC.Marc internal data storage in any user subroutine that is in an element loop element data is at the element, integration point and layer level, e.g. stresses, strains etc. NODVAR utility routine allows the user to retrieve nodal data from the MSC.Marc internal storage nodal data is at nodal point level e.g. displacements external forces, reaction forces. The main problem with this data is the read only characteristics and can not be altered by the user.

Description of each of the available user subroutines is given in the manuals provided by the programs. The UFORMS allows the definition of a constraint condition. MSC.Marc's capability for applying arbitrary homogeneous constraints between nodal displacements is used through this user subroutine. The constraint conditions can be supplied by using the user subroutine UFORMS. The definition of the subroutine is as followed:

$$\{u^a\} = [S] \begin{Bmatrix} u^b \\ u^c \\ etc \end{Bmatrix} \quad (5.1)$$

The vector on the left hand side is the displacement at node *a*, referred to as the tied mode. The vector on the right-side corresponds to displacements at *b*, *c*, etc.; these nodes are referred to as the retained nodes. The displacements can only be defined in rectangular coordinates; it is not possible to use cylindrical coordinates. In the matrix [S], a row of zeros indicates that particular degree of freedom at node *a* is not constrained. To apply a constraint between degrees of freedom at the same node, the node must appear on both sides of the equation, with rows of zeros in [S] corresponding to the degrees of freedom on the left-hand side, which are retained

on the right-hand side, and columns of zeros in **[S]** corresponding to the tied nodes appearing on the left-hand side.

The tying is an attractive way of coupling the nodes or in other words linking them. And the relation with tied and retained node can be given in UFORMS subroutine with **[S]** matrix.

Finding [S] matrix

The primary issue is to find the **[S]** matrix to define the boundary condition and the constraint of keeping circular motion by updating the rotation axis. **[S]** matrix consists of a geometry dependent variables that relates the tied and the retained nodes. Hence geometrical analysis should be performed. **Figure 5.13** shows the relation of angular configurations of an arbitrary couple of retained and the tied node. The first figure is the configuration at time t, whereas the second one is for time equal to t+Δt. The ring rotates Δβ in clockwise direction, in the first configuration.

In the **Figure 5.13** is obvious that $\alpha + \beta + \phi = \pi$. However another important relation is the equality of the velocities in θ- and r- directions. The UFORMS subroutine does not support relating the velocities directly, but the displacements. Hence the incremental displacements in these directions which are indicated with θ_1, θ_2 and r_1, r_2 and are can be equated as follows:

$$\theta_1 = \theta_2 \tag{5.2}$$

$$r_1 = r_2 \tag{5.3}$$

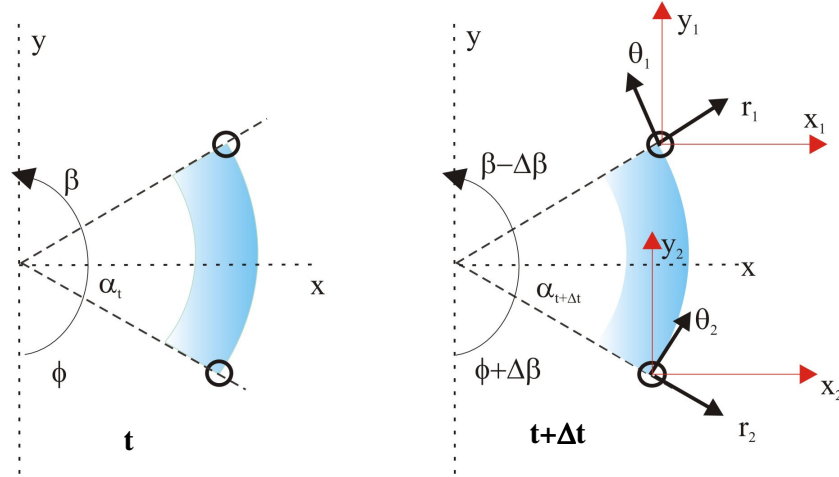


Figure 5.13 The relation of angular configurations of any retained and the tied node.

As mentioned before, the UFORMS can be utilized in rectangular domain not in cylindrical. Therefore, it is required to transform the displacements in to rectangular domain before equating them. The transformation of the displacement is shown in **Figure 5.13**. The x_i and y_i are the incremental displacements for tied and retained node and can be obtained using **Eqns.5.4-7**.

$$x_1 = r_1 \sin(\beta - \Delta\beta) - \theta_1 \cos(\beta - \Delta\beta) \quad (5.4)$$

$$x_2 = r_2 \sin(\phi + \Delta\beta) - \theta_2 \cos(\phi + \Delta\beta) \quad (5.5)$$

$$y_1 = r_1 \cos(\beta - \Delta\beta) + \theta_1 \sin(\beta - \Delta\beta) \quad (5.6)$$

$$y_2 = -r_2 \cos(\phi + \Delta\beta) + \theta_2 \sin(\phi + \Delta\beta) \quad (5.7)$$

The matrix representations of the coordinates are as follows:

$$\begin{Bmatrix} x_1 \\ y_1 \end{Bmatrix} = \begin{bmatrix} \sin(\beta - \Delta\beta) & -\cos(\beta - \Delta\beta) \\ \cos(\beta - \Delta\beta) & \sin(\beta - \Delta\beta) \end{bmatrix} \begin{Bmatrix} r_1 \\ \theta_1 \end{Bmatrix} \quad (5.8)$$

$$\begin{Bmatrix} x_2 \\ y_2 \end{Bmatrix} = \begin{bmatrix} \sin(\phi + \Delta\beta) & \cos(\phi + \Delta\beta) \\ -\cos(\phi + \Delta\beta) & \sin(\phi + \Delta\beta) \end{bmatrix} \begin{Bmatrix} r_2 \\ \theta_2 \end{Bmatrix} \quad (5.9)$$

After obtaining the coordinates in rectangular coordinates, *Eqns. 5.2-3* is used for derivation of the relation between the nodes.

$$\begin{Bmatrix} x_1 \\ y_1 \end{Bmatrix} = \begin{bmatrix} \sin(\beta - \Delta\beta) & \cos(\beta - \Delta\beta) \\ -\cos(\beta - \Delta\beta) & \sin(\beta - \Delta\beta) \end{bmatrix} \begin{Bmatrix} x_2 \\ y_2 \end{Bmatrix} = \begin{bmatrix} \sin(\phi + \Delta\beta) & -\cos(\phi + \Delta\beta) \\ \cos(\phi + \Delta\beta) & \sin(\phi + \Delta\beta) \end{bmatrix} \begin{Bmatrix} x_2 \\ y_2 \end{Bmatrix} \quad (5.10)$$

The relation between the tied node and the retained node was given in *Eqn.5.1*, the **[S]** matrix and the displacement vector of the retained nodes should be kept in right hand side.

$$\begin{Bmatrix} x_1 \\ y_1 \end{Bmatrix} = \begin{bmatrix} \sin(\beta - \Delta\beta) & \cos(\beta - \Delta\beta) \\ -\cos(\beta - \Delta\beta) & \sin(\beta - \Delta\beta) \end{bmatrix}^{-1} \begin{bmatrix} \sin(\phi + \Delta\beta) & -\cos(\phi + \Delta\beta) \\ \cos(\phi + \Delta\beta) & \sin(\phi + \Delta\beta) \end{bmatrix} \begin{Bmatrix} x_2 \\ y_2 \end{Bmatrix} \quad (5.11)$$

$$\begin{Bmatrix} x_1 \\ y_1 \end{Bmatrix} = \begin{bmatrix} -\cos(\beta + \phi) & -\sin(\beta + \phi) \\ \sin(\beta + \phi) & -\cos(\beta + \phi) \end{bmatrix} \begin{Bmatrix} x_2 \\ y_2 \end{Bmatrix} \quad (5.12)$$

In the above equation, the $\beta + \phi$ arguments in the sine function can be substituted with $\beta + \phi = \pi - \alpha$ using the relation $\alpha + \beta + \phi = \pi$

$$\begin{Bmatrix} x_1 \\ y_1 \end{Bmatrix} = \begin{bmatrix} -\cos(\pi - \alpha) & -\sin(\pi - \alpha) \\ \sin(\pi - \alpha) & -\cos(\pi - \alpha) \end{bmatrix} \begin{Bmatrix} x_2 \\ y_2 \end{Bmatrix} \rightarrow \begin{Bmatrix} x_1 \\ y_1 \end{Bmatrix} = \underbrace{\begin{bmatrix} \cos(\alpha) & -\sin(\alpha) \\ \sin(\alpha) & \cos(\alpha) \end{bmatrix}}_{[S]} \begin{Bmatrix} x_2 \\ y_2 \end{Bmatrix} \quad (5.13)$$

$$[S] = \begin{bmatrix} \cos(\alpha) & -\sin(\alpha) \\ \sin(\alpha) & \cos(\alpha) \end{bmatrix} \quad (5.14)$$

Hence the [S] matrix is a simple transformation matrix. It is only dependent of segment angle α . The difference of this model with the other models is that the segment angle does not remain same. In the incremental ring rolling, as mentioned before, the surfaces on the boundaries do not remain planar, warpage on the surface are observed, hence the rotation axes of the nodes change. This is a continuous change due to ring growth and tilting motion. Hence it is better to express the segment angle as α_t , where the t designates the time increment. The [S] matrix also becomes time dependent.

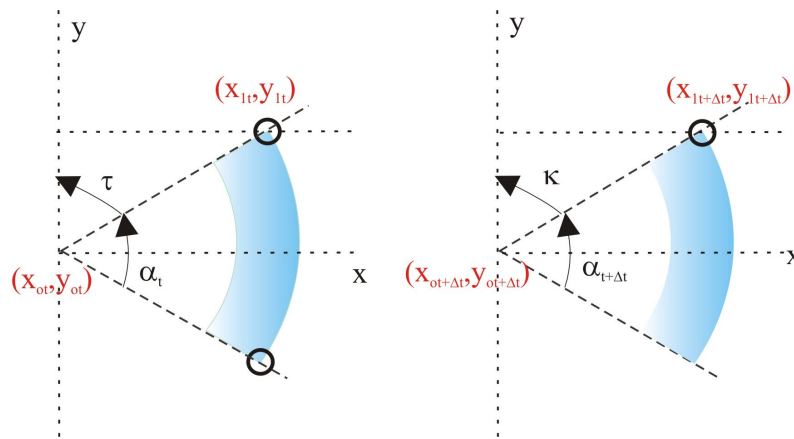


Figure 5.14 Representation of change in segment angle

The angle at any time t can be computed at each step by finding the center and uses geometrical relations that can be derived from **Figure 5.14**. As shown in the figure, the angle change can be derived using the nodal coordinates. The angle change derived should be accumulated in each step. The UFORMS subroutine is called in every cycle of an increment, what is missing in this subroutine are the updated nodal coordinates per iteration. There is only one variable related to nodal coordinates given in the user subroutine the *xord*, which only provides the coordinates at the beginning of the increment. Therefore additional variables should be defined by using the functions supported by program. These variables can be obtained by writing a FORTRAN code into the subroutine that picks up the original coordinates, the displacements at the beginning of the current increment and the iterative displacements (displacements from begin of current increment up

to current cycle). By adding these variables the actual coordinates of the nodes are found, which are exactly needed for the calculation of the current segment angle. As the coordinates are updated the following equations can be used to determine the angle change.

$$\tau = \arctan \left[\frac{x_{1t} - x_{ot}}{y_{1t} - y_{ot}} \right] \quad (5.15)$$

$$\kappa = \arctan \left[\frac{x_{1(t+\Delta t)} - x_{ot}}{y_{1(t+\Delta t)} - y_{(ot+\Delta t)}} \right] \quad (5.16)$$

$$\Delta\alpha = \alpha_{t+\Delta t} - \alpha_t = (\tau \pm \kappa) \pm r \quad (5.17)$$

where r is the rigid body rotation angle of the ring, this variable can be called from user utility routines. The angle change can only be found when the instantaneous center of rotation of corresponding node is found ($x_{ot}, x_{o(t+\Delta t)}, y_{ot}$ and $y_{o(t+\Delta t)}$). The algorithm to find the center of rotation of the node is more complicated. In this algorithm, the updated nodal coordinates are again utilized. The initial coordinates of the nodes on the boundary planes and initial coordinates of their center of rotations are stored in different variables, and they are used to find the initial distance of center of rotation. At each update of nodal coordinates, the displacements in x,y,z directions are taken from the previous update and they are accumulated on to initial distance. By this way, final orientation of the center of rotation is found for each increment.

The results of the velocity coupling method will be discussed in next chapters. It is found out to be the most powerful model in terms of accuracy in residual stresses.

CHAPTER 6

APPLICATION OF NUMERICAL MODELS

In this chapter the applications of numerical models introduced in the previous chapter will be presented. The results will be analyzed in terms of geometry, strain/stress distributions. The performance of the numerical models: accuracy and the computation time will be examined. The material flow characteristic for a single type of incremental rolling process will also be explained. The effects of assumptions, i.e. segment angles for simplified models, will be discussed. The validity of assumptions and the special boundary conditions will be investigated with the geometrical and the stress results obtained from the experiment results presented in *Chapter 4*.

The accuracy in geometry is a vital criterion, since the incremental ring rolling process is aimed to be used in near net shaping processes. The stress comparisons are also important for estimating the rolling forces and torques (these analyses are not performed in this study, only residual stresses are concerned). Furthermore, the residual stresses on the workpiece are important for the fatigue life concerns. The analyses on residual stresses on even ring rolling process have not been dealt extensively before; this study is the first study investigating the residual stress distribution.

In the first section, the segment model developed for the conventional ring rolling will be analyzed. These analyses construct the basis of next ones. In the latter section the models for incremental ring rolling will be presented and the models will be compared within each other and with experiments in the last section. In *Table 6.1* the investigated are given and the scope of the analysis are also given.

Table 6.1 Summary of analyzed models

Conventional Ring Rolling	
Two-Dimensional (2D) Full Models	These models were investigated to understand numerical modeling and simplification methods.
Two-Dimensional (2D) Segment Model	However comparisons are not given in this thesis since, an extensive study on these models has already been done by Music (2005).
3D Full Model	
3D Segment Model	The effect of segment angle is investigated. The material flow and stress distribution are compared with full model.
Incremental Ring Rolling	
3D Full Model	The geometry and stress comparisons of models with different mesh topologies are given. Also the material flow characteristic of the process is investigated.
3D Segment Model	The effect of segment angle on accuracy in geometry and residual stress results are investigated and results are compared with full model.
3D Segment Model with Soft Elastic Region	The effect of modulus of elasticity in accuracy is shown and the results are compared with full model
Velocity Coupling Model	The geometry and stress comparisons of the model is done for both high and low deformation processes.

6.1 3D Segment Model for Conventional Ring Rolling

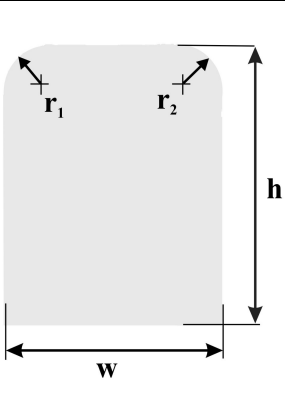
This model was adapted from 3D full model and 2D segment model developed for conventional ring rolling. The main assumption is simulating the ring as a partial segment and remaining part as rigid. The validity of this assumption was investigated by examining the main parameter: the angle of the ring segment. The model validated against the 3D full model results. The results presented in this part correspond to a deformation of 1.0 mm of bite.

6.1.1 Geometrical Comparison

The comparison in geometry is based on the four dimensions of the ring profile for different segment angles shown in **Table 6.2**. The figure shown on the left hand side of the table corresponds to half cross section of the ring, cut from the middle of the ring. The measurements are taken from three points for each dimension. The average values and the deviations from the full model for each dimensions are calculated.

Table 6.2 Geometrical comparison of 3D segment model for conventional ring rolling

Segment Angle	Error (%)			
	r_1	r_2	w	h
30°	0.47%	2.01%	0.66%	0.40%
60°	0.21%	1.07%	0.12%	0.52%
90°	0.05%	1.03%	0.14%	0.20%



The table shows the error percentages for four models with different segment angles. It is observed that there is no significant deviation in geometry from the

full models, although there is a decreasing trend with increasing the segment angle. The largest deviation is observed for the r_2 dimension; this area has a contact with the profiled form roll, in other words there is a die filling problem. However this amount is not significant, the radius is supposed to be 1 mm hence the error cause only a 0.02 mm difference.

6.1.2 Total Equivalent Strain Analysis

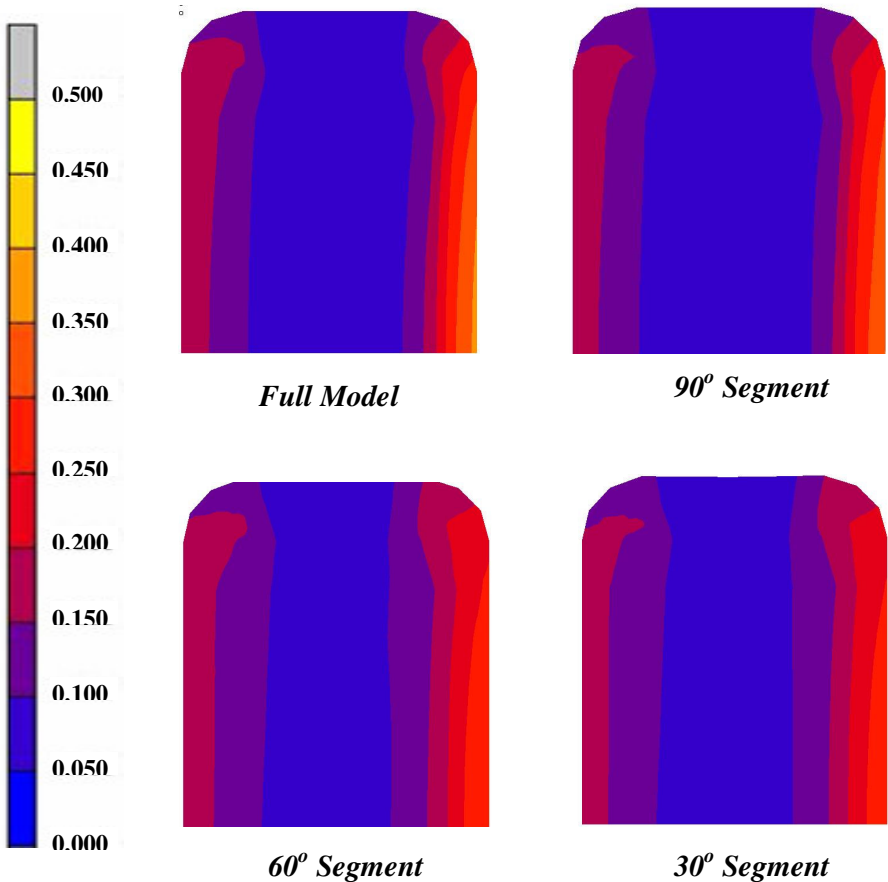


Figure 6.1 Total equivalent strain comparison of 3D segment model for conventional ring rolling

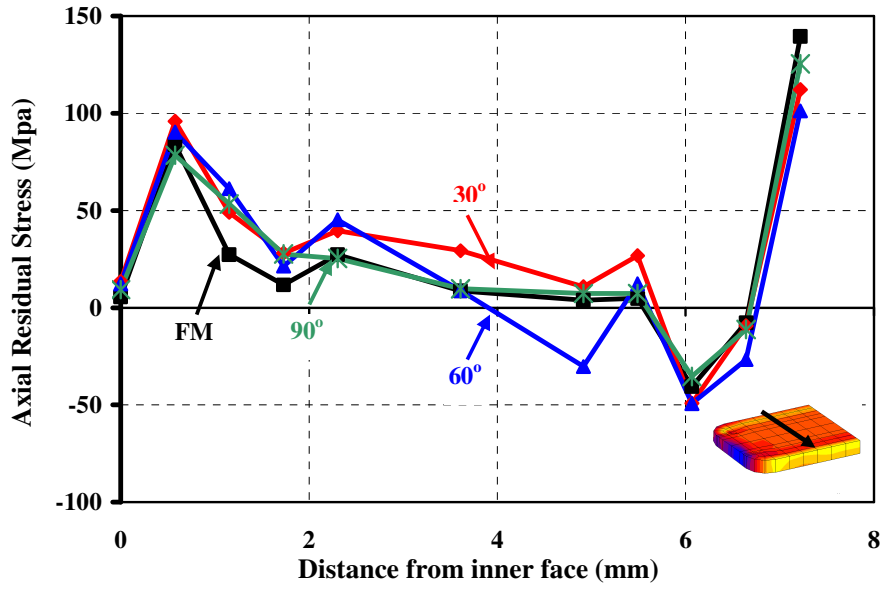
The total equivalent strain analysis is also important for determining the efficiency of the model in predicting the material flow. It is expected to have similar strain distribution for all models when the geometry is considered. In *Figure 6.1*, total equivalent strain results are shown, the left side is the form roll side, and right is

the mandrel. As the full model result is examined, it is observed that the strain values are higher at the outer surface of the ring where the form roll touches (left side), and the highest strain values are observed on the mid part of the ring; close to symmetry plane. The strain distribution on the inner side is more uniform and there is an increase towards inner part near the filleted region. These characteristics are similar for 3 models with different segment angles.

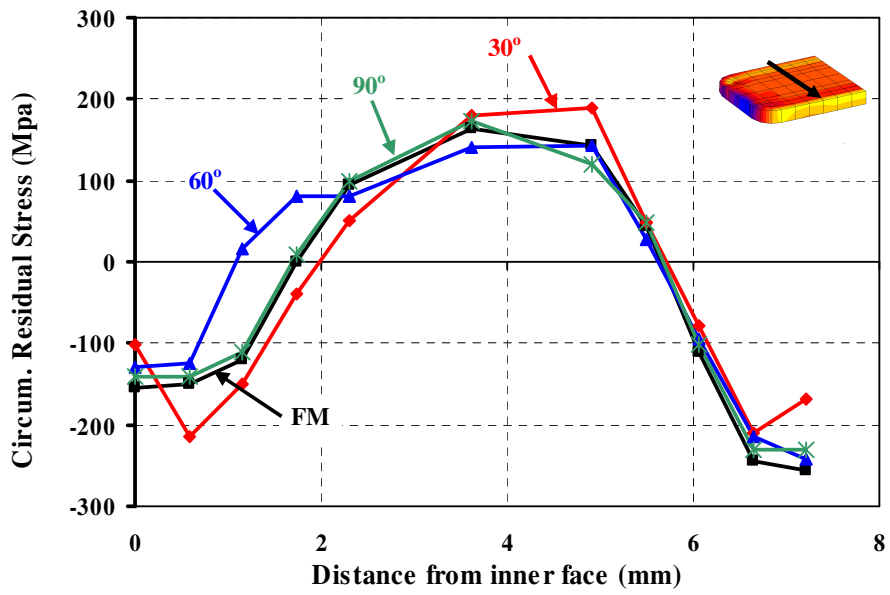
There are minor differences: for example; the strain bands are larger on the inner side of the ring for 60° and 30° segment angles. The reason for this is the amount of the part assumed rigid. The segment angle brings the assumption of keeping the remaining part of the ring as rigid. In real case the elastic deformation exist on this region due rolling force which leads growth in the ring. The rolling force and the deformation amount are same for all models; thus the deformation energy is same. This deformation energy is composed of plastic deformation (which is dominant) and elastic deformation energy terms. The amount elastic energy is same but the volume of the rigid modeled part is not same. As the angle decreases the region considered as rigid obviously increases. Therefore for small angle models the accumulated elastic energy can cause plastic deformations.

6.1.3 Residual Stress Analysis

The residual stress analyses are performed with the results of the same 3D full model (*FM*). The ***Figure 6.2a-b*** show the axial, circumferential residual stress distribution. The results are averages of the data taken from three distinct planes of the ring segment, in radial direction from inner to outer surface of (as shown in ***Figure 6.3a***)



a)



b)

Figure 6.2 Comparison of residual stress distribution in a) circumferential axial directions for different segment angles

The *Figure 6.2b* shows that all models catch the stress gradient in circumferential and axial stresses on the outer surface, which has already mentioned in numerical modeling chapter. There is a difference between inner and the outer stress distribution and the variation is not uniform along the radial direction. This is an expected result as the strain distribution is considered. The circumferential residual stress results are also in agreement with the full model, most of the deviations are observed at the 30° and 60° model cases. The reason for this difference is explained in previous section, the variation is larger for the smaller segment angles and more stresses induced on the small angled models.

6.1.4 Accuracy and Computation Time

The accuracy of the model is based on the differences in Von Mises equivalent stresses, since it is more comprehensive parameter including effects of all stress components. The ring segment is divided by three surfaces and the residual stress data are collected on these planes, the average values are used.

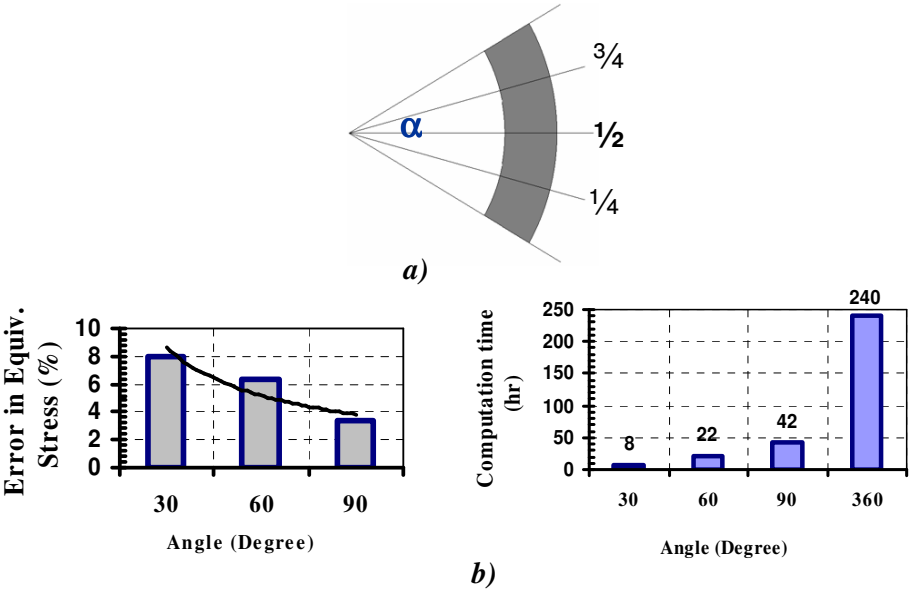


Figure 6.3 a) Planes of measurement on the ring segment b) Accuracy of measured

After finding the averages, the each stress value is compared with the correspondent full model result and local error values are calculated. The averages of these errors are taken and a global error is found for each model. The error for the 30° model is approximately 8%, and there is a non-linear decreasing trend with respect to increase in segment angle. The error 90° model is about 3.5% which is more than half of the error accumulated for 30° model. However when the computation time is considered, it lasts as 5 times as longer as it does in 30° degree model. The accuracy in geometry has already discussed in first part which is less than %1 for each model. Therefore it is more flexible to use 30° model, with its low computation time and high accuracy in geometry and reasonable accuracy in the stress results. This model and all of the models are performed on machine with Pentium IV HT 3.0 GHz, and 1.5 GB RAM.

6.2 3D Full Model for Incremental Ring Rolling

As mentioned in previous chapter, this model is a straight forward representation of the incremental ring rolling process investigated. The model should be reference model for the simplified numerical models; hence the reliability of the model should be validated with experiments. As stated before, the numerical modeling was performed in two sets, given in previous chapter in *Figure 5.8*. The analyses were conducted, for two rings differ in width (20 mm and 16 mm), and these rings are formed with 5 mm and 10 mm mandrels. Among four models, one model was investigated in detail: the process in which ring 16 mm in width was formed by 10 mm mandrel. This model is also validated with the experiments and is repeated for different mesh topologies. In this section the results of this model will mainly be focused. The analyses of this model consist of comparisons in geometry, strain/stress distributions of the models with different mesh topologies and the experiments. The other sets will also be discussed in the material flow point of view in the last part of this section.

6.2.1 Geometrical Comparison

The geometrical analyses are performed for 3D full models with different meshes and the results are compared with the experiments in **Table 6.3**. In the table, cross-section of the incrementally rolled ring is given; the comparisons are based on the deflections shown on the figure. These deflections were previously defined in experimental analysis part. These deflections directly represent the characteristics of the incrementally rolled part; the degree of fishtailing out (Δ_1), the amount of the tilt which can be defined as the deflection from the form roll surface (Δ_3), degree of climbing towards to mandrel (Δ_4).

Table 6.3 Geometrical comparison of 3D Full Model for different meshes

	Mesh # 1 Mesh # 2			
			Mesh # 3	
Deflections (mm)	Δ_1	Δ_2	Δ_3	Δ_4
<i>3D Full Model (#1)</i>	0.52	1.01	1.0	1.52
<i>3D Full Model (#2)</i>	0.41	1.29	1.31	1.42
<i>3D Full Model (#3)</i>	0.38	1.15	1.51	1.62
<i>Experiments</i>	0.17	1.35	1.4	1.74

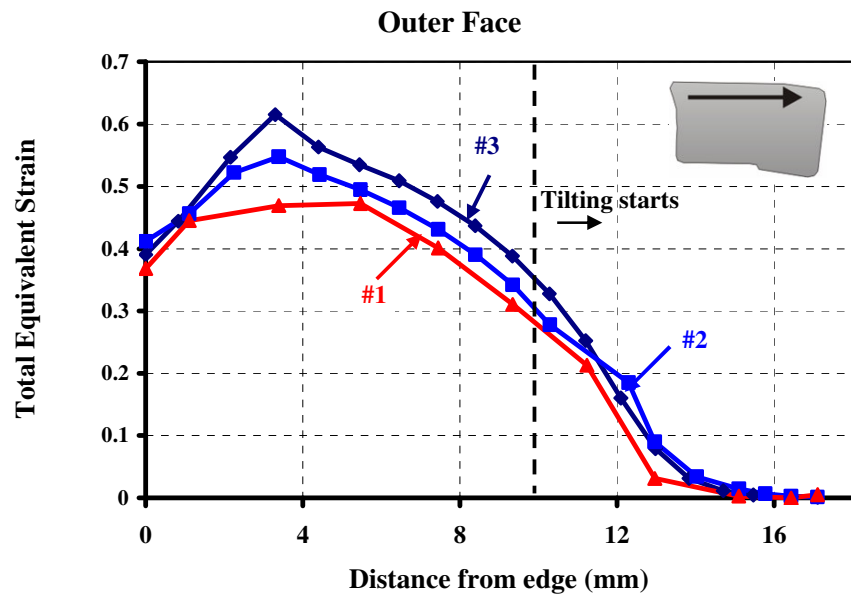
The experimental data are obtained by using profile measurement device. In the table, it seems that the deflections are different from the experimental data even for the refined mesh (3rd mesh). However, when the dimensions of the ring is considered which is about 17.1 mm in height (average) and about 9.06 mm

(average) in width the maximum difference in deflection corresponds to error of 4.4% for 1st mesh, 3.5% for 2nd mesh and %1.3 for mesh 3, respectively. The third mesh gives the best prediction in geometry among all. The comparisons in geometry for simplified models will be based on this model.

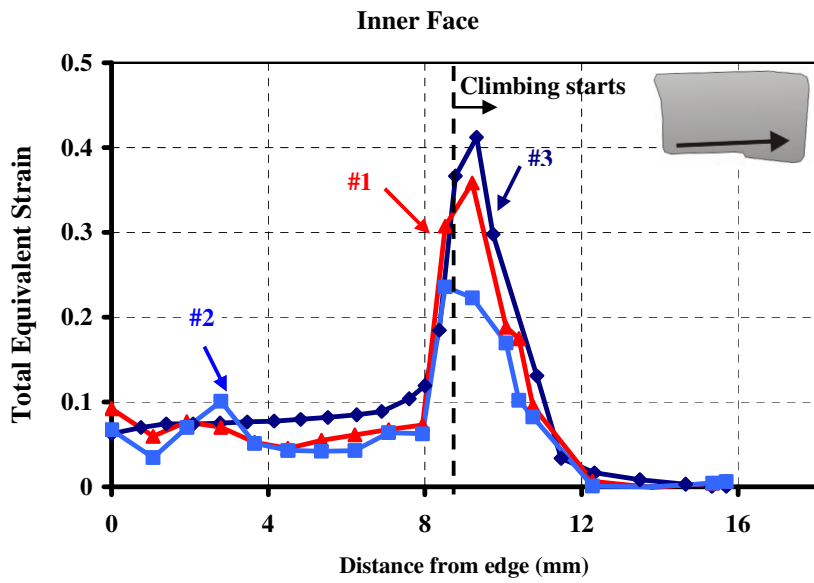
6.2.2 Total Equivalent Strain Comparison

The equivalent strain comparison on the outer and inner surface ring is compared for different mesh topologies (*Figure 6.4a-b*). The strain data are taken along the direction shown in small figures on the graphs. The point where the tilting starts is indicated in the figure, the left hand side is the region where the form roll touches the ring. It can be observed that there is a non-uniform strain distribution on this side. The strain attains higher values on the left side; this is an expected result since on this region there is a growth in radial direction due to rolling forces. On this part shear stress due to friction, during forming induced. The strain is maximum at the end of the left fillet of the ring; the strain starts to decrease from this point and it converges to zero at the right side. This indicates that the material flow through left side of the ring is more than it is through the right side, on the outer surface. There is a steep decrease in strain after the tilting starts. It was also observed in the experiments that the ring does not grow radially on tilted region so this kind of distribution is expected.

The maximum strain values are observed for the model with 3rd mesh. This is an expected result since the elements on the outer surface of this mesh is finer than others. The maximum value is observed at the end of the fillet where the element is smaller since than the all others and has a distorted shape due to geometry. It has already discussed in *Chapter 5* that it is not possible to obtain convergence on the outer part of the ring with these models. There are variations among stress values of different models however the distribution is quite similar.



a)



b)

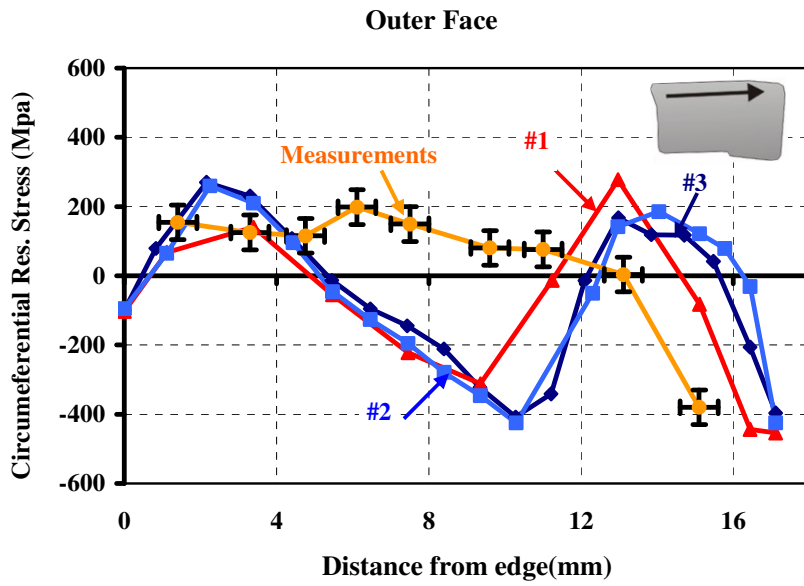
Figure 6.4 Total equivalent strain distribution on a) outer b) inner surfaces of the ring

The convergences of the models are better at the inner side except for the region where the climbing towards to mandrel starts. The high strain gradient observed towards this region. The ring bends over the fillet of the mandrel. In all topologies the mesh can not be fitted on the fillet, the discretization is not enough, however more discretization will lead excessive computation time and this is not required at this stage.

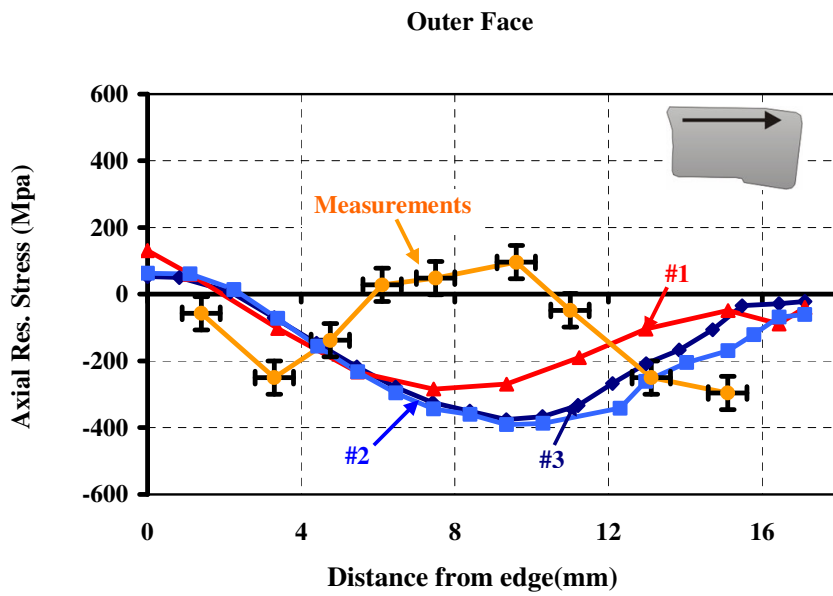
6.2.3 Residual Stress Comparison

The residual stress comparison is a vital part of this study. The residual stresses are measured on XRD mentioned in the experimental analysis part. The verification of the model with the experiments is necessary to construct a reference for other models. In this part, circumferential and axial stress distributions, on the outer and inner surface of the rings with different mesh topologies are compared. In the *Figure 6.5 a-d*, these comparisons are shown, respectively.

In *Figure 6.5a-b*, it can be observed that the results for the 2nd and 3rd meshes are in agreement; this is expected because the meshing topology on the outer surface of the ring, contact parameters are step size, are similar on these two models. Although there is a convergence for these two models, they do not agree with the experiments. In *Section 5.1.1* it was explained that it is difficult to catch the gradient on the outer surface. In this section *Figure 5.4*, the results have been given along radial direction and the steepest gradient has been observed on the outer surface. The difference reduces as the mesh gets finer; however it is not reasonable to use a finer mesh because of the extremely long computation time. The stress distribution for the 1st mesh differs extremely from other two. The outer surface of this model is 2 times coarser than the 2nd and 3rd meshes. There is less number of nodes, so in the graphs the curve fitted with less number of data points, this increases the linear interpolation error of on the curves.



a)



b)

Figure 6.5 Residual stress distribution on the **a)** circumferential **b)** axial direction on the outer surface of the ring, for different mesh topologies

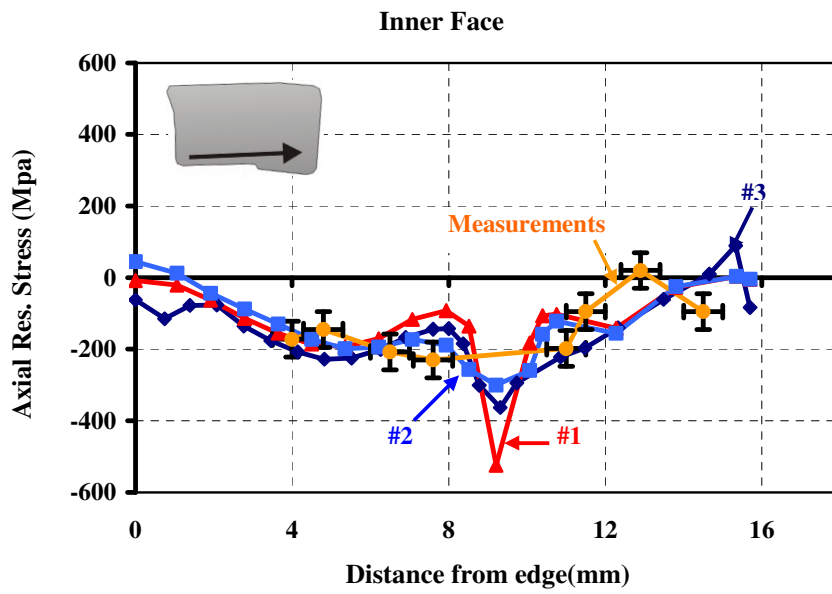
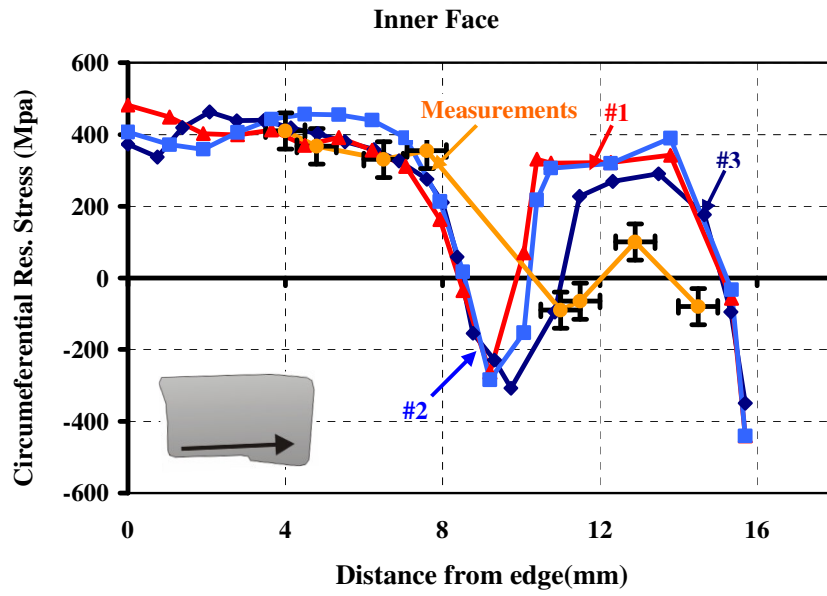


Figure 6 6 (Residual stress distribution on the a) circumferential b) axial direction) on the inner surface of the ring, for different mesh topologies

There is a better agreement in the residual stress distribution on the inner surfaces among the models and the experimental measurements. This is an expected result because even 1st mesh has a finer mesh structure on this area. The steepest gradient is observed about the point where the climbing starts, it is almost impossible to catch the gradient with these meshes, it should be more refined. The difficulty in this refinement will be discussed in next part.

6.2.4 Accuracy and Computation Time

Table 6.4 Accuracy and computation time of the 3D Full Models

		<i>Mesh #1</i>	<i>Mesh #2</i>	<i>Mesh #3</i>
<i># of elements</i>		26,880	39,600	51,600
<i>computation time(hours/days)</i>		~98/4.1	~192/8	~336/14
<i>avg. error(%) residual stresses</i>	<i>outer surface</i>	%53	%39.2	%35.7
	<i>inner surface</i>	%21.2	%16.8	% 13.1

The computation time of the models are shown in the **Table 6.4**. The accuracy of the model is based on residual stress deviations from the experiments, measured on the outer surface in two directions. The average error is calculated for each direction and a global error is found using the others. The refined model gives the better prediction in inner stress distribution with a 13.1%, this is an acceptable results. If the accuracy of this model in the geometry is re-considered, which is about 1%, this model can be considered as a reliable model for further investigations on numerical modeling. Although its accuracy, the computation time for the 3rd model is extremely long; about 14 days. If the modeling time is also considered (trial and errors for band of numerical parameters, necessities of restart and the re-submissions due to lack o accuracy), the time spent for this model is approximately 5 weeks. The computation time can be reduced by using a more

powerful computer, so this model can be more effective if a workstation or any super computer is used.

6.2.5 Material Flow Characterization

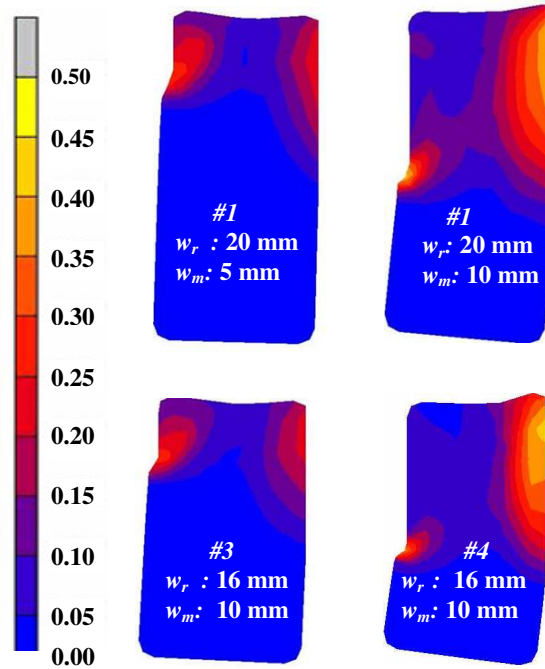


Figure 6.7 Material flow characterization with different sets of models.

In the *Figure 6.7*, the equivalent strain results for the models mentioned in previous chapter are given. This study is performed to observe the material flow characteristics for the edge aligned mandrel configuration. In the first analysis a wider ring is formed. It is observed that the strain induced on the outer surface of the ring, rolled with the wider mandrel (10 mm) is larger than the one, rolled with the smaller. The strain distribution trends in the inner part is similar, on the part where the ring climbs over the mandrel there is a high stress concentration and the strain values are maximum at these points. It can be observed for all models that the ring does not grow in radial direction just after the point tilting starts. Although there is a radial movement in this region there is no strain induced. This means that on this region there is no plastic deformation, the elements only rigidly

translates in radial and axial direction (there is two-dimensional motion). The mesh on this region can be coarser; this will not affect the results significantly.

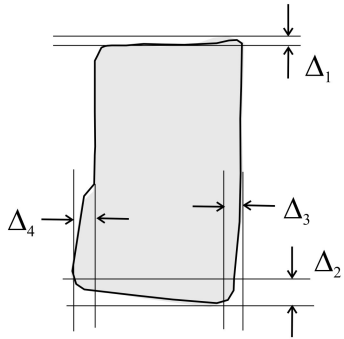
6.3 3D Segment Modeling for Incremental Ring Rolling

This model is the direct implementation of the conventional ring rolling process on the incremental ring rolling. In this part, the results of the angle analyses were performed for the segment model and the effect of the angle on accuracy of the results was investigated. A similar analyses was performed for the conventional ring rolling case, however it is expected to observe differences in the nature of the process. These results were compared with the full model and the experiments. The analyses are performed under same boundary conditions with the 3rd meshing configuration. In these analyses the effect of the rigid boundary planes on the ring segment will also be mentioned.

6.3.1 Geometrical Comparison

The geometrical analyses are performed for 3D full models with different meshes and the results are compared with the experiments in ***Table 6.5***. In the table, cross-section of the incrementally rolled ring is given; the comparisons are based on the deflections shown on the figure. In the table only results for 30° is given because, the geometry for different angles does not vary significantly with changing angle, this was also same for the conventional ring rolling. In the table it can be observed that there are slight differences. The most significant difference is on the top of ring, fishtail out is more than the measured value. This can be due to the of the extra compressive stresses induced on the rigid boundary planes,

Table 6.5 Geometrical comparison of 3D Segment Model



Deflections (mm)	Δ_1	Δ_2	Δ_3	Δ_4
<i>3D Full Segment Model (with 30°)</i>	0.49	1.19	1.21	1.5
<i>3D Full Model (#3)</i>	0.38	1.15	1.51	1.62
<i>Experiments</i>	0.17	1.35	1.4	1.74

6.3.2 Total Equivalent Strain Comparison

The total equivalent strain comparison for the model is shown in contour plot views, in **Figure 6.8**. The results are taken from the mid-plane of the segment. The total equivalent strain distributions for these two models are quite similar, the most significant difference is observed on the outer surface. The agreement in geometry can also be seen in this figure. In the figure, it can be observed that the equivalent strain distributions have peaks on the region where there is a small contact area with the mandrel edge. The error in equivalent strain results in the inner part of the ring is less than it is in the outer part. On the outer surface of the ring the strain profile is similar but there is a high gradient in strain for the first model.

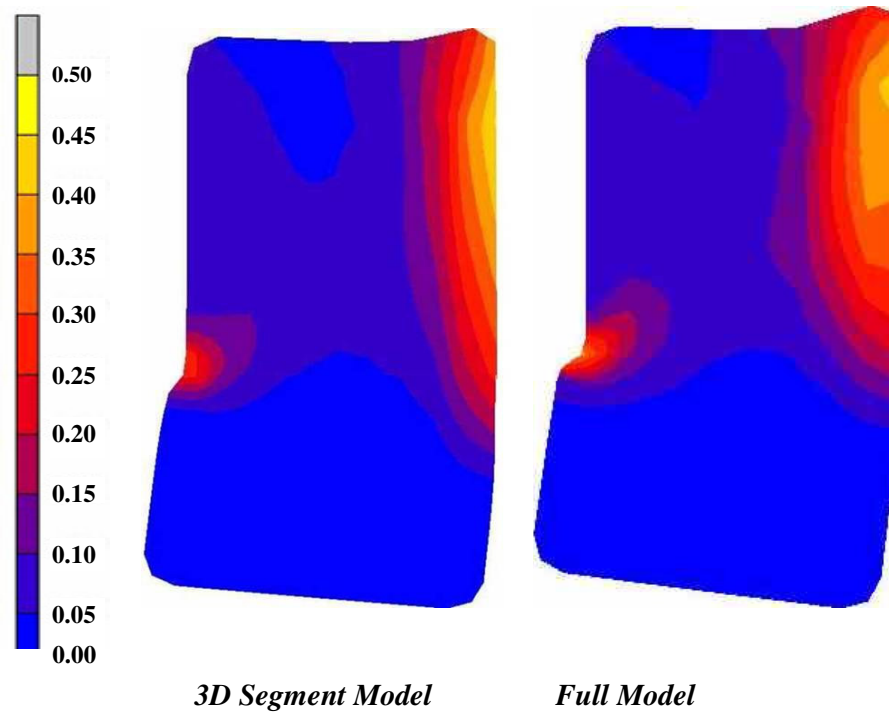


Figure 6.8 Total equivalent strain distributions for 3D Segment Model

6.3.3 Residual Stress Comparison

The residual stresses are compared for different segment angles and the variation from the full model is compared on basis of equivalent stresses in *Figure 6.8*. The results show that there is no significant stress variation as segment angle changes but the variation is larger for the smaller segment angles and more stresses induced on the small angled models. The reason was explained in *Section 6.1*. However there is also difference between the full model and all of the segment angle models.

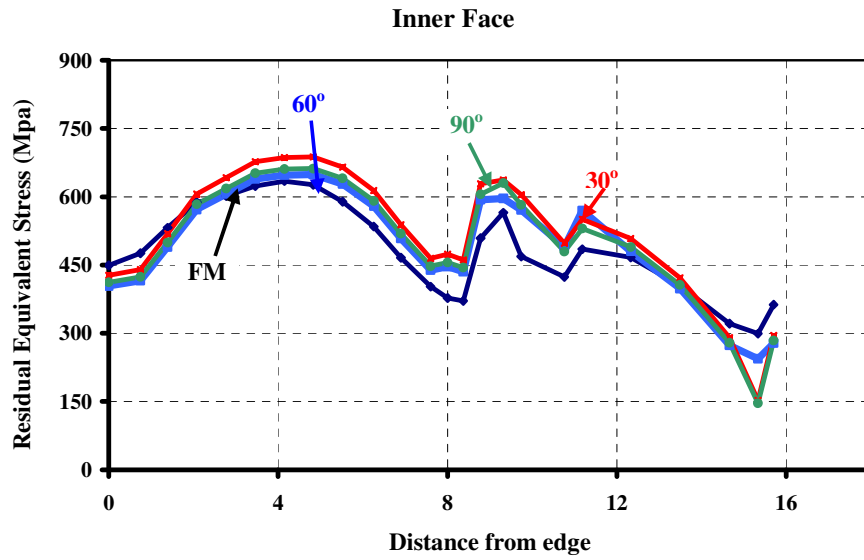
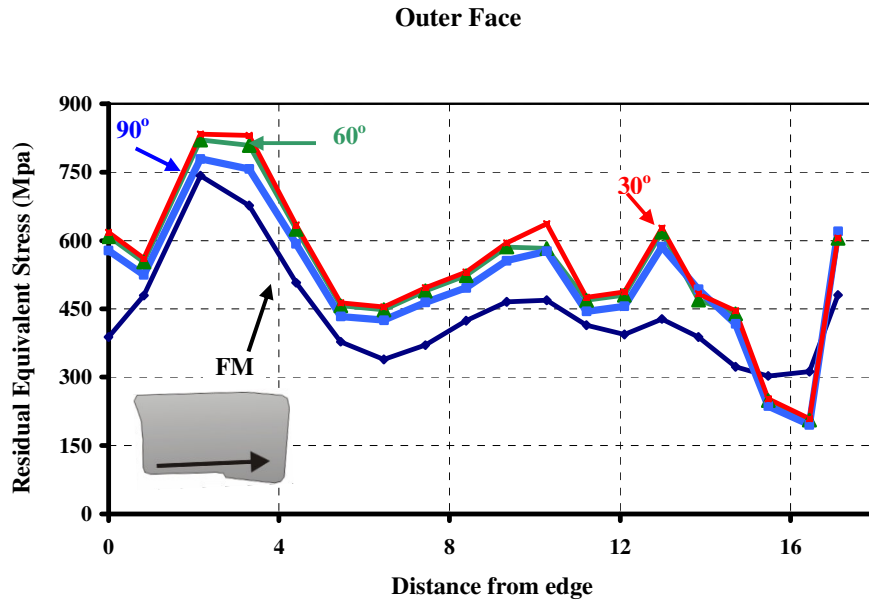


Figure 6.9 Residual equivalent stress distribution on the a) outer b) inner surface of the ring, for different segment angles

The main crude assumption of this model was explained as the fixing the boundary surfaces as rigid planes. This assumption is absolutely valid for a conventional ring rolling process, since the growth in circumferential direction is uniform. However as it was also observed in the experiments, the material flow is non-uniform in radial and axial and so in circumferential direction. The tilting motion, which is an outcome of non-uniform flow, creates bending moment on the boundary surfaces. Therefore, the boundary surfaces can not remain plane in the real process ring rolling. The planes start to warp.

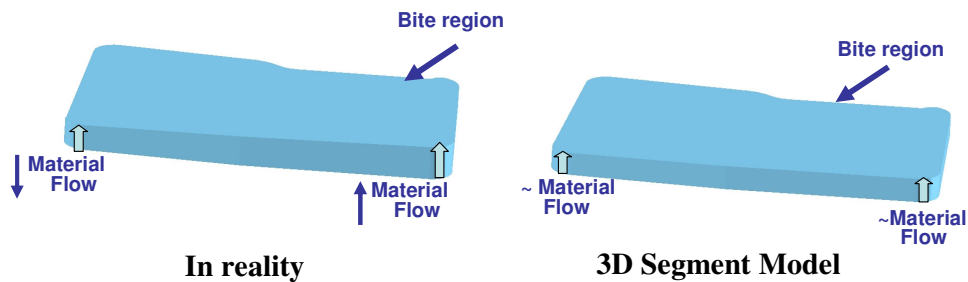


Figure 6.10 Material flow on the boundary plane

A simple representation of the boundary planes are shown in the *Figure 6.9*. In the real case, the material flow on the left side is less than it is on the right side, however rigid boundary planes do not let this kind of motion. This warpage induce excessive stress on the boundary planes and the flexibility of the ring on the boundaries is restricted. Then this restriction induces, compressive stresses especially in circumferential directions, which will also be shown in the comparison part. This causes higher stress values. The boundary planes should be relaxed to simulate the real process conditions.

6.3.4 Accuracy and Computation Time

It was shown that the stress values are higher in this model however the total error which depends on segment angle is reasonable and if the accuracy of the geometry is considered this model can be considered as reliable in terms of accuracy. The

accuracy is based on comparison of equivalent stress distribution with the full model. In the *Figure 6.11*, the error for the models and the computation time are given. The error accumulated is also maximum, for 30° segment angle model with minimum computation time of 11 hrs. It is approximately one thirty fourth of the full model.

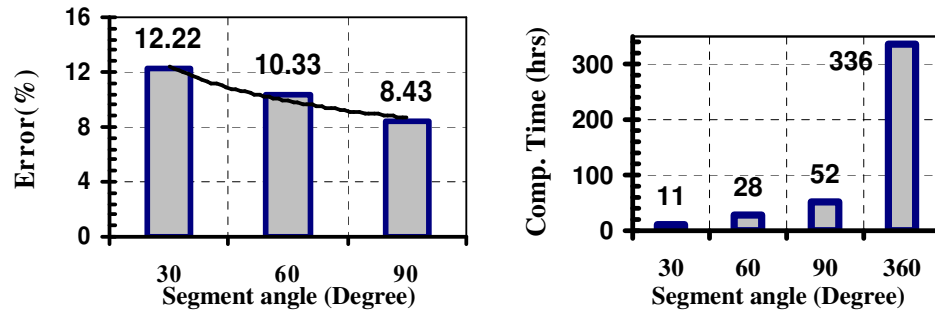


Figure 6.11 Accuracy and computation time of the model

6.4 3D Segment Model with Soft Elastic Region

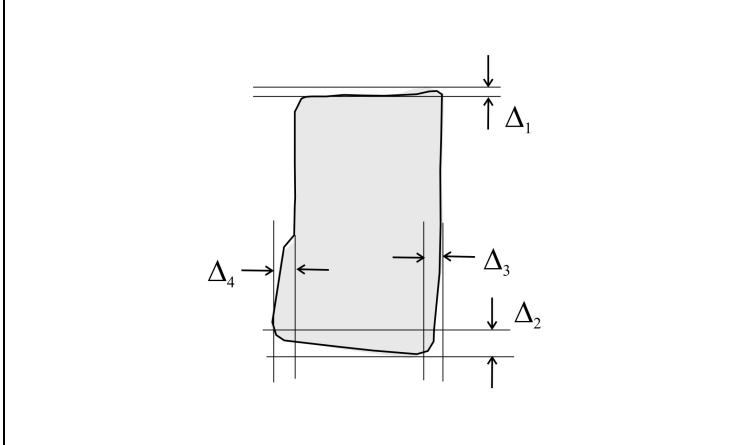
This model is similar to previously investigated one. An improvement based on the higher stress results due to restrictions in the boundary plane, is made. In this model the boundary planes are relaxed with the soft elastic regions as mention in the previous chapter. The most important parameter to investigate is the modulus of elasticity of the region. The analyses are performed for 4 different values; 50, 1000, 10000, 50000 MPa.

6.4.1 Geometrical Comparison

It is observed from that for different modulus of elasticity values, the geometry of the simulated ring does not change significantly. The comparisons on geometry are based on the results of the model with 1000 MPa of modulus of elasticity. In the table it can be observed that there are slight differences. These differences were

higher for plain 3D segment model. This model can be considered as high accurate in terms of geometry when the width and the height of the ring are considered.

Table 6.6 Geometrical comparison of 3D Segment Model with Soft Elastic Region



Deflections (mm)	Δ_1	Δ_2	Δ_3	Δ_4
<i>3D Full Segment Model with Soft Elastic Region (with 30°)</i>	0.42	1.10	1.28	1.49
<i>3D Full Model (#3)</i>	0.38	1.15	1.51	1.62
<i>Experiments</i>	0.17	1.35	1.4	1.74

6.4.2 Total Equivalent Strain Comparison

The total equivalent strain distributions for these two models are quite similar (**Figure 6.12**), the most significant difference is also observed on the outer surface. The results are taken from the mid-plane of the segment. In the figure, it can be observed that the equivalent strain distributions have peaks on the region where there is a small contact area with the mandrel edge. The error in equivalent strain results in the inner part of the ring is less than it is in the outer part. On the outer surface of the ring the strain profile is similar. The equivalent strain distributions are also based on the model with 1000 Mpa. The graphical representation of the

distribution will be presented in the proceeding parts. The comparisons with previous model will also be presented.

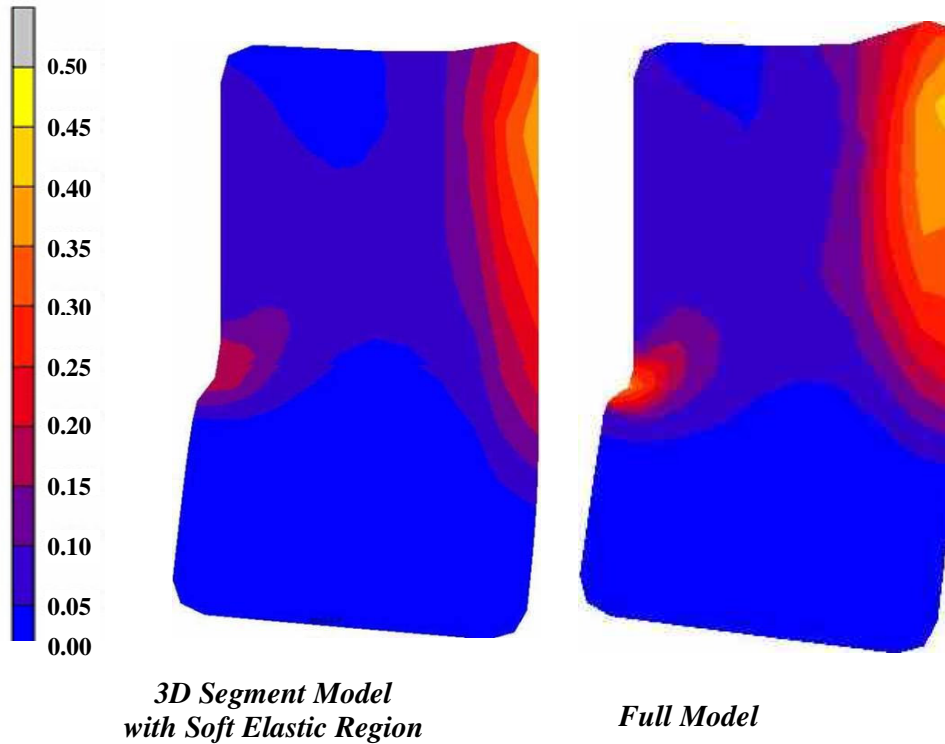


Figure 6.12 Total equivalent strain distributions comparison for 3D Segment Model with Soft Elastic Region

6.4.3 Residual Stress Comparison

The residual stresses are compared for all models with different modulus of elasticity. The variation from the full model is compared on basis of equivalent stresses in *Figure 6.8*. The results show that there is no significant stress variation as segment as the modulus of elasticity changes but the variation is larger for the models with larger modulus of elasticity. As the modulus of elasticity decreases the variation also decrease. 50 and 1000MPa gives the closest results, however 50 MPa is resulted in some contact problems on the boundary surfaces, due to excessive elastic deformation sticking on the boundary planes is observed.

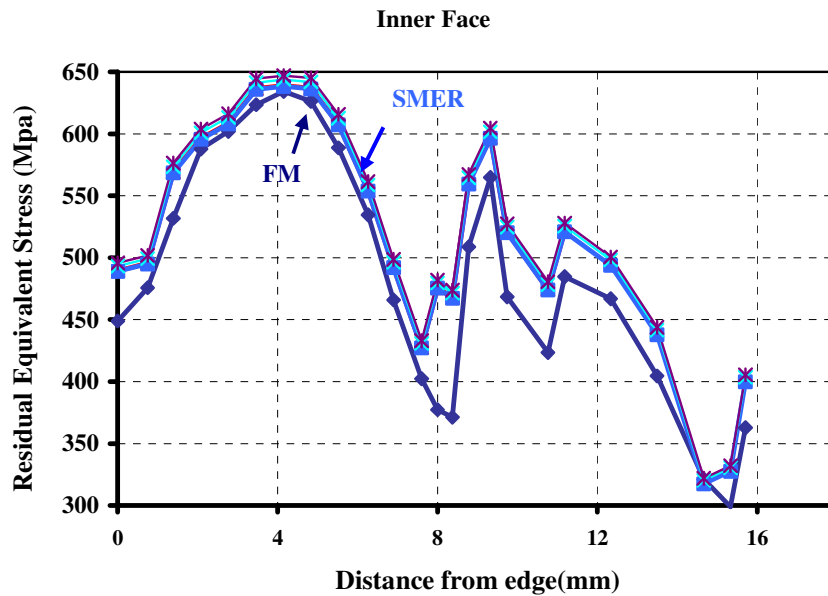


Figure 6.13 Total equivalent stress distributions comparison for 3D Segment Model with Soft Elastic Region

It is observed that there is a stress relief on the ring. The stress values are smaller for this model. However the results of this model correspond to process with 1.1 mm bite. In excessive deformation, relieves on the boundary planes will be inadequate.

6.4.4 Accuracy and Computation Time

It was shown that the stress values are lower in this model and the total error which slightly depends on modulus of elasticity is reasonable. The minimum error is observed for the 1000 Mpa. This amount is also reasonable for giving adequate flexibility in warping *Figure 6.13*. The model is performed with a 30° segment angle and its accuracy is about 8.05% with a computation time of 13 hrs. If the accuracy of the geometry is considered this model can be also considered as reliable in terms of accuracy as well as being efficient in terms of computation time. The accuracy is based comparison of equivalent stress distribution with the

full model results. In the *Figure 6.13*, error for the models and the computation time are given. The error accumulated is also maximum, for 30° segment angle model with minimum computation time of 13 hrs. It is approximately one thirty fourth of the full model.

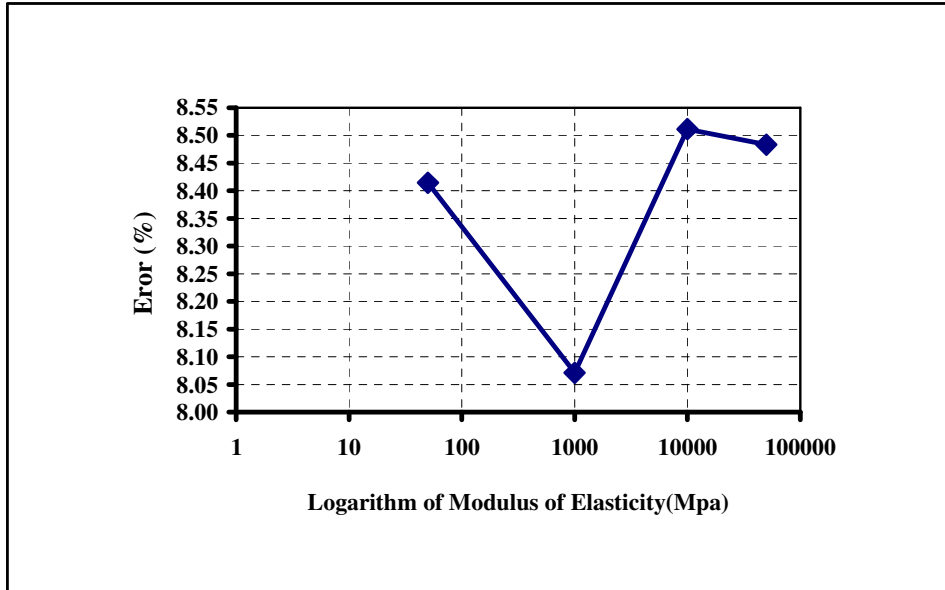


Figure 6.14 Accuracy of the model for different modulus of elasticity.

6.5 3D Velocity Coupling Model

This model is the most complicated one among all other models, despite its complexity there is no specific parameter to examine. The model is also based on the concept of relaxation of the boundaries. It enables the flexibility of modeling the processes even at high deformations. In this section, the effectiveness of the model will be investigated for both low (1.1 mm of bite) and high (2.2 mm of bite) deformations. The results of the former will be validated using the full model and the experiments whereas the latter will be validated with only a full model.

The results are taken from a model with 30° segment angle. In previous models, the accuracy is enhanced as the segment angle increases. The results of this model

showed that the accuracy is adequate for 30° and there is no need to check for the variation of the results for larger segment angles.

6.5.1 Geometrical Comparison

a) Low Deformation (Bite: 1.1 mm)

Table 6.7 Geometrical comparison of velocity coupling method at low deformation

Deflections (mm)	Δ_1	Δ_2	Δ_3	Δ_4
<i>Velocity Coupling</i>	0.40	1.12	1.43	1.55
<i>3D Full Model (#3)</i>	0.38	1.15	1.51	1.62
<i>Experiments</i>	0.17	1.35	1.4	1.74

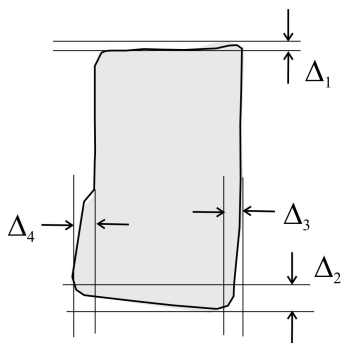
It can be observed from **Table 6.7** that the geometry of the model is approximately same for the velocity coupling model. There are small differences in the deflections, and if it is compared with the dimensions of the ring, these can be neglected.

b) High Deformation (Bite: 2.2 mm)

In **Table 6.8**, the results of velocity coupling model show that the increase in deformation reflected non-uniformly to the deflections. For example the amount of

fishtail out (Δ_1) tripled whereas the amount of the tilt and climbing increased to 1.5 times of their previous values. The full model verifies the simplified model. The results for two models are close and the order of differences is approximately same as it is in the lower deformation case. Therefore, the geometric accuracy is sustained at high deformations.

Table 6.8 Geometrical comparison of velocity coupling method at high deformation



The diagram shows a cross-section of a ring that has been deformed. The original shape is a rectangle, and the deformed shape is a rounded rectangle with a 'fishtail' at the top and bottom. Four deflection measurements are indicated: Δ_1 is the vertical distance from the top edge of the original rectangle to the top edge of the deformed ring; Δ_2 is the vertical distance from the bottom edge of the original rectangle to the bottom edge of the deformed ring; Δ_3 is the horizontal distance from the right edge of the original rectangle to the right edge of the deformed ring; and Δ_4 is the horizontal distance from the left edge of the original rectangle to the left edge of the deformed ring.

Deflections (mm)	Δ_1	Δ_2	Δ_3	Δ_4
Velocity Coupling	1.10	2.12	2.43	2.64
3D Full Model (#3)	1.22	2.34	2.32	2.79

6.5.2 Total Equivalent Strain Comparison

a) *Low Deformation (Bite: 1.1 mm)*

The non-uniform strain distribution discussed in previous parts can also be observed in this model. The profiles of the strain on the outer and inner surfaces of the ring are similar for two models. There are minor differences; on the region where the climbing starts and on the outer surface where mandrel contacts with. The higher strain values are observed at these regions. On the outer surface, the strain decreases gradually just after tilting starts. The strain distribution becomes

more uniform as getting closer to inner part of the ring. The model is also good at predicting the strain distribution.

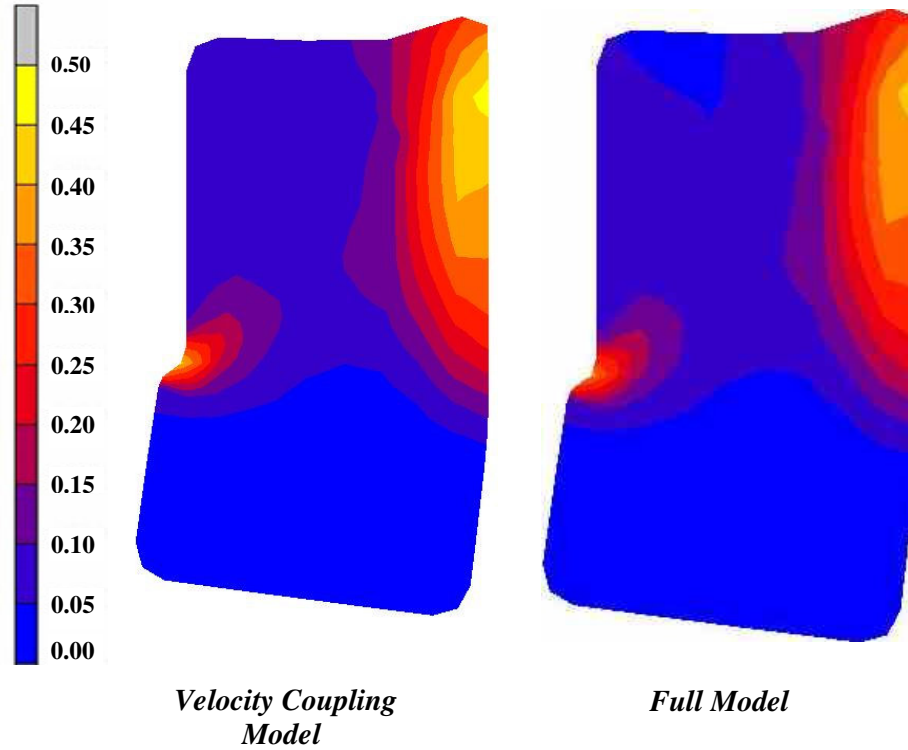


Figure 6.15 Total equivalent strain distributions comparison for velocity coupling model (1.1 mm of bite)

b) *High Deformation (Bite: 2.2 mm)*

The profile of strain distribution for high deformation process has similar trend with the low deformation one. The degree of non-uniformity is higher for this model and strain values at the outer surface are doubled. The profiles of the strain on the outer and inner surfaces of the ring are similar for two models. There are also minor differences; on the region where the climbing starts and on the outer surface where mandrel contacts with the ring. The higher strain values are observed at these regions for the velocity coupling model. This small difference is due to two main assumptions of the model; equating the velocities of boundary

planes and finding the instantaneous center of rotation with stored data of previous increment. Both of these assumptions accumulate error as the number of increment increases. In real case, the normal velocity of the boundary planes slightly differs, so there is a local error (shown in *Figure 5.11*), equating these velocities at each increment accumulates error and it increases with number of increment.

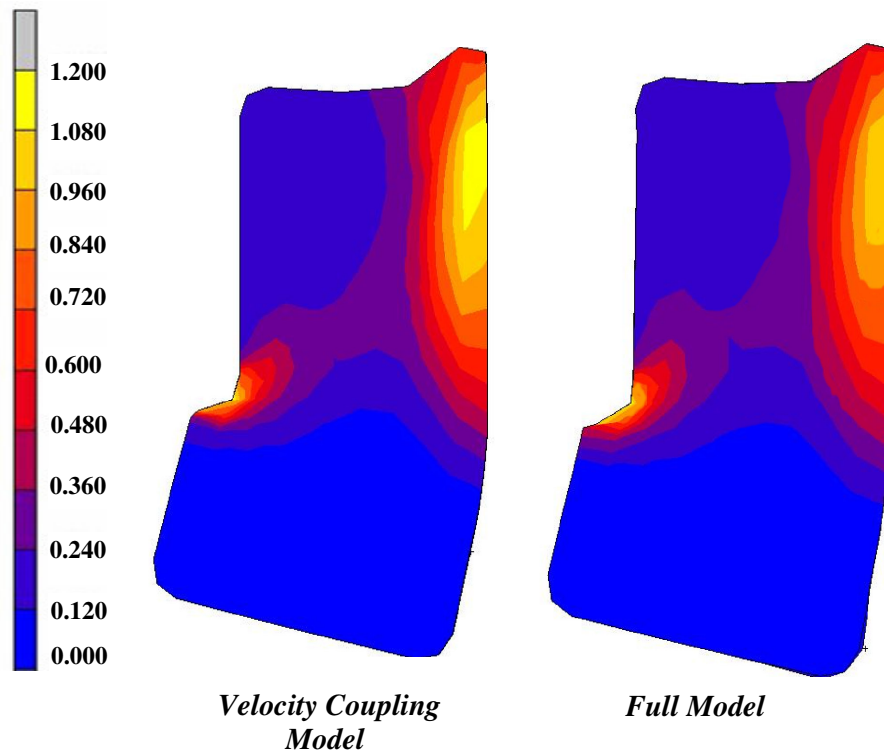


Figure 6.16 Total equivalent strain distributions comparison for velocity coupling model (2.2 mm of bite)

6.5.3 Residual Stress Comparison

a) *Low Deformation (Bite: 1.1 mm)*

The residual stress comparison for the low deformation will be given in *Section 6.6* in comparisons of all models. The characteristics have already mentioned in other models.

b) *High Deformation (Bite: 2.2 mm)*

The residual stress results are compared with the full model (*FM*) results in **Figure 6.18 a-d**. The comparisons are made in circumferential and axial directions for inner and outer surfaces. On the outer surface, there is a gradient between the middle and edge of the ring. The stresses on the middle part of the ring are compressive. In order to understand the residual stress distribution in circumferential direction on the outer surface of the ring, the deformation in the circumferential direction is given in **Figure 6.17**. The undeformed view of the plane is also shown.

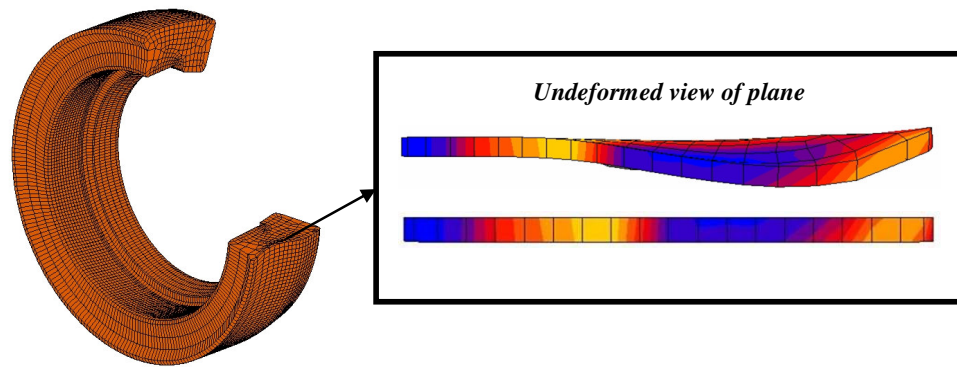


Figure 6.17 *Circumferential deformation of the ring*

The blue bands represent the compressive stresses and remaining bands are for tensile stresses. The warpage on the plane can be easily observed. There is a curvature on the right part of the ring which squeezes the middle part over the planar part, thus the compressive stresses in both circumferential and axial directions are observed on this part (**Figure 6.18a-b**). The tensile stresses in circumferential direction have peak values at the tip of the curvature. The axial stress distribution has also similar trend, however the compressive area is more than the tensile area. The ring stretches in axial direction (this can be easily observed in **Figure 6.16**), and it tends to recover its shape after the tools are released, hence the compressive stresses are observed dominantly.

On the inner surface, the stress is uniformly distributed in both circumferential and axial direction, except for the climbing region (*Figure 6.18c-d*). The gradient at the climbing region is high and the stress distribution at this region is not reliable due to high stress concentration. The stress values on this region can be improved by mesh refinements, however if the computation time for this model is considered (702 hrs \approx 29.5 days) it is costly. The axial stresses converge to zero at the edges; this is an expected result.

This small difference is due to the main assumptions of the model; equating the velocities on boundary planes. There is difference in the velocities due to elastic deformations in reverse direction. Each increment of the ring rolling looks like simple upsetting process due to squeezing motion of the form roll then material flow is expected to be in two directions. However, the dominant material flow is provided by the rolling force in the direction of rotation, and the material only elastically deforms in reverse direction. This is neglected at solution of each increment, and the results are used in the next increment and the error increases. Neglecting the elastic deformations in reverse direction leads to higher stress results for this model. An analytical model was tried to be developed to calculate this effect at each step. The main idea was assigning the elastic effects to the boundary nodes. However the nature of the process is extremely complex, there are no closed formed analytical equations for even conventional ring rolling.

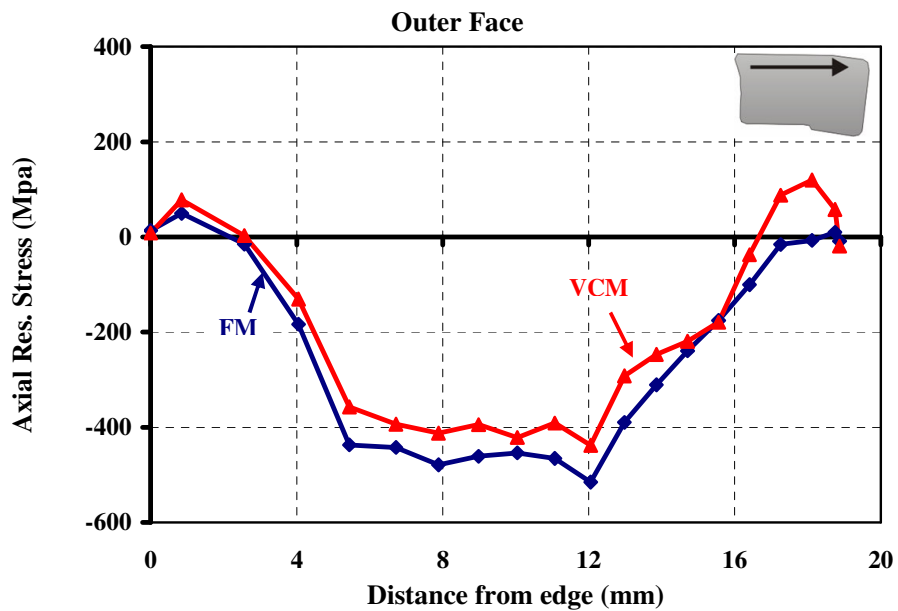
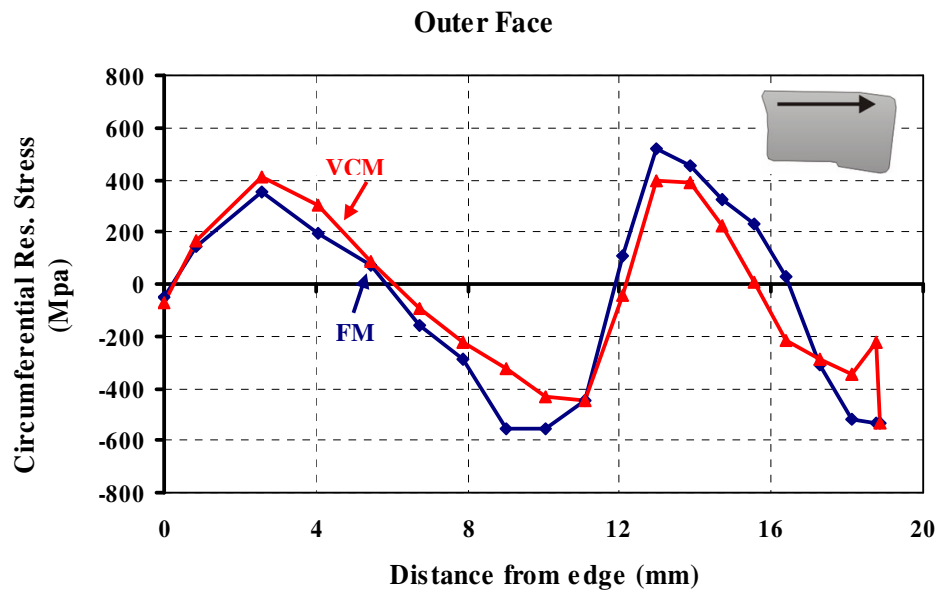
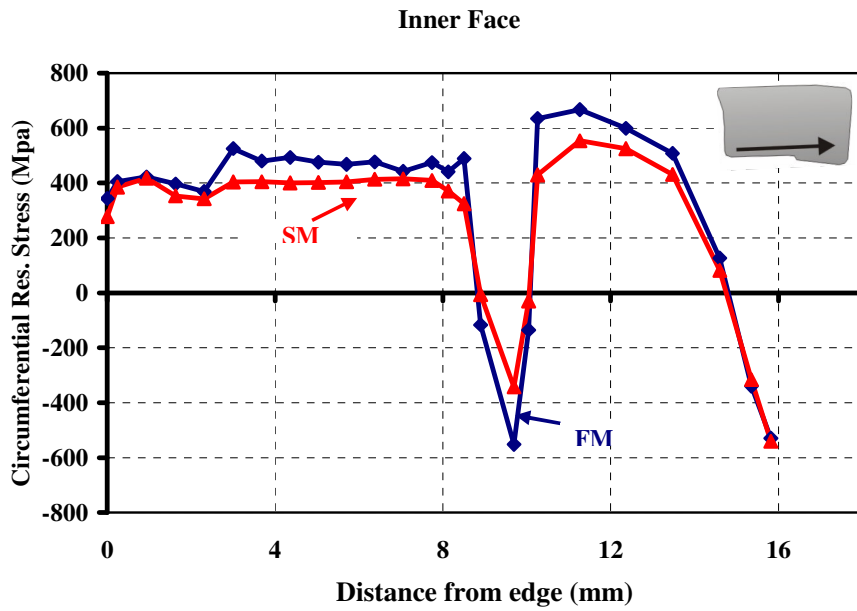
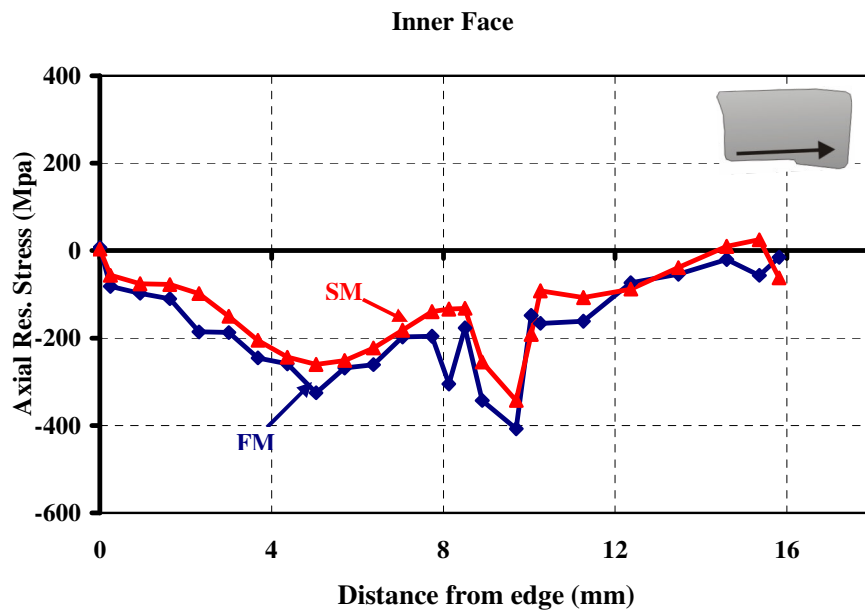


Figure 6.18 Residual stress distribution in the **a)** circumferential **b)** axial direction, on the outer surface of the ring, for different mesh topologies



c)



d)

Figure 6.18(continued) Residual stress distribution in the *c*) circumferential *d*) axial direction, on the inner surface of the ring, for different mesh topologies

6.5.4 Accuracy and Computation Time

The comparison for the residual stresses for low deformation process has not presented yet, however the error is calculated on the basis of the equivalent stress distribution for both processes. The stress values are higher in velocity coupling model due to reasons mentioned before. In the **Table 6.9** errors of the models and the computation time is given. The computation times of the velocity coupling models are approximately one twenty fifth of the full model with a high accuracy in results.

Table 6.9 Accuracy and computation time of the velocity coupling models.

<i>Velocity coupling model</i>	<i>Error in Equivalent Stress (%)</i>	<i>Computation time (hrs)</i>	<i>Computation time for Full Model (hrs/days)</i>
<i>Low deformation (1.1 mm)</i>	<i>%3.2</i>	<i>~18</i>	<i>~336 / 14</i>
<i>High Deformation (2.2 mm)</i>	<i>%4.1</i>	<i>~38</i>	<i>~702 / 29</i>

6.6 Comparisons of all models

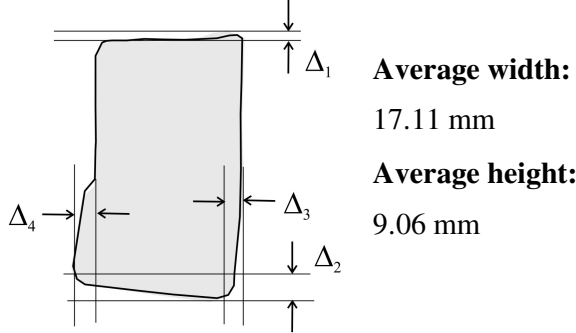
In this part, the models will be compared within each other and with the experiments. The comparisons stated in previous part will be summarized. The reason for differences in the results will be explained and requirements for further improvements will be discussed. The efficiency of the models will be evaluated in terms of computation time and the error.

6.6.1 Geometrical Comparison

The **Table 6.10** shows the amount of the deflections that have been defined previously for all models. The error for each deflection value is calculated with respect to results of the experiments and the maximum is taken as the global error. The error decreases as the model gets more complex and the computation time

increases. A performance index (PI) for prediction of geometry can be defined as the product of the percentage error with computation time, the minimum of which will be most efficient. This product is minimum for the 3D segment model, thus the most effective model in geometrical prediction is the 3D segment model.

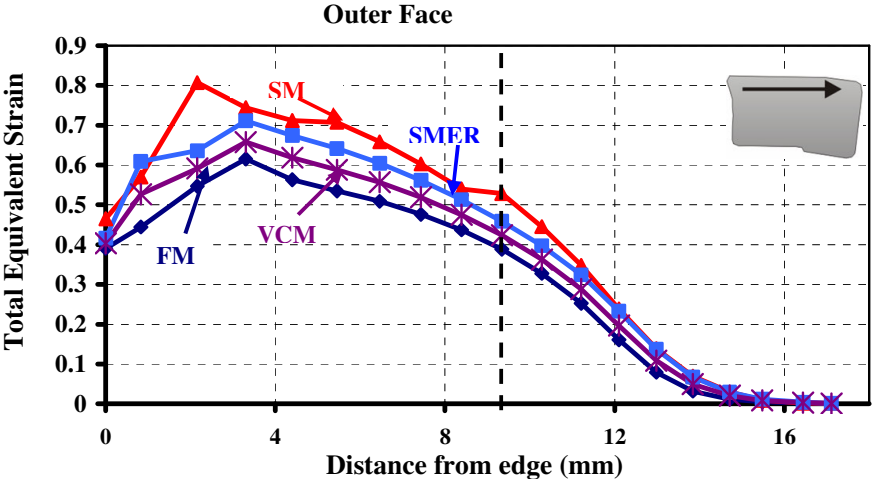
Table 6.10 Geometrical comparison of all models

							
Deflections in mm	Δ_1	Δ_2	Δ_3	Δ_4	Error (%)	Comp Time (hrs)	PI
<i>3D Segment Model (SM)</i>	0.49	1.19	1.21	1.51	2.65	11	29.2
<i>3D Segment Model with Elastic Region (SMER)</i>	0.42	1.10	1.28	1.49	2.43	13	31.6
<i>Velocity Coupling(VCM)</i>	0.40	1.12	1.43	1.55	2.10	18	37.8
<i>3D Full Model (FM)</i>	0.38	1.15	1.51	1.62	1.32	336	443.4
<i>Experiments</i>	0.17	1.35	1.4	1.74	-	-	-

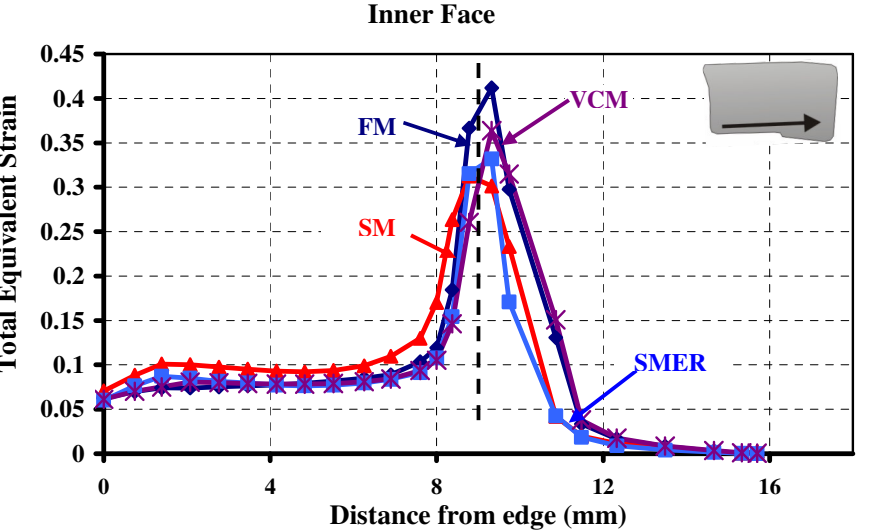
6.6.2 Total Equivalent Strain Comparison

The total equivalent strain values are compared in *Figure 6.19a-b*. The strain data are taken along the direction shown in small figures on the graphs as in previous cases. All models successfully predict the region where tilting and climbing starts(the starting points are shown in dash lines), however there is a small shift towards left for the 3D segment model.. The non-uniform strain distribution can be

seen in results of all models. The strain values are higher in 3D Segment model and the maximum difference with the full model is observed in this model. These higher results are due to restricted boundary planes. The 3D segment model with soft elastic region has better approximation to the full model; as the boundaries are relaxed, the excessive forces decreases and the deformation decreases.



a)



b)

Figure 6.19 Total equivalent strain comparison of all models on the a) outer b) inner surfaces

The velocity coupling model gives the better approximation for all regions on the outer and inner surface of the ring. The reason for the minor differences is the accumulated error due to assumption of equating the velocities and calculation of center of rotation using the data for previous increment.

6.6.3 Residual Stress Comparison

In *Figure 6.20-24*, the residual stresses in circumferential and axial direction on the inner and the outer surface of the ring has been shown respectively. It has been already mentioned that it is difficult to catch the stress on the outer surface. Further refinement should be performed.

The stress results in circumferential direction are similar for all models but there are differences in magnitudes (*Figure 6.20*). The most significant differences in stress results are observed between the 3D segment model and the full model. The differences are bigger where tilting starts; at this region, the maximum difference is 250 MPa. The reason for this big difference is the restricting effect of the boundary planes. This difference corresponds to error of 40%. The differences are also because of the small differences in the nodal positions. The data are collected from nodes and the position of the nodes can vary for different models. For example there is a small shift in the results of 3D segment model towards left.

The results between 8.5-17 mm distances have a good convergence trend. As the boundary planes are relaxed with elastic regions; the circumferential stress directly decreases. The most accurate results are obtained from velocity coupling model, both the trend and the magnitudes are successfully predicted. It can be considered as most efficient model to predict outer stress distributions.

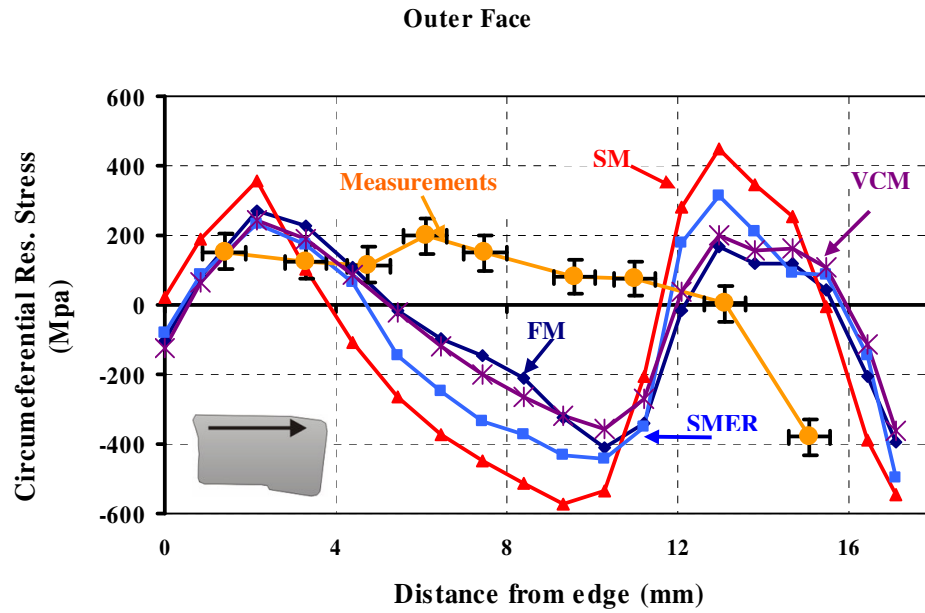


Figure 6.20 Residual stress distribution in the circumferential direction on the outer surface of the ring, for all models.

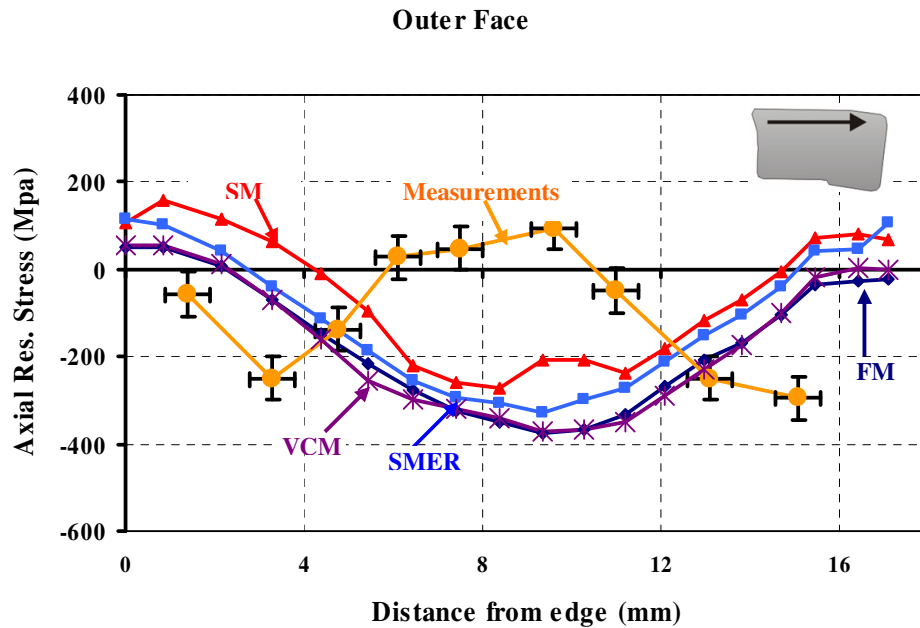


Figure 6.21 Residual stress distribution in the axial direction on the outer surface of the ring, for all models.

It can be observed from *Figure 6.21* that there is a better agreement in the results of axial stresses on the outer surface. The restriction on the boundaries does not affect the axial stress dominantly however still the segment angle model with soft elastic region gives better results compared to plain segment model. The maximum difference is also about the tilting point. The agreement of the velocity coupling model to full model is perfect. Therefore, the most effective model in prediction of axial and the circumferential stresses is the velocity coupling model

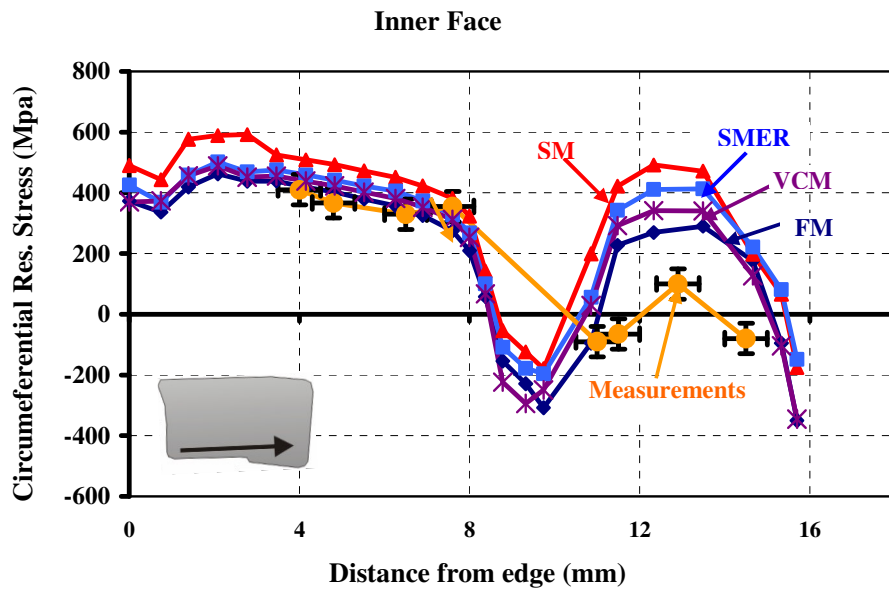


Figure 6.22 Residual stress distribution in the circumferential direction on the inner surface of the ring, for all models.

There is a better agreement with the experiments in axial and radial residual stress distribution on the inner surface. The circumferential stress distribution is shown in the *Figure 6.22*. The maximum variation from the stress values of the full models is also observed in results of 3D segment model. However the error is smaller. The velocity coupling model has again perfect agreement with the full model; there are minor differences in the climbing region in which the experimental results are not also reliable because of the difficulties in the measurements at this part. Therefore,

the velocity coupling model is the most efficient model also for prediction of circumferential stresses on the inner surface.

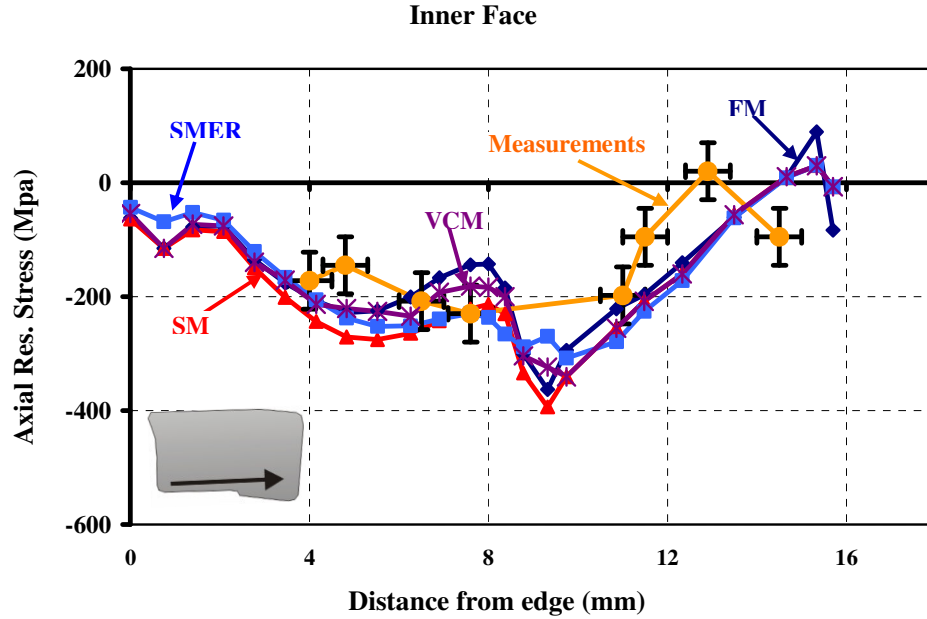


Figure 6.23 Residual stress distribution in the axial direction on the inner surface of the ring, for all models.

The axial stress distributions for all models are in a good agreement as shown in **Figure 6.23**. The trend in the results of the experiments is predicted successfully; however there are minor differences in values.

6.6.4 Accuracy and Computation Time

The accuracies of the all models are compared on the basis of error on the equivalent stress. The **Table 6.11** shows the error accumulated for all models and the corresponding computation times. Among simplified models the velocity coupling has the longest computation time. However, when performance index (PI) which can be defined as the product of computation time and the percentage

error is calculated, the velocity coupling model is considered to be most effective one in predicting the residual stress distribution.

Table 6.11 Accuracy and computation time comparison of all models.

Models	Error (%)	Computation Time (hrs)	PI
<i>3D Segment Model (SM)</i>	12.22	11	134.4
<i>3D Segment Model with Elastic Region (SMER)</i>	8.05	13	104.7
<i>Velocity Coupling(VCM)</i>	3.2	18	57.6
<i>3D Full Model (FM)</i>	-	336	

CHAPTER 7

DISCUSSION AND CONCLUSION

The incremental ring rolling process is a hot topic and has not been studied extensively neither experimentally nor numerically. This study, involving both experimental and numerical works, is an intermediate work in the examination of the nature of the process.

The studies were started with intensive literature survey. Since the process has not been dealt before, similar processes were identified and numerical studies on these processes were investigated. The studies were focused on numerical modelling. The pitfalls on the numerical modelling of the incremental forming processes were examined and proposed methods were discussed. It was observed that the implicit codes are preferred in modelling metal forming process despite the computation time is costly.

The experimental studies which were performed in ORS Bearing Company, gave the basic information about the material flow for different configurations of mandrel and its width. Three series of experiments were performed. In the first series, the mandrel was aligned from the edge and the effect of increase in bite was investigated. In the second series four different configurations were tried to examine the stability and observe the shapes resulting from straight paths. In this series the residual stress distributions were taken from XRD machine and the results compared with the conventional ring rolling. It was observed that the residual stresses were more tensile in incremental than it was in conventional ring

rolling. The third series of experiments were performed to investigate the effect of rolling parameters on the profile. The aim of this series was to investigate the effect of rolling parameters on the profile, the residual stresses and stability. It was shown that the difference between the residual stresses for the inner and outer surfaces increases when the mandrel is aligned to middle of the ring.

The numerical investigations were started with examining the conventional ring rolling and working on the previous studies to understand the modeling issues. A 2D simplified model which had been developed previously was combined with 3D full model and an alternative method was proposed for modeling conventional ring rolling. This model consists of modeling the ring partially, and assuming remaining part as rigid by means of rigid boundary planes. The results of the residual stresses agreed with full model with high accuracy and computation time decreased significantly.

The investigations for incremental ring rolling were started with the studies on finding a reliable numerical model. The analyses on 3D full model were performed and the results were validated with the experiments. The selected 3D full model was used as the reference model in proceeding studies.

The simplified model developed for conventional ring rolling was adapted to incremental one and also called as *3D Segment Model*. Although the geometrical accuracy was high, the reliability of results of residual stresses was lower. The assumption of keeping the boundary planes as planar was not valid for this process. The boundary planes needed relaxation. This was provided by a new model called as *3D Segment Model with soft Elastic Region* in which boundary planes were relaxed using soft elastic regions on the boundaries. The accuracy in stress results was significantly increased.

The final improvement was performed by removing the boundary planes, and imposing new boundary conditions using a special subroutine. This new model

was called as *Velocity Coupling Model*. The normal velocities of the nodes on the boundary planes of the partially modeled ring were equated. The validity of this assumption was discussed. The highest accuracy in stresses was obtained from this model.

All of the models were compared with the reference model and the experiments. It was observed that all provide perfect approximation in geometry and reasonable accuracy in the residual stress results. The effectiveness of the models were discussed and the velocity modeling was observed to be the most efficient model when the ration of computation time to the amount of error in predicting the stress was considered. These models can be used in further investigations of the incremental ring rolling to determine the material flow and residual stresses.

CHAPTER 8

RECOMMENDATIONS AND FURTHER STUDIES

The incremental ring rolling process was investigated by narrowing the definition to a single step, which did not involve the simultaneous movement of mandrel in both radial and axial direction. However as it was mentioned before, it is a difficult task to model this kind of process numerically; even the computation time for the full model of the investigated process was about 29 days for 2.2 mm of bite. The computation time for a moving mandrel model would be much more than this, since a more refined mesh would have to be used and the contact parameters would be re-analyzed.

Another restriction for a moving the mandrel model was in validation. The experimental set up was not convenient to support this kind of analyses. Therefore, the validation of the numerical model would not be possible. In the further analyses of this process; more powerful computers should be used to decrease the computation time and the limitation in the experiments should be eliminated, by modeling a simple modeling machine. The modeled machine can use plastic or wax material instead of steel (as the modeled machine in Cambridge University mentioned in first part).

The simplified models should be used to model the moving mandrel problems to observe the material flow and the stress distributions. The reliability of the models for different kind of mandrel alignment configurations should be proved. The

residual stress distributions for all of configurations should be performed to validate the results.

This study is a “warming up” stage of the incremental ring rolling process. The feasibility of the new process can be investigated by designing new tools to control the shape of the ring according to material flow. Therefore, the material flow and the stress distribution profiles obtained from the current study can be used in this kind of feasibility study.

REFERENCES

Allwood, J.M.; Tekkaya, A.E.; Stanistreet, T.F: The development of ring rolling technology. *Journal of Steel Research* Vol. 76/2/3, (2005) 111-120.

Allwood, J: A Periodic table of ring processes. *Proceedings of 8th ICTP, Verona/Italy, 2005.*

Allwood, J.M.; Kopp, R.; Michl, D.; Music, O.; Oztop, M.; Stanistreet, T.F; Tekkaya, A.E; Tiedemann, I: The Technical and Commercial Potential of an Incremental Ring Rolling Process, *Annals of CIRP* 54(1) (2005) 233-236.

Bartnicki, J.; Pater Z.: Numerical simulation of three-rolls cross-wedge rolling of hollowed shaft, *Journal of Materials Processing Technology* 164–165 (2005) 1154–1159.

Bührer, R.: Orbital Forming-Challenges of Simulation Methods. *ICFG/Vif Workshop on Modelling of Incremental Bulk Forming Processes, Darmstadt/Germany, May 17-18, 2006.*

Cai,Z.Y.: Precision design of roll-forging die and its application in the forming of automobile front axles. *Journal of Materials Processing Technology* 168, 95–101, (2005)

Eruc, E.; Shivpuri, R.: A summary of ring rolling technology--II. Recent trends in process modeling, simulation, planning, and control. *International Journal of Machine Tools & Manufacture*, 32 (1992) 379-398.

Davey, K.; Ward, M.J.: A successive preconditioned conjugate gradient method for the minimisation of quadratic and non-linear functions. *IMACS, Appl. Numer. Math.* 35 (2000) 129–156

Davey K.; Ward M. J.: A Practical Method for Finite Element Ring Rolling Simulation using the ALE Flow Formulation. *International Journal of Mechanical Sciences*, Vol. 44, (2002)165-190

Domani, G.: Experiences with Simulation of Incremental Forming Processes at HILTI. *ICFG/Vif Workshop on Modelling of Incremental Bulk Forming Processes*, Darmstadt/Germany, May 17-18, 2006.

ERATZ-Engineering Company: http://www.eratz.de/index_e.htm, Last accessed; September 2006.

Fang, G.; Lei,L.P; Zeng,P: Three-dimensional rigid-plastic finite element simulation for the two-roll cross-wedge rolling process. *Journal of Material Processing Technology* 129 (2002) 245-249.

Fritsche, D.: Efficient Simulation of Cyclic Processes Using Similarity Methods, *ICFG/Vif Workshop on Modelling of Incremental Bulk Forming Processes*, Darmstadt/Germany, May 17-18, 2006.

Fu, P.F.; Yang, S.H.; Huang, L.J.: The new development of roll forging technology and its application in China, Rotary forming: *Proceedings of International Conference*, International Academic Publishers, Beijing, (1989) pp. 205–210.

Ghaei, A.; Movahhedy, M.R.; Taheri A.K: Study of the effects of die geometry on deformation in the radial forging process. *Journal of Materials Processing Technology* 170 (2005) 156–163

Groche, P.; Rathmann, T.: Development of a technological process for 3D-FEA of rotary swaging processes. 4th ICFG Workshop on Process Simulation in the Metal Forming Industry, Shanghai/China, 2004

Güley, V.: Experimental investigation of residual stresses and their effect on fatigue life of ball bearings, Master of Science Thesis, Middle East Technical University, 2004.

Hartely, P.; Alsamhan, A.; Pillinger, I.: The development of real time re-meshing technique for simulating cold-roll-forming using FE methods. *Journal of Materials Processing Technology* 147 (2004) 1–9

Heislitz, F.; Livatyali, H.; M.A. Ahmetoglu: Simulation of roll forming process with the 3-D FEM code PAM-STAMP, *J. Mater. Process. Technol.* 59 (1996) 59–67

Hosford, W.; Caddell, R.M.: *Metal Forming Mechanics and Metallurgy*, Prentice Hall, 1993

Hu, Z.M; Pillinger, I.; Hartley, P.; McKenzie, S.; Spence, P.J., Three-dimensional finite-element modelling of ring rolling, *Journal of Materials Processing and Technology* 45 (1994) 143–148

Hu, W.; Wang, Z.R.: Theoretical analysis and experimental study to support the development of a more valuable roll-bending process. *International Journal of Machine Tools & Manufacture* 41 (2001) 731–747

Jang, D.Y. ;Liou, J.H.: “Study of stress development in axi-symmetric products processed by radial forging using a 3-D non-linear finite-element method” *Journal of Materials Processing Technology* 74 (1998) 74–82

Joun M.S.; Chung J.H.; Shivpuri R.: An axisymmetric approach to preform design in ring rolling using a rigid-viscoplastic finite element method. *International Journal of Machine Tools and Manufacture* 38 (1998) 1183-1191.

Just,H.;Meeting the Challenge of Simulating Incremental Forming Processes, Workshop Darmstadt. ICFG/Vif Workshop on Modelling of Incremental Bulk Forming Processes, Darmstadt/Germany, May 17-18, 2006.

Karacaovali, H.: Analysis of Roll-Forging Process, Master of Science Thesis, Middle East Technical University, 2005.

Kawabe, T.;S, Katayama:“Rigid-plastic fem analysis of deformation property in rotary forging”.*Journal of the Japan society for technology of plasticity* 44 (2003)513

Kim, N; Oh S.I. “Analysis Tool for Roll Forming of Sheet Metal Strips by the FEM” *Annals of CIRP* Vol. 48/1 (1999) 235-238

Kim , N; Kobayashi,S: Three-dimensional simulation of gap-controlled plate rolling by the finite element method. *International Journal of Machine Tools Manufact* 30/2 (1990)269-281

Kim, N.; Machida, S.; Kobayashi, S.: Ring rolling process simulation by three dimensional finite element method. *International Journal of Machine Tools Manufacturing* 30 (1990) 569-577.

Kim,N.;Yea,Y.;Ko,Y;Lee,J.:Prediction of spread, pressure distribution and roll force in ring rollingprocess using rigid–plastic finite element method. *Journal of Materials Processing Technology* 140 (2003) 478–486

Kiuchi, M. ;Yanagimoto, J., Computer aided simulation of universal rolling processes, *ISIJ,International*, 30 (1990) 142-149

Knight, W.A; Biswas, S.K. :Towards an Integrated Design and Product System for Hot Forging Dies. *Int. Journal of Production Research*, (1976) 23.

Koppers, U. *et al.*: *Stahl und Eisen*, 106 (1986) No. 14-15, 789-795.

Lange, K.: *Handbook of Metal Forming*. Michigan, Society of Manufacturing Engineers, 1985.

Li, G.J.; Kobayashi, S: Rigid-plastic finite element analysis of plane strain rolling. *Trans. ASME Journal of. Engineerin Industry* 104 (1982) 55.

Lin, Y.H.; Hua, M.: Influence of strain hardening on continuous plate roll-bending process.*International Journal of Non-Linear Mechanics* 35 (2000) 883-896

Lindgren,M: *Modelling and Simulation of the Roll Forming Process*, Master of Thesis, Luleå University of Technology,2005.

Mamalis, A.G.; Hawkyard, J.B.; Johnson, W.: Spread and flow patterns in ring rolling, *Int.J. Mech. Sci.*, 18 (1976) 11-16.,

Marcál,P,V.; Kanazawa,K: Finite element analysis of the steel rolling process. *Applications of Numerical Methods to Forming Processes, ASME, AMD-28* (1978) 81.

Marczinski,H.J.: *Neue Verfahren in der Massivumformung*, Deutsche Gesellschaft für Metallkunde. (1981) 151-161.

Meyer, L. W.: Incremental Forming: Materials Behavior and Description. ICFG/Vif Workshop on Modelling of Incremental Bulk Forming Processes, Darmstadt/Germany, May 17-18, 2006.

Montmitonnet,P.: FEM Strategies for Modeling Two Incremental Forming Processes:Comparison of Hot Ring Rolling and Cold Tube Pilgering. ICFG/Vif Workshop on Modeling of Incremental Bulk Forming Processes, Darmstadt/Germany, May 17-18, 2006

Moon, H.K.; Lee, M.C.; Chung J.H.; Joun M.S.: Finite element analysis of a rotary forging process for bearing assembly, Proceedings of 8th ICTP, Verona/Italy, 2005.

Moore, M. G.; Evans, W.P.: Mathematical Correction for Stress in Removed Layers in X-Ray Diffraction Residual Stress Analysis. SAE Transactions, Vol. 66, 1958.

Munshi, M; Shah, K.; Cho, H.; Altan,T: Finite element analysis of orbital forming used in spindle/inner ring assembly. Proceedings of 8th ICTP, Verona/Italy, 2005.

Music,O: Analysis Of Cold Ring Rolling Process. Mechanical Engineering Department, Middle East Technical University, 2005

Music,O; Güley,V;Öztop, M.S; Savaş,T; Özhan,F; Tekkaya, A.E: Analysis of cold ring rolling process, Proceedings of 8th ICTP, Verona/Italy, 2005.

Noyan, I. C.; Cohen, J. B.: Measurement by Diffraction and Interpretation. 1st ed., Springer-Verlag, New York, 1987.

Pauskar, P.: Finite Element Modeling of Incremental Forming Processes at The Timken Company. ICFG/Vif Workshop on Modelling of Incremental Bulk Forming Processes, Darmstadt/Germany, May 17-18, 2006.

Oztop,M, ;Tekkaya, A.E; Music,O: Two Novel Elastic-Plastic FE Model for Incremental Ring Rolling Process, ICFG/Vif Workshop on Modelling of Incremental Bulk Forming Processes, Darmstadt/Germany, May 17-18, 2006.

Pater,Z.: “Numerical simulation of the cross wedge rolling process including upsetting” Journal of Materials Processing Technology 92-93 (1999) 468-473.

Pater,Z.: Finite element analysis of cross wedge rolling. Journal of Materials Processing Technology 173 (2006) 201–208.

Peng, Y.; Li, D.; Luo,Y. ;Wang, F.: Roll Forming Simulation With Solid Shell Element. Proceedings of 8th ICTP, Verona/Italy, 2005.

Quigley, E.; Monaghan, J: “The finite element modeling of conventional spinning using multi-domain models”, Journal of Material Processing Technology 124 (2002) 360-365.

SAE International, Residual Stress Measurement by X-ray Diffraction, 2003 Edition.

Sawamiphakdi, K.; Pauskar, P.M.; Jin, D.Q.; Lahoti, G.D: Ring rolling process modeling using explicit finite element analysis Advanced Technology Of Plasticity, Vol. 1 Proceedings of the 7th ICTP,Yokohama/JAPAN, Oct. 28-31, 2002

Sebastiani, G; Brosius, A.; Ewers, R.; Kleiner, M.; Klimmek, C.: Numerical investigation on dynamic effects during sheet metal spinning by explicit finite-element-analysis. Journal of Materials Processing Technology 177 (2006) 401–403

Senanayake, R.S.; Cole, I.M.; Thiruvarudchelvan, S.: The application of computational and experimental techniques to metal deformation in cold-roll-forming. *Journal of Material Processing Technologies* 45 (1994) 155–160.

Sheikh, M.A.; Palavilayil R.R.: An assessment of finite element software for application to the roll-forming process. *Journal of Materials Processing Technology* (2006) (in press)

Standring, P.: Characteristics of rotary forging as an advanced manufacturing tool. *Proceedings of the I MECH E Part B Journal of Engineering Manufacture*, Volume 215, Number 7(2001) 935-945

Standring, P.: Modeling of Rotary Forging. ICFG/Vif Workshop on Modeling of Incremental Bulk Forming Processes, Darmstadt/Germany, May 17-18, 2006

Tekkaya,A.E.: Incremental Bulk Metal Forming,Process Planning. 56th CIRP General Assembly, Kobe/Japan, August 20-26 2007

Takizawa,H.; Matsui,T.; Kichi,H.: Rigid-plastic finite element analysis of partially modeled ring rolling. *Simulation of Materials Processing: Theory,Methods and Applications Mori.ed.* (2001) 601-606

Tszeng, T.C: Residual stress calculation by finite element method in manufacturing, Ph.D. dissertation, University of California, Berkeley, CA, 1987.

Tszeng T.C.; Altan T. :Investigation of ring rolling by pseudo plane strain FEM analysis, *Journal of Materials Processing Technology*, 27 (1991) 151-161

Utsunomiya H.; Saito Y.; Shinoda T.; Takasu I.: Elastic–plastic finite element analysis of cold ring rolling process. *Journal of Materials Processing Technology* 125–126 (2002) 613-618.

Wang, G.; Xue, K.; Lu, Y.: Methods of dealing with some problems in analyzing rotary forging with the FEM and initial application to a ring workpiece. *Journal of Materials Processing Technology* 71 (1997) 299-304

Wen , J.; Petty, D.M. : A novel method for prediction of rolled cross section shape *Journal of Materials Processing Technology* 80–81 (1998) 356–36

Yang, G.; Mori,K; Osakada,K.: Determination of forming path in three-roll bending using FEM simulation and fuzzy reasoning. *Journal of Materials Processing Technology* 45(1994)161-166

Yang, Y.S.; Hua, F.A.; Zhang, Y.N.; Guo, M.H.; Guo, D.Y.; Tong, W.H.; Hu, Z.Q. Three-dimensional finite element analysis of tube spinning .*Journal of Materials Processing Technology* 168 (2005) 68–74

Yang D.Y.; Kim K.H.: Rigid–plastic finite element analysis of plane strain ring rolling. *Int. J. Mech. Sci.* 50 (1988) 541-550.

Xie,C.; Dong, X.; Li, S.; Huang, S.: Rigid–viscoplastic dynamic explicit FEA of the ring rolling process. *International Journal of Machine Tools & Manufacture* 40 (2000) 81–93

Xu,Y.; Zang, S.H.; Li, P.; Yang, K.; Shan, D.B.: 3D rigid-plastic FEM numerical simulation on tube spinning. *Proceedings of 8th ICTP, Verona/Italy, 2005.*